ΕΛΛΗΝΙΚΗ ΔΗΜΟΚΡΑΤΙΑ
Εθνικόν και Καποδιστριακόν
Πανεπιστήμιον Αθηνών

ΤΜΗΜΑ ΓΕΩΛΟΓΙΑΣ ΚΑΙ ΓΕΩΠΕΡΙΒΑΛΛΟΝΤΟΣ

Τομέας Δυναμικής, Τεκτονικής και Εφαρμοσμένης Γεωλογίας

ΜΕΤΑΠΤΥΧΙΑΚΟ ΠΡΟΓΡΑΜΜΑ ΣΠΟΥΔΩΝ

ΕΠΙΣΤΗΜΕΣ ΓΗΣ ΚΑΙ ΠΕΡΙΒΑΛΛΟΝΤΟΣ

Ειδίκευση: Εφαρμοσμένη Γεωλογία και Γεωφυσική

FACULTY OF GEOLOGY AND GEOENVIRONMENT

Department of Dynamic Tectonic and Applied Geology

POSTGRADUATE PROGRAM

Specialization: Applied Geology and Geophysics

DEBRIS FLOW MODELLING: THE CASE OF MANDRA

ΠΡΟΣΟΜΟΙΩΣΗ ΡΟΩΝ ΚΟΡΗΜΑΤΩΝ: Η ΠΕΡΙΠΤΩΣΗ ΤΗΣ ΜΑΝΔΡΑΣ

Contents

List of figures

List of tables

Abstract

The purpose of this thesis is to present and describe debris flow phenomena during a flash flood. On November 15, the city of Mandra and the surrounding countryside were flooded unexpectedly. The upstream watersheds, which received massive amounts of rainfall with a cumulative rainfall of nearly 300mm in less than 8 hours, suffered considerable damage, many human casualties, and significant geomorphological consequences.

The distribution of debris flows in the Agia Aikaterini stream is of great importance for the research of their processes. The pre-existing maps that depict the points where there were debris flows were the first data needed for the simulation. The simulation was run based on these to ensure the program's reliability.

The Rapid Mass Movements Simulation(RAMMS:: DEBRIS FLOW) is a surprisingly great software for simulating flow streams, with several useful tools and the ability to present them as editable graphics pretty quickly.

The following chapters discuss the concept of landslides and how to deal with the problems they cause, the factors that influence the appearance and onset of debris flows, the classification of debris flows, their deposition and morphology, failure analysis and stability, the characteristics and failure mechanisms of debris flows, the elimination of weak layers, and finally the study area and the simulation results.

ΠΕΡΙΛΗΨΗ

Σκοπός της παρούσας εργασίας είναι η παρουσίαση και η περιγραφή των φαινομένων ροών κορημάτων κατά τη διάρκεια μιας ξαφνικής πλημμύρας. Στις 15 Νοεμβρίου 2017 η πόλη της Μάνδρας και η ευρύτερη περιοχή αναπάντεχα δέχτηκαν μεγάλη πλημμύρα. Οι ανάντη λεκάνες απορροής, οι οποίες δέχθηκαν τεράστια ποσότητα βροχόπτωσης σχεδόν 300mm σε λιγότερο από 8 ώρες, υπέστησαν πολλές σημαντικές ζημιές, απώλειες ανθρώπων αλλά και σημαντικές γεωμορφολογικές επιπτώσεις.

Η κατανομή των ροών κορημάτων στο ρέμα της Αγίας Αικατερίνης παρουσιάζει ιδιαίτερο ενδιαφέρον έχοντας μεγάλη σημασία για την μελέτη των διεργασιών που συνέβησαν. Τα πρώτα δεδομένα που χρειάστηκαν για την προσομοίωση των ροών κορημάτων ήταν οι ήδη προυπάρχοντες χάρτες που απεικονίζουν που συνέβησαν οι ροές κορημάτων. Με βάση αυτά πραγματοποιήθηκε η προσομοίωση με σκοπό την αξιοπιστία του λογισμικού. Το Rapid Mass Movements Simulation (RAMMS:: DEBRIS FLOW) είναι καλό λογισμικό που χρησιμοποιείται για τη προσομοίωση των ροών κορημάτων, έχοντας πολλά εργαλεία και τη δυνατότητα να παρουσιάζονται τα αποτελέσματά του με μεγάλη ευκρίνεια.

Τα ακόλουθα κεφάλαια αναφέρουν την έννοια των κατολισθήσεων και τον τρόπο αντιμετώπισης των προβλημάτων που προκαλούν, τους παράγοντες που επηρεάζουν την εμφάνιση και την έναρξη των ροών κορημάτων, την ταξινόμησή τους, την εναπόθεση και τη μορφολογία τους, την ανάλυση, την ευστάθεια και τα χαρακτηριστικά της αστοχίας , τέλος, τις απαραίτητες πληροφορίες για την περιοχή μελέτης.

Thanksgiving

First, I would like to thank Dr.Stavropoulou Maria for the faith she has shown me in every work-related difficulty, as well as her advice and prompt assistance in completing this assignment.

Subsequently, a key factor was Mr. Andreadakis Emmanuel, PhDc. With his hydrogeology expertise, experience, and recommendations, he will be critical to the fulfillment of the project's results.

Also, I would like to thank Sofia Laskari, PhD, whose help was equally important in completing this project.

Besides, I would like to thank Mark Cristen, a RAMMS team member, as well. We communicated throughout the program's difficulties, and he assisted me in any way he could. In addition, I would like to show my thankfulness to Marianna Igoumenidou and Sofia Polykreti for their expertise in the field of English and for pointing out my grammatical and vocabulary issues.

Finally, I would like to thank my whole family, especially my mother and my sister ,and my fiancé Dimitris, where every step of the way they are by my side and support me.

Introduction

Debris flows are fast-moving mixtures of water, clay, and granular sediments that are typically caused by strong and localized storms in mountain catchments. Debris flows' destructive character is exacerbated by their high density, velocity, and discharge. Front velocities of over 10 m/s have been seen, with peak discharges that are one or two orders of magnitude larger than torrential floods. They have the ability to convey large volumes of sediment from the bottom of steep slopes to the fan termination, where deposition normally takes place (Simoni & Graf, 2012). Flash floods are a common occurrence in the Mediterranean, resulting in a variety of small and large-scale tragedies. High-intensity storms that cause ephemeral watercourses to overflow are a usual flood phenomenon in the region. Flash floods, despite their importance, have been poorly understood until recently due to monitoring challenges, capable of attributing to the temporal and spatial scales on which they occur, as well as to the inadequacy of traditional observational networks when it comes to effectively measure their characteristics.

These observational difficulties, which are usually accompanied by a lack of instrumental data (as demonstrated in many of the examples examined here) or even destroyed instruments, have focused on post-event research and hydro meteorological analysis (Diakakis, et al., 2019).

The results of mathematical models that depict the depositional process, such as flow depth, velocity, and impact force, can be utilized to calculate the debris flow hazard. The current routing models are based on one-dimensional and two-dimensional continuum mechanical equations. They frequently exploit simple rheological relationships and ignore the physics of debris flows to simulate the bulk behavior of one-phase mixtures at the macroscopic scale (Iverson , et al., 1997).

A number of viscoplastic fluid models are based on a rheological formulation for a Bingham fluid or the more generalized Herschel Bulkley representation (Simoni & Graf, 2012). Their application needs extensive topographical and volume data as well as difficult-to-assess rheological qualities. As a result, a back-analysis can only provide useful rheological information and produce predictable results (Sosio, et al., 2007).

In this study, the research findings of the Mandra area incident (November 2017) are being presented. The depositional behavior of the events was back-analyzed using the RAMMS technique. RAMMS is a useful tool for engineers working with avalanches and other natural hazards that is based on the solution of two-dimensional continuum mechanical equations for a Voellmy rheological scheme. Indeed, it was created by WSL/SLF as a useful tool for engineers working with avalanches and other natural hazards (Cristen, et al., 2010).

We evaluated the model's reliability in the simulation of debris flows in the Katsimidi stream by including a hydrograph as calibration parameters. The overall behavior of the model and its sensitivity to the basic input parameters are explained through simulations. The findings show that a range of rheological parameters can accurately describe debris flows in the Katsimidi stream. The model exaggerates the likelihood of overflow, which might be limited. Field data validates velocity, flow height, and pressures, and

there appear to be miniscule to no deviations based on previous results, which can helpful with regard to risk assessment.

CHAPTER 1

1.1. Landslide Categories

In general, many individual landslides, creeps and mass movements have been described. Occasional observers have recorded these movements out of curiosity. In the past, few geologists in the past had dealt extensively with mass movement (Rapp, 1960).

Rainfall-induced landslides and debris flow, which occur around the world erode slopes and scour channels contribute to the formation of alluvial fans, resulting in infrastructure damaging and life loss (Bollschweiler, et al., 2012).

Various definitions have been proposed for the term "landslide". According to Terzaghi, landslide is the mass movement of a slope (rock or ground) whose gravity center moves downwards and outwards (Terzaghi, 1950). However, Cruden and Varnes 1996, describe the term of landslide as «the movement of a mass of rock, debris or earth down a slope", but sinking, avalanches and ice movements are not included.

One of the main criteria for landslide classification has to do with the landslide kinematics. Landslides are divided into rapid and creep. Creep are described landslides with slow or very slow movement. The surface layer being in motion is of the order of a few centimeters per year. The theory of creep is considered similar to that used in the mechanics of materials, i.e. a deformation that continues under constant pressure. According to Varnes 1996, "creep means different things to different persons, and perhaps, it is inappropriate to use this term or use it in a well-defined manner". In general, there have been a variety of landslide classifications; however, the prevailing one proportional to the landslide movement (Cruden & Varnes, 1996).

The rapid mass movements are classified as follows:

Falls: in this case, the ground or rock is detached from a steep slope along a surface. There is little or no shear displacement. Then the material moves downwards bouncing or rolling through the air. Usually, the motion is very fast but in case the displaced mass has receded, the fall will be preceded by small sliding or tipping movements that separate the displacement material from the undisturbed mass. Undercutting is most common in cohesive soils or rocks near the cliff-side that is being eroded by waves, or in eroding riverbanks (Cruden & Varnes, 1996).

- Rockfalls: The flow consists of small pieces of rock. They involve abrupt, downward movements of rock or earth or both. These are detached from steep slopes or cliffs. The material bounces when it falls because when it falls it collides with the lowest slope, which has an angle less than the angle of fall. As the mass falls, there is a chance that it will break if it hits. Thus, it has the ability to roll on very steep slopes until the ground is leveled (Highland & Bobrowsky, 2008).

Slides: The term slip refers to a downslope movement of a ground or rock. It occurs mainly on ruptured surfaces or in thin zones of shear strain.

The slides are distinguished in translational and rotational.

-Rotational slides: the slide is made on a surface where it is curved and concaved while the sliding material is subject to slight deformation. When the sliding surface is circular then the displaced mass moves along the surface with a small internal deformation. Often the surface is not circular but follows pre-existing geological surfaces. There is the possibility of moving the head of the displaced material almost vertically while its upper surface has the ability to tilt backwards towards the scrap. Sliding is called a slump when it is rotational and has many parallel curved planes of movement. This category of landslide occurs more often in "fill" materials because it appears in many instances in homogeneous materials. The slopes on which it occurs range from 20 to 40 degrees. In addition, in soils the rupture surface has a depth- to -length ratio between 0.3 and 0.1. Rotational slide is extremely slow to moderately fast. This means that in the case of being extremely slow it is less than 0.3 meters or 1 foot every 5 years whereas when it is moderately fast, it does not exceed 1.5 meters or 5 feet per month. The reasons for which it is caused are the intense or uninterrupted rain as well as a rapid melting of snow. These result in the saturation of the slopes and the increase in groundwater within the mass. It should be noted that the base of the slopes is eroded by a rapid fall of the river level after floods, by the rise of the groundwater level after the filling of reservoirs and by the increase of the level of streams, lakes and rivers. They obviously cause problems in structures and especially in those being just above the moving mass due to deformation; however, if their movement is slow they do not pose a threat to human lives. The volume is difficult to stabilize permanently so after such failures can dam rivers causing floods (Highland & Bobrowsky, 2008).

-Translational landslides: the movement of a translational landslide is done outwards or downwards and outwards along a relatively flat surface with a slight rotational motion or tilt backwards. If the rupture surface is completely inclined then this type of slip can reach long distances. Their material may consist of loose, unconsolidated soils to extensive slabs of rock, or both. These slides fail along geological discontinuities. They can move along the layer of permanent frost. This type of landslide is the most common. The distance to length ratio of the rupture surface is less than 0.1. The movement when it is slow , is equal to 5 feet per month or 1.5 meters per month. However, it can be moderate to extremely fast reaching 5 feet a day or 1.5 meters a day. The landslide mass of translational failures when the speed is extremely fast can be extended to debris flow. It is caused by heavy rainfall, rising groundwater and melting snow, floods or other inundation of water resulting from irrigation, or leakage from pipes or human-related disturbances such as undercutting. When their speed remains slow, they can destroy structures but only when their speed increases can they threaten human lives. They can certainly cause floods if they dam rivers (Highland & Bobrowsky, 2008).

Topples: These are the forward rotations of masses of soil or rocks, around a point or axis located below the center of gravity of the moving masses. This type of movement can then gradually develop into a fall or slip depending on the geometry of the slope, the moving mass and the detachment surface. The speed of a reversal ranges from extremely slow to extremely fast while as a movement it manifests itself mainly on rocky slopes (rock topples). On the contrary, debris topples and earth topples are rare cases, the

occurrence of which is mainly due to natural processes (eg differential erosion) and human interventions (Cruden & Varnes, 1996).

Spreads: It concerns the complex lateral motion of the earth's cohesive materials, which rest on a weak substrate, which is subject to liquefaction or plastic flow. The cohesive material blocks retreat from the weak substrate and the slow downward movement extends over long distances. This is a result of the retrograde extensions from the zone of origin. Zones of origin can be riverbanks or coastlines that have been eroded. Liquefaction due by water saturation or earthquake shock in substrates like loess, a weakly cemented windbreak, causes spreads. -silt that has been buried (Highland & Bobrowsky, 2008).

-Lateral spreads: Lateral spreads are related to movements relevant to the lateral dimension of the material. The slopes on which they appear have a slight slope and are distinguished in the block spreads and liquefaction spreads.

-Block spreads: Rocky geological formations are placed on top of weak formations and are separated by vertical cracks in pieces. The underlying material is crushed to cover the cracks that are created. The displacement that usually occurs is slow and is distributed throughout the extending mass.

-Liquefaction spreads: They are formed mainly in sensitive clays and sludges, which, when disturbed, show a loss of their strength. Fracture is gradual and usually begins as extensive subsidence with reverse progressive expansion. The movement starts without warning and its speed is high to very high.

Flows: In a flow, the movement is continuous and the shear surfaces are short-lived, at close range and not maintained. The materials contained in the flow have velocities similar to those in a viscous liquid. They consist of loose materials as the moving mass undergoes intense deformations. When their speed is extremely slow then they are classified as creep. When the flows are fast then there is a constant motion of the particles that make up the moving mass, which moves in the form of a viscous fluid. They are distinguished in earthflows and debris flows.

The existence of debris flows occurs when steep gullies and canyons have been stripped, in case they have no vegetation due to fires or forest logging. They extend over long distances and the runout is large. However, their movement is relatively shallow. The debris fans are called the fanlike and triangular deposits, which are created by debris and mud that end at the bases of the slopes.

-Debris Flow: This is a form of movement that has high speeds. It includes loose soil, rocks and organic matter in combination with water, forming a slurry that flows downwards. Often, on account of the content of fine material, it is called mudslide. Frequently, rotational and translational slide develop into a debris flow because they gain great speed and by losing their internal mass their coherence acquires water. In addition, there are dry flows (or sand flows) that occur in sand without cohesion. Flows are extremely fast and if they occur without warning, whereas they can, also, cause

-Earthflows: They occur on slopes of small to moderate slope in loose fine-grained soils, such as clays and silt but in very weathered, clay bearing bedrock. The movement of the mass of the materials is subject to

intense internal deformation as it has the form of a viscous fluid. Speed varies reaching long distances. When disturbed the marine clay becomes vulnerable. It can also lose all its shear strength if its moisture content changes and liquefies. When the mass exceeds 60% water content then the flow is also referred to as mudflow (Highland & Bobrowsky, 2008).

Some parameters of debris flows can be obtained and are useful for risk assessment as well as for mitigation. In addition, they are useful in predicting flow time and help in timely evacuation (Matthias, 2005). The figure includes the total volume of debris, peak discharge, flooded area and possible consequences.
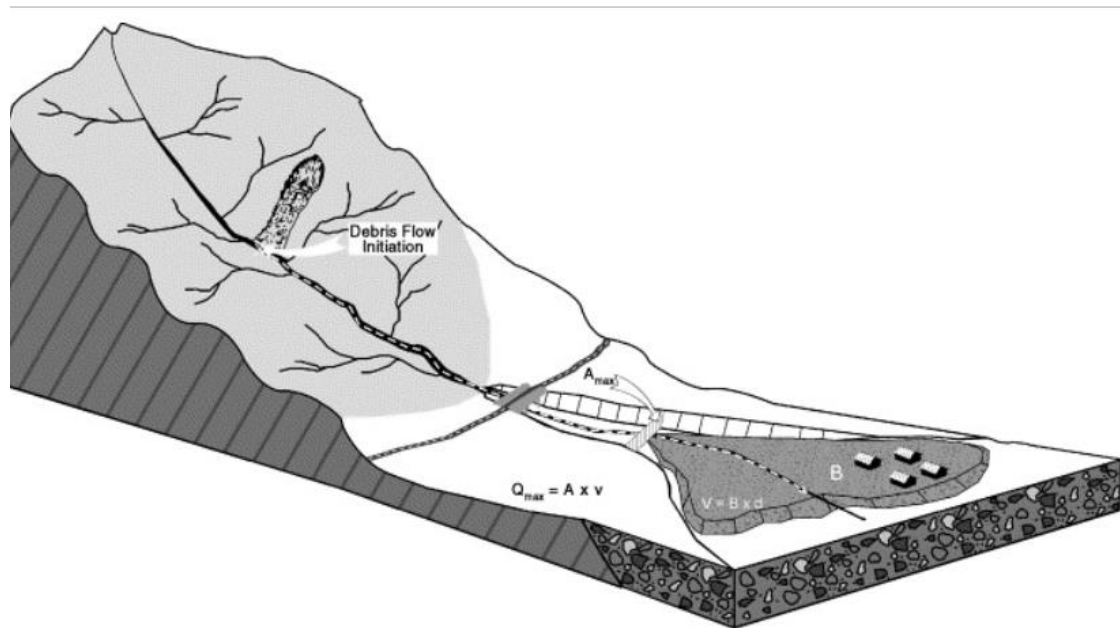
FIGURE 1 THE DESCRIPTIVE SIZE CATEGORIES "SMALL", "MEDIUM" AND "LARGE" ARE NOT USED BECAUSE THEY ARE VAGUE AND CAN ONLY BE OBJECTIVE IF USED IN CONJUNCTION WITH NUMBERS. DEBRIS FLOWS CAN COVER A WIDE RANGE OF VOLUMES DUE TO THE LARGE VOLUME OF MATERIALS AVAILABLE (MATTHIAS, 2005)

A landslide can be seen in the following parts (Cruden & Varnes, 1996):

1. Main scrap: is the steep surface of undisturbed soil around the periphery of the movement, caused by the removal of the sliding material from the undisturbed material. The extension of the surface of the steep side, below the displaced material constitutes the rupture surface.

2. Head: It's at the very top of the landslide, and it's made up of the higher parts of the sliding mass along the contact between the displaced material and the main scrap.

3. The tip: It is the highest point of contact between the displaced material and the main section.

4. Crown with cracks: It is the essentially immovable material that is located at the highest points of the main scrap.

5. The main body: It is the displaced mass of the material. It is formed by the accumulation of material which, after moving along a path, stops its course and is concentrated in the lower part of the landslide body (at this point its kinetic energy is zeroed).

6. Surface of rupture: is the surface that forms the lower limit of the displacement material and separates the sliding mass from the fixed background. Its upper part corresponds to the sliding surface of the material.

7. The detachment surface: It is a part of the initial surface of the ground covered by the foot of the landslide.

8. Foot: is the part of the displaced material that is downstream of the finger. The often-buried cross section is located between the lower part of the burst surface and the initial ground surface.

9. Toe: is the margin of the slipped material being the farthest point from the main front.

10. Surface of rupture toe: It is the cross section (often buried) between the lower fracture surface boundary and the initial ground surface.

11. The tip: That is, the farthest point from the top of the landslide, which is at the foot

12. The immersion zone: It is the area of the landslide in which the displaced material is below the initial surface of the soil.

13. Swelling zone: It is the area of the landslide in which the displaced material is above the initial surface of the ground.

14. The flap: It is the immovable material located next to the sides of the fracture surface. Described as right or left based on the posture of the crown with cracks.

15. Displaced materials: Materials that are displaced from their original position on the slope

16. The initial ground surface: That is, the surface of the slope that existed before the landslide.

1.1.1 How to approach Landslide problems

The stabilization of the slopes aims to reduce the loads and increase the landslide resistance forces. The driving forces of a landslide have the ability to decrease if the material is excavated from the appropriate part of the unstable soil and by draining the water in order to reduce the hydrostatic pressures, which act on the unstable mass.

Furthermore, to avoid the unstable slope, a new construction site location could be selected or the construction site adjusted (Μπούνου, 2012). In order to select any stabilization measure, the actual or possible causes of failure must be precisely identified because there is a possibility of recurrence of the failure (Abramson, et al., 2002).

The basic measures to solve landslide problems on the slope are the collection and drainage of surface water, groundwater drainage, elimination of weak layers and possible failure zones, construction of support structures or other supports and soil reinforcement. Anchor reinforcement will be analyzed below.

Collection and Drainage of surface water: The water is directed to the landslide area, the capture of which is achieved in two ways. The first way is to level the ground. In this way the waters do not find an obstacle in the movement and they are not retained. The second one is to build a permanent peripheral trench with a suitable slope and its configuration so that it is not filled with materials of the surrounding soil mass (Μπούνου, 2012).

Underground Drainage: Groundwater is a key factor in slope instability. Thus, underground drainage is considered an effective method of stabilization. Drainage is possible in various ways but it must be borne in mind that it can be successful only when its design is done in combination with the integrated geological and hydrogeological research of the area. A simple way to drain the soil is to build open canals or otherwise drainage ditches. Their construction is built at an angle and depth to the fixed background of the landslide. They are filled with coarse-grained rocks, which allow the removal of groundwater and help increase the shear strength of the soil. Nonetheless, there is a limitation to the effectiveness of this method because after some time there is a risk that the voids of the coarse layer will be filled with fine-grained materials from the surrounding soil mass. An alternative way of draining groundwater is to perform almost horizontal drillings from the base of the slope, which act as filters. If there are old boreholes and wells in the area of failure or their reconstruction then drainage is achieved due to the continuous pumping of water from them.

However, the most effective way to drain groundwater is to drill a drainage tunnel in combination with horizontal boreholes from the surface or inside the tunnel roof. This method is not profitable at all from a financial viewpoint. Therefore, it is selected only in failures of great depth and long length (Μπούνου, 2012).

1.2. Factors affecting the occurrence of debris flow

The availability of loose sediments, torrential rainfall, and topographic characteristics are all important elements in the commencement of runoff. Various meteorological factors influence the occurrence of debris, mud, and lahar floods. Their research contributes to a better understanding of soil hydrology and the interpretation of the impact of climate on the occurrence of phenomena. In addition, if there is a high risk, it is important for the development of early warning systems. These variables have a lot of spatial and temporal diversity. Most shallow landslides, and especially debris flows, are thought to be caused by rapid infiltration of sustained heavy rainfall, which causes soil saturation and a brief rise in pore water (Iverson, 2000).

Peak flow appearance is influenced by both primary and secondary climatic factors. The most important are those that are a direct cause of the phenomenon, such as severe storms and rapid melting snow. Secondary climatic elements are the ones that influence whether precipitation flows and are activated during an earthquake, a volcanic eruption, or a heavy storm. The related metrics (rainfall, rainfall intensity, and so on) have value limitations that can be used in risk assessment as well as mitigation (Wieczorek & Glade, 2005). The induction of precipitation flows has been observed all over the world, and it can begin as early as the first five minutes of rainfall if the intensity is greater than 20mm/h, with an intensity greater than 9mm/h for a duration of one hour or more, or with an intensity less than 1mm/h for a continuous rainfall of more than 60 hours, depending on the case (Γραμμένου, 2021).

Depending on the type of onset, debris flows in alpine settings are grouped into three categories: a) shallow landslide, b) riling, and c) firehose effect. In an alpine landscape, the firehose effect is generated by masses of detritus being eliminated by a condensed jet of water. Research has often investigated the relationship between drainage basin topography and runoff, and GIS has been used to model the starting sites of runoff in relation to channel gradation area, discharge, and sediment contribution (Chien-Yuan Chen & Fan-Chieh Yu, 2011). The position of the head of a ridge channel is controlled by its topographic form, and there is a threshold relationship between the degree of inclination and the area it encompasses (Montgomery & Dietrich, 1994). For instance, in the Central Front Range of Colorado, inclination angles greater than 32 degrees and areas less than 3,000 m^2 are conducive to the commencement of slope flows (Godt & Coe, 2007). Other studies (Hungr, et al., 1984) (Rieckenamnn & Zimmermann, 1993) have shown an association with the onset of steep currents in the slope of the source areas, with typical values between 27 ° and 38 °. A slope of more than 25 degrees is also required to commence runoff flows, which reduces as the catchment area grows. According to Millard (1999), runoff flows from a canal's sidewalls are bigger and appear at steeper slopes than those from the canal's central walls. Although this finding supports the concept of a sediment transport limit, it was based on data from the coastal environment and may have limited applicability in the mountains (Chien-Yuan Chen & Fan-Chieh Yu, 2011).

External factors such as rainfall, snowmelt, human activity and geological form are not the only factors influencing the formation of debris flows. The properties of loose materials such as particle

classification, soil dispersion and water content are some of the factors that contribute to their formation. The key to revealing the mechanism of initiation of debris flows is the analysis of critical coupling relationships between these factors (Jun-Du, et al., 2021). There is no specific standard for their classification. Some researchers have classified the debris flow according to the way it is caused, i.e. by shallow landslides and runoff. Other researchers divided the debris flow into landslides that moved rapidly and mixed with water, forming them by hydraulic erosion of sediment in the canal or streambed and by formation of drift deposits from bank collapse. In the first and third case, there was a development of viscous debris flow due to the wider grading of the grains while in the second case a stony flow of debris developed due to pebbles and gravel in the riverbed in mountainous areas (Jun-Du, et al., 2021).

The findings can be used to estimate the disaster-prevention potential of catastrophic flows. Loss of life, destruction of homes and facilities, damage to the road network, railways, and pipelines, road accidents and train derailments, environmental impacts due to leaks, agricultural land, livestock, and forests, interruption of water supply systems, degradation of aquaculture and similar phenomena are all immediate effects of spillovers. The disruption of traffic and communications along road networks is one of the most serious indirect effects of leakage flows. Another indirect effect of the gusts is the clearing of land.

Variable	Description	Units	First Introduced
D	Rainfall duration; the duration of the rainfall event	h or days	Caine (1980)
D_c	Duration of the critical rainfall event	h	Aleotti(2004)
E	Cumulative event rainfall; The total rainfall measured from the beginning of the rainfall event to the time of failure; also known as storm rainfall	mm	Innes (1983)
E_{MAP}	Normalized event rainfall; cumulative event rainfall normalized to MAP (E_{MAP} =E/MAP); also known as normalized storm rainfall	-	Guidicini and Iwasa(1977)
C	Critical rainfall ; the total amount of rainfall from the time of a distinct Increase in rainfall intensity(t_o) to the time of triggering of the first landslide(t_t)	mm	Govi and Sorzana(1980)
C_{MAP}	Normalized critical rainfall; critical rainfall divided by MAP (C_{MAP} = C/MAP)	-	Govi and Sorzana (1980)
R	Daily rainfall; the total amount of rainfall for the day of the landslide event	mm	Crozier and Eyles (1980)
R_{MAP}	Normalized daily rainfall; daily rainfall divided by MAP(R_{MAP}=R/MAP)	mm	Terlien (1998)
I	Rainfall intensity; the average rainfall intensity for the rainfall event	mm h^{-1}	Caine(1980)
I_{MAP}	Normalized rainfall intensity; rainfall intensity divided by MAP (I_{MAP}=I/MAP)	h^{-1}	Cannon(1988)
I_{MAX}	Maximum hourly rainfall intensity; the maximum hourly rainfall intensity	mm h^{-1}	Onodera et al. (1974)
I_P	Peak rainfall intensity; the highest rainfall intensity (rainfall rate) during a rainfall event; available from detailed rainfall records	mm h^{-1}	Wilson et al. (1992)
I(h)	Mean rainfall intensity for final storm period; *h* indicates the considered period, in hours, most commonly from 3 to 24 h	mm h^{-1}	Govi and Sorzana(1980)
I_F	Rainfall intensity at the time of the slope failure; available from detailed rainfall records	mm h^{-1}	Aleotti (2004)
I_C	Critical hourly rainfall intensity	mm h^{-1}	Heyerdahl et al. (2003)
I_RMAP	Normalized rainfall intensity at the time of the slope failure; rainfall intensity at the time of the slope failure divided by MAP (I_RMAP=I_R/MAP)	h^{-1}	Aleotti (2004)
A(D)	Antecedent rainfall. The total(cumulative) precipitation measured before the landslide triggering rainfall event; *D* indicates the considered period in days	mm	Govi and Sorzana(1980)
A_{MAP}	Normalized antecedent rainfall; antecedent rainfall divided by MAP (A_{MAP}=A/MAP)	-	Aleotti(2004)
MAP	Mean annual precipitation; for a rain gauge, the long term yearly average Precipitation, obtained from historical rainfall records; a proxy for local climatic conditions	mm	Guidicini and Iwasa (1977)
RD_s	Average number of rain days in a year (rainfall frequency); a rain day is a day with at least 0.1 mm of rain; for a rain gauge, the long term yearly average of rain days obtained from historical rainfall records; a proxy for local climatic conditions	#	Wilson and Jayko (1997)
RDN	Rainy-day normal; for a rain gauge, the ratio between the MAP and the average number of rain days in a year (RDN=MAP/RDs)	mm/#	Wilson and Jayko(1997)
N	Ration between MAPs in two different areas	-	Barbero et al. (2004)

In terms of morphological slope and exposure to river floods, many mountainous places are best suited for the formation of these geomorphs (Matthias, 2005). Rainfall and landslide data were utilized to inform Caine's 1980 determination of the minimal rainfall amount and intensity that is likely to cause shallow landslides and runoff (Caine, 1980). When the minimum average intensity, which is likely to cause insufficient surface failures was plotted in logarithmic coordinates, it was observed that as the duration of rainfall tends to increase, the minimum average intensity, which is probable to cause insufficient surface failures decreases linearly from 10 minutes to 35 minutes. The minimum ID required for the initiation of shallow landslides and runoff flows has been calculated. An objective statistical technique was used to create the lower curve from rainfall data. Rainfall data was smoothed by half yearly rainfall and normal daily rainfall to address discrepancies in the strength and duration of rainfall that may lead to shallow slope failures in places with varying climatic conditions. The Climate Research Unit of the University of East Anglia produced the Global Climate Data System, which provided the climate data. The received global ID thresholds (intensity and duration) are much lower than Caine's recommended limit and the other global thresholds proposed (Caine, 1980). Where local and regional lower limits are unavailable, the new global intensity and duration limits can be employed in a global landslide warning system based on global precipitation measurements (Bollschweiler, et al., 2012).

The table 1 lists the variable, the most often used units of measure for the parameter, and the creator (s) who first entered the parameter. In the literature, several definitions for the same or related variables have been employed, and nomenclature is inconsistent

Number	Author	Landslide Type	Threshold Type	Equation	Range	Notes
1	Caine (1980)	Shallow landslides and debris flows	ID	$I = 14.84 * D^{-0.39}$	0.167<D<500	S,P
2	Innes (1983)	Debris flows	ID	$I = 4.93 * D^{-0.50}$	0.1<D<100	S,P
3	Clarizia et al.(1996)	Soil Slips	ID	$I = 10 * D^{-0.77}$	0.1<D<1,000	S,P
4	Crosta and Frattini(2001)	Shallow Landslides	ID	$I = 0.48 + 7.2 * D^{-1.00}$	0.1<D<1,000	S,H
5	Cannon and Gartner(2005)	Wildfire related debris flows	ID	$I = 7.00 * D^{-0.60}$	0.1<D<3	S,P,M
6	This work	Shallow landslides and debris flows	ID	$I = 2.20 * D^{-0.44}$	0.1<D<1,000	S,P
7	This work	Shallow landslides and debris flows	ID	$I = 2.28 * D^{-0.20}$	0.1<D<48	C,P
8	This work	Shallow landslides and debris flows	ID	$I = 0.48 * D^{-0.11}$	48≤D<1,000	C,P
9	This work	Shallow landslides and debris flows	I_{MAP}D	$I_{MAP} = 0.0016 * D^{-0.40}$	0.01<D<1,000	S,P
10	This work	Shallow landslides and debris flows	I_{MAP}D	$I_{MAP} = 0.0017 * D^{-0.13}$	0.1<D<48	C,P
11	This work	Shallow landslides and debris flows	I_{MAP}D	$I_{MAP} = 0.0005 * D^{-0.13}$	48≤D<1,000	C,P
12	This work	Shallow landslides and debris flows	I_{RDN}D	$I_{RDN} = 0.25 * D^{-0.39}$	0.1<D<1,000	S,P
13	This work	Shallow landslides and debris flows	I_{RDN}D	$I_{RDN} = 0.24 * D^{-0.14}$	0.1<D<48	C,P
14	This work	Shallow landslides and debris flows	I_{RDN}D	$I_{RDN} = 0.06 * D^{-0.12}$	48≤ D< 1,000	C,P

TABLE 2 RAINFALL INTENSITY-DURATION ID (GUZZETTI, ET AL., 2008)

Caine reports 73 cases of excessive rain and harsh weather around the world that resulted in tiny landslides and streams. Based on these data, Caine was the first to suggest an overall intensity-duration (ID) limit for the occurrence of shallow landslides and runoff. Caine's lower curve is as follows (Caine, 1980):

EQUATION 1: $I = 14,82 * D - 0,39 (0,167 < D < 500)$

where D is the rainfall duration in hours and I is the rainfall intensity in millimeters per hour.

Information was collected on rainfall conditions that resulted in slope failure in various places or regions around the world as a result of Caine's pioneering work (Caine, 1980) and different rainfall limits were proposed at local, regional, and global scales of published thresholds and rationale for establishing and using rainfall thresholds. Despite the criticism, which is based on the observation that it is not the amount of rainfall that causes damage, but the (largely unknown) amount of water that penetrates and moves in the ground to cause damage, continuous rainfall measurements are used to predict the occurrence of shallow landslides and runoff (Aleotti, 2004) (Caine, 1980). In order to consider, the climatic effects, the intensity of rainfall is divided into the average annual rainfall (MAP), [1]the average number of rainy days (RD) and the normal rainfall (RDN) (Raymoncd & Angela, 1997). Individual climatic zones have thresholds set to further explore the effect of climate on the start of shallow landslides and runoff flows (Bollschweiler, et al., 2012).

Research-wise Caine (1980) presented the first I-D rainfall limit, as previously stated, for shallow landslides and debris flows worldwide. Since then, similar I-D limits or other types of critical conditions have been proposed. Crosta (1998) investigated the effect of local soil characteristics and rainfall conditions associated with location on the I-D threshold in northern Italy. Chen et al. (2005) used a combination of moderate intensity and duration of rainfall to monitor the flow of debris in Taiwan. Godt et al. (2006) calculated previous humidity conditions of slope materials and an I-D rainfall threshold to determine landslide seasons in Seattle. Osanai et al. (2010) set as a criterion based on the cumulative rainfall of 60 minutes and the soil-water index in each 5 km grid that covers the whole of Japan (Liu, et al., 2020). It is considered that due to climatic, topographic and geological differences, the spatial variability of critical rainfall conditions occurs (Guzzetti, et al., 2007).

Many factors can affect the presence of a debris flow. Some factors are characterized as predisposing, which make an area more and more sensitive to the flow of debris without actually activating it, such as in the case of availability in a catchment area. Other factors that cause debris flow are considered as triggers, e.g. the intense flow of surface water. Here are some factors that affect the appearance of debris flows (Highland & Bobrowsky, 2008).

Slope Angle: A fundamental factor influencing the appearance of debris flow is the angle of inclination. It is important to distinguish between the angle of inclination required to activate debris flow and the angle of inclination required to maintain flow mobility in the evacuation zone. The angle of inclination required to activate the flow may not be the same as the angle of inclination to maintain flow mobility. Debris flows can be activated at angles over 30°. Large slopes are particularly prone to the occurrence of debris flow, and intense soil erosion is created. The factor that is considered to be of primary importance is that any risk assessment for the first crossing should include slopes from 26° to 50°. However, when the geological formation is being peat, then a lower minimum angle should be embrased (Nettleton, et al., 2005). According to (Takahashi, et al., 1998) (Takahashi, 1978), it was estimated that the critical slope for debris flow was only about 14.5° based on the mechanical equilibrium.

Slope Height: It is not yet known if a correlation exists between the height of the slope and the sensitivity to the flow of debris. If the materials involved behave as granular soils and are modeled with c = 0, then based on the slope stability theory then it is argued that the probability of failure is independent of the slope height. It is generally not believed that the height of the slope should be considered in relation to risk models. A flow below 400 meters is likely to cause more damage than a flow below 40 meters, with all other factors being equal (Nettleton, et al., 2005).

Slope Aspect: The slope aspect is a key factor in predicting landslides. If the slope face and the direction in which a smooth rock profile sinks coincide, then debris flow is triggered, while a stepped rock head profile, or one with inward-facing cuts relative to the sloping face may not be involved with the onset of debris flow (Nettleton, et al., 2005).

Other topographic factors are active channels and gullies, which give weight to the surface runoff of water and are more likely to channelized flow. Positive or negative effect on the formation of debris flows depending on the shape and location can have terraces, ditches (natural or otherwise), and breaks in slope. Besides, a flow may be delayed due to natural or man-made obstructions in the source, transportation or deposition zones (Nettleton, et al., 2005).

Geology: Geological formations are a predisposing factor for debris flows and have the ability to mobilize unconsolidated deposits. An important factor for a mantle of superficial deposits is the lithology of the underlying bedrock. An area is prone to failure due to soil and rock erosion. Weather conditions create some products that form a weak soil mantle that covers the substrate that feeds a surface. Along this surface, there may be slope failure or debris flow. What is more, low shear strength occurs in bedrocks that are discontinuous. Beyond that, when there are discontinuities within the bedrock, they are used by the debris flows resulting in more rock debris (Nettleton, et al., 2005).

Geotechnical Elements: The geotechnical behavior of the soil includes cohesion, grain size, shear strength, moisture content, void ratio, relative density and permeability. All of the above are important for the occurrence of debris flow. Loose unconsolidated deposits such as mud, sand, gravel, cobblestones and boulders are usually predisposed to debris flows. Restrictions on groundwater flow and increase in the

relative water pressure of the pores are caused because the thickness or permeability of the surface deposits varies (Winter, et al., n.d.).

HYDROLOGICAL ELEMENTS

Drainage Network: A drainage basin is the area where water flows forming a stream. A stream consists of flowing surface waters, which can be a mighty river. All rainfall that falls into a drainage basin, moves into it. However, part of this rainfall can pass through groundwater to a neighboring catchment area (Earle, 2020).

Obviously, the morphometric parameters of the drainage basin play an important role in the occurrence of debris flow. These parameters include the area and perimeter of the catchment, the average length, the maximum, the minimum and the average altitude, the average angle of inclination, the shape factor and the circularity rate. The cross-sectional and longitudinal shape of the stream affects the length and volume of the runoff. Additionally, a flood can be delayed because the inclination of a current can absorb the flood energy. The material along the banks of the stream is eroded and the flow of debris is affected by the effect of erosion. Thus, the thick deposits of saturated materials can be weakened with the result that the base of the slope has no support and hence, debris flows are caused (Calligaris & Zini, 2012).

Groundwater and Hydrological settings: The basic parameter for the instability of the slopes is the depth and the position of the underground aquifer. Besides, for the activation of debris flows the permeability of the formations is a key factor. When permeable and relatively impermeable formations come into contact, then there is an increase in pore water pressures which can cause slope failure as well as mobilization of debris flow (Nettleton, et al., 2005).

Meteorological Elements: Debris flows occur when there are many strong weather events in a short period of time. When the pace of penetration exceeds the intensity of rainfall, a saturated layer forms on the surface, causing a strong flow of surface water and the aquifer to rise to a critical point, or vice versa, when the rate of penetration exceeds the intensity of rainfall. Because a new system of forces is created as a consequence of penetration phenomena, the slope failure rate increases. More particularly, heavy rainfall, quick melting of snow and humidity are all factors that contribute to debris flows (Highland & Bobrowsky, 2008).

1.3 Factors affecting the start of debris flow

Debris flow is a rapid flow with a high amount of water and a scattering of grains throughout the depth, as has been documented numerous times. The manner that water is provided and combined with the granules shortly after onset is referred to as the mechanical interpretation of its onset.

The reasons attributed to the onset of debris flow are the following (Takahashi, 1981):

1. under certain conditions a landslide turns into a debris stream

2. A naturally constructed dam that controls a gully can collapse in a debris flow

3. With the appearance of surface water from heavy rainfall

Topography: Topography is one of the most well-known variables in the commencement of debris flow. A requirement for this is that the material is able to move. Fine-grained materials include sand and gravel while coarse-grained materials include coarse-grained materials with a wide grain distribution. Research has shown that topography appears to be a significant aspect in the starting process, although there is no single, sufficient, or necessary pattern for the debris flow to begin. (Klubertanz, et al., 2009).

Parameters of materials: The characteristics of the materials are another issue to consider while analyzing the onset of debris flows. Some researchers have focused on the shear strength of the material and others on the parameters of steady state and critical condition. Density, porosity, and plasticity index are some of the fundamental variables. Almost all field studies examine grain size distribution; however, there appear to be no common features for comparable flows and debris locations (Klubertanz, et al., 2009).

State of stress: The initial pressure state on the affected slope is considered by some, and the prestressing pressure is referred to as the influencing factor in this case. (Klubertanz, et al., 2009). *Water:* Water has an effect on the slopes' stability, as evidenced by its presence. When there is local inhomogeneity as well as highly porous layers, the stability is greatly impacted. Increased water pressure in the pores as a result of heavy rainfall, as well as variations in level, intensity, and other factors, all influence the commencement of debris flow. (Klubertanz, et al., 2009).

The commencement of debris flow is influenced by a number of other factors. In high alpine areas, for example, the occurrence of permanent frost has an impact on slope stabilization. The most common starting mechanism is due to water, and Takahashi (1981) studied the onset of debris flow under these conditions. Let us consider a thick uniform layer of loose non-cohesive grains whose slope angle is θ (figure 2). When the shallow depth water h_0 flow occurs, the pore spaces between the granules are assumed to be saturated, so a parallel flow occurs without excessive pore pressure. The characteristic distribution of shear stress in the bed should be like one of those depicted below; in which τ is the applied tangential stress and τL the internal resistive stress.
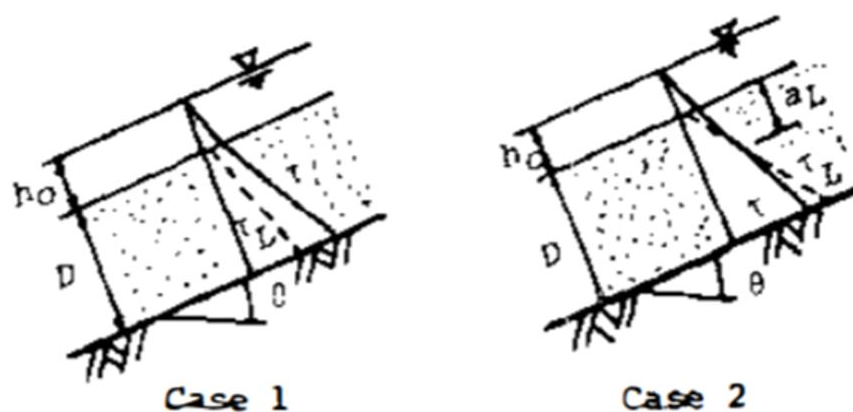
FIGURE 2 CHARACTERIZATIONS OF SHEAR-STRESS DISTRIBUTIONS

Case 1 in the figure is shown by the equations (2) and (3):

EQUATION 2: $\qquad tan\theta \geq \begin{cases} c * (\sigma - \rho) \\ c * (\sigma - \rho) + \rho \end{cases} tan\varphi$

in which c * is the concentration of granules by volume in the bed of static residues, σ and ρ are the densities of the granules and the fluid respectively, and ɸ is the internal friction angle.
When the second case occurs then

EQUATION 3: $\qquad tan\theta = \dfrac{c*(\sigma-\rho)}{c*(\sigma-\rho)+\rho(1+h_0 L^{-1})} \, tan\varphi$

which aL is the depth where τ and τL coincide.

As soon as the surface runoff occurs in the first example, the entire bed and the portion above the depth aL in the second case will begin to flow. Because static disequilibrium rather than the dynamic force of fluid flow causes this sort of bed instability, the flow should be referred to as sediment gravity flow. For the occurrence of sediment gravity flow the basic condition is aL;> d, in which d is defined as the diameter of the granules. If this condition is replaced in Equation 2 then:

EQUATION 4 : $\quad tan\theta \geq \dfrac{c*(\sigma-\rho)}{c*(\sigma-\rho)+\rho(1+h_0 d^{-1})}$

Even though the condition $a_L >/$ d is satisfied, when a_L is far less than h_o grains it cannot be uniformly dispersed throughout the whole depth of the flow due to the rather small colliding dispersibility. Therefore, a sediment gravity flow, which is appropriately called a debris flow should meet the condition $a_L >/k_{ho}'$ in which k is a numerical coefficient, determined from experiments to be about 0.7. Substitution of the condition $a_L>/k_{ho}$ into Equation (2) gives:

EQUATION 5 : $\quad \boldsymbol{tan\theta \geq \dfrac{c*(\sigma-\rho)}{c*(\sigma-\rho)+\rho(1+k^{-1})} tan\varphi}$

When equations (4) and (5) are satisfied simultaneously, a debris flow occurs. Attention is required in the first case where equations (4) and (5) are satisfied. Even if the seepage flow does not reach the surface, a grain bed that meets Equation (2) may slip. In such a case, in the neighborhood of the surface layer, τL would be larger than τ, and there the structure of the bed would be maintained. Rather than debris flow, this phenomenon should be referred to as a landslide. Thus, in such a steep permeable bed a landslide would occur before the increase of the leakage flow stage reached the surface of the bed.

After a landslide the pile of debris that has been caused has a smaller slope than the beginning on the slope of the mountain; it can therefore move with the appearance of surface water as a flow of debris. The time lag between the occurrence of a landslide and the removal of its deposition by creating a debris flow could depend on the water supply. In addition, sometimes it was difficult to recognize the transition between the two phenomena due to its brevity (Takahashi, 1981).

1.4 Distinguishing the methods of initiation

The methods of discrimination or prediction refer to basic elements of monitoring and initial identification in the area of possible formation, that is, in the source area of material that can provide important reports for early warning of debris flow disasters. Some of the tools used to monitor the flow of debris and early warning are the use of geophones, seismometers and other seismic monitoring facilities based on the ground amplitude, frequency and energy of the event. Furthermore, it was possible to distinguish the flow of debris from the flow of flood (Schimmel, et al., 2018). However, the latter method is very sensitive to the process of moving the debris flow. In addition, there is a limitation due to cost, noise and installation so it cannot be promoted in a large area. Furthermore, some researchers have tried to use lightning data from cloud to ground and available dynamic energy to correlate (Underwood, et al., 2016). However, this method was difficult to support due to the scale conversion.

There are three basic methodologies for distinguishing between the onset of debris flow where they are summarized in a safety factor already analyzed, the rainfall index method and the overall assessment method. The last two methodologies will be mentioned moving forward, but the material and technology of the sensors and the network communication are not included (Jun-Du, et al., 2021). Rainfall indicator method: For most debris flow events, rainfall, which is an external force, played a key role. It is the most popular method for monitoring debris flow ascribable to low technical limit and maintenance costs and its representative method is the power equation (ID method) proposed by Caine (1980) (Guzzetti, et al., 2007) (Caine, 1980) (Guzzetti, et al., 2008) .

EQUATION 6: $\quad I = \alpha D^\beta$

where I is the critical rainfall per unit time, which may be the maximum intensity (Cannon, et al., 2008) or the average intensity (Brunetti, et al., 2010), D is the rainfall duration; and α and β are the empirical calibration parameters, respectively. In the method, it is assumed that there is a non-linear relationship between the critical intensity of rainfall and its duration. With the first decreasing as the second increases. In practice two ways of the method are commonly used, the upper limit method and the lower limit method. In the upper limit method, the maximum intensity of rainfall is taken as a critical point, which cannot cause debris flow events at a specific time and place. On the other hand, the lower limit method takes as a point the minimum intensity of rainfall, which can cause debris flow events (Guzzetti, et al., 2007). Comparing the two, the upper limit method is a relaxed method and prone to failure alarm while the lower limit method is a conservative method and subject to false alarms. Depending on the empirical judgment and subjectivity, any interval value is taken as a crucial point (Jun-Du, et al., 2021).

In general, methods for determining empirical rainfall limits can be either of practical or statistical procedures (Guzzetti, et al., 2007). In terms of practical methods, they are based on the visual inspection of the point cloud representing the duration and conditions of heavy rainfall that have led to debris flows and drawing of a threshold line as a heuristic lower limit on the empirical data. Statistical methods allow the

determination of rainfall limits in a coherent framework and bring about thresholds that are reproducible and for which uncertainty measures are calculated. The uncertainty that concerns and affects the estimation of the intensity-duration limit is a result of the heterogeneity of the natural process and / or the uncertainty of the estimation of rainfall (Nikolopoulos, et al., 2014). To determine the ID limit, the intensities and durations of rainfall used are obtained through spatial estimation. When the estimation of rainfall properties is done according to the available rainfall measurements then there are errors in estimating the intensity and duration of rainfall at the debris flow sites. The sources of uncertainty in the spatial estimation of rainfall are related to (i) the density and geometry of the grids, (ii) the estimation procedures and (iii) the spatial variability of the precipitation (Nikolopoulos, et al., 2014).

1.5 Size classification of debris flow

The hazard assessment cannot be done using the debris flow volume (V) alone. Knowledge of this parameter alone is insufficient. For studies, it is important to know the maximum discharge (Q) and the area most likely to be flooded by debris (B). Debris basins are designed based on the debris volume variable. They aim to stop the flow of debris before it reaches an area. In addition, debris flow volume affects the discharge distance and the area covered by a debris flow. Flow volume, on existing models, is required as an input parameter (Matthias, 2005). Thus, the volume affects hazard maps or the intensity of the cash flow. This fact makes it a more reliable parameter than the mass. The entire volume of debris transported beyond a place of interest is referred to as debris-flow volume (usually the apex of a creek fan on which development occurs). It should be noted, however, that deposit thickness is often very difficult to determine (Matthias, 2005).

Peak discharge is used as an input variable for the design of bridges, culverts, pipeline crossings and channelization. It specifies the cross-sectional area required for flow passage (O'Brien, 2001). Peak discharge is the highest point on the hydrograph when the rate of discharge is the greatest. Below is a description of the size categories used. The volume estimates that reflect the total volume transferred from the top of the fan should be noted.

In the first category of debris flows, the volume is from 10 to 10^2 m^3. These occur in small channels or gullies where the material they carry is small and flowing downwards. Usually, these happen after a landslide or rock fall. Early deposition is encouraged by limited sediment supply, water scarcity, rapid drainage into coarse and permeable colloidal deposits, and finally, a slight slope. There is no smaller category than category 1 because debris flows with a volume of less than $10m^3$ are not of great interest. Mud is generally composed of water, clay, solid particles and organic matter. Colloidal ingredients work with water, for example, through ionized double layers (clay particles). This means that the behavior of the sludge can be quite different from the behavior of a forceless particle suspension with the same total solid concentration. More particularly, the muds are thick and have a non-Newtonian behavior (Coussot & Piau, 1994).

On the other hand, the debris flows belonging to the second category have a volume of 10^2 to 10^3 m^3. These occur in small creeks that are often limited in supply. When there is a limited supply, a recharging period is required before each debris flow event. In addition, they have a low frequency of activity. In contrast to unrestricted supply, basins, are controlled by hydro-climatic events because the provision of a sediment that can move easily is rarely a limiting condition for the occurrence of debris flow. Debris flows of this category can destroy small wood or brick buildings up to 20,000 m^2 in the catchment area as the maximum discharge reaches up to 30 m^3 / s (Matthias, 2005).

The third category with a volume of 10^3 to 10^4 m^3 produces debris flows in return periods of decades. They occur in non-volcanic catchments and when longer return periods are reported, it concerns unlimited supply channels (Matthias, 2005). This category of debris flows has peak discharges of up to 200

m^3 / s and the flooded area is 90,000 m^2. It is a catastrophic event but it is not easily recognized because the period of their return to small catchments <5 km^2 can occur after decades (Matthias, 2005).
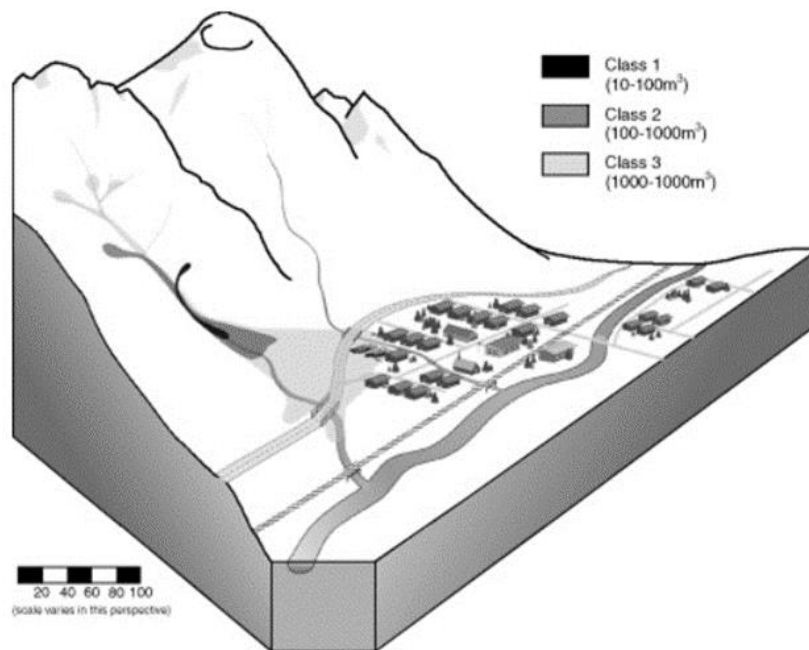
FIGURE 3 DEBRIS FLOWS IN CATEGORIES 1 TO 3 (MATTHIAS, 2005)

Regarding the rest, category 4 is related to category 3 only that debris flows refer to return periods of hundreds of years for limited supply catchments. Their volume is from 10^4 to 10^5 m^3 and only experts can identify them as a danger. With regard to catchments of 5 km^2 in category four, the ceiling of this category is the maximum that can be achieved (Matthias, 2005).

Category 5 debris flows, with a volume of 10^5 to 10^6 m^3, come mainly from volcanoes or areas with many sources of sediment. The more flexible flows are the ones of volcanic debris with high clay content and poorly developed or non-existent boulder front while the flows of sandstone debris with sandy clause are less flexible. These characteristics are responsible for the long runoff distance (Matthias, 2005).

Finally, the waste streams of category 6 have a volume from 10^6 to 10^7 m^3. Their maximum discharge is up to 30,000 m^3 / s as they can flood an area of up to 30 km^2. They erupt usually triggered by volcanoes by edifice flank or sector collapses, eruption-triggered snowmelt or subglacial melting or lake outbreaks. This category is responsible for thousands of deaths worldwide (Matthias, 2005).

There are also larger classes of flows, which are caused only by volcanoes. Examples are given of four additional categories that refer to the largest volcanic events (Γραμμένου, 2021). An example of a Class 7 waste stream is the one in Casita, Nicaragua in 1998 with a volume of 1.8×10^6 m^3. Examples of class 8 that have been studied are the Toutle River in 1980 with runoff flows of 1.3×10^7 m^3 and a maximum discharge of 68,000 m^3 / s to Mount St. Helens and the runoff in Huascaran, Peru (V = 1.3×10^7 m^3) in 1962, again in 1970 (V = 5 to 10×10^7 m^3) (Γραμμένου, 2021) (Fort, et al., 2010). Class 9 debris flows include the 4000-year-old BP event on Mount Meager, British Columbia with an estimated volume of $1-2 \times 10^8$ m^3 and debris flows into the Toutle River (V = 1.4×10^8)m^3, Q = 7200m^3 / s) at Mount St. Helens. Class 10 debris flows include the Osseola Mudflow with a volume of 3-4km^3 and a flow (0.25 km^3) at Mount Rainier. Debris flows, especially in the order of 7 to 10, if left unannounced can cause hundreds of deaths and destruction on a regional scale (Γραμμένου, 2021).

Debris flows in the last 20 years are some of the most harmful geomorphic processes in mountainous areas. They produce extremely large cutting-edge benefits with boosting processes. When a given channel receives a low frequency of debris flows, it is more dangerous because the amount of material is stored in time-limited channels that is proportional to the time period since the last debris flow (Matthias & Jordan, 2001).

The appearance of mudflows takes place both in nature and industry. Their main common feature is that they are more or less composed of a large number of natural fine particles, which are suspended in

water (Coussot & Piau, 1994).The concepts that describe them need to correspond to practical aspects of the problems. Between the flood and the flow of waste is difficult to distinguish based on the concentration of sediment due to their spatio-temporal change. The maximum flow observed is a good distinguishing feature during the phenomenon. The maximum flow of a flood is 2 to 3 times higher than a flood runoff. In addition, it has a shallow flow depth and has few catastrophic consequences. Unusually catastrophic water release events from basins are an exception (Matthias & Jordan, 2001).

1.5.1 Debris flow starting from a slope

In this case, debris flows down a slope, including small streams and hollow landfills. They are driven by external forces such as rainfall etc. Experiments and research have shown that slope debris flows begin with the process of softening, cracking, and creeping of loose material and failure. Subsequently, slope failure develops into local collapse as well as liquefaction under constant shear stress. Next, the forces have the ability to expand into the surrounding areas and eventually to the onset of debris flow (Gabet & Mudd, 2006). Slope materials could also be converted to debris flow without collapsing or slipping processes. Many case studies have revealed that rainfall of 10 mm/h or less can produce landslides and debris flows in some regions (Jun-Du, et al., 2021). The two most important characteristics for initiating the flow of debris are the composition of the granules and the porosity of the loose materials. The porosity and permeability of the soil layer are determined by the granule composition. By increasing the fine content of the soil, the porosity of the soil is reduced, and the permeability coefficient or hydraulic conductivity of the soil layer is reduced. As a result, low rainfall intensity may surpass the critical point for soil saturation, resulting in an increase in water pressure in the pores and a decrease in effective stress, for example (Jun-Du, et al., 2021). It turned out that the larger volume of fine particles did not necessarily trigger the onset of debris flow. When it reaches a critical point, corrosion occurs (Zhou, et al., 2018). In addition, the clay or sand content can also contribute to the effectiveness of initiating debris flow and the sandy soil has higher water permeability which helps to reach the critical point faster (Gabet & Mudd, 2006).

According to the critical state theory of soil mass (Casagrande, 1936), under the action of continuous shear stress the soil mass can reach a critical porosity through expansion or contraction, regardless of whether its initial state is solid or loose. If the initial state of the soil is loose then the high porosity can lead to a huge positive pore pressure during the shrinkage process and thus will increase the chance of debris flow (Gabet & Mudd, 2006). During soil deformation, continuous expansions and contractions frequently occur, resulting in a dynamic change in soil porosity, which influences the water content and the pressure of the soil pores. As a result, the importance of porosity is represented more in its water storage and pressure conduction capabilities, as well as in the changes in soil stress state that ensue (Jun-Du, et al., 2021). Criterion Mohr-Coulomb refers to the shear strength of the soil mass, which is determined by the effective stress and cohesion. The criterion can also be used to interpret slope instability and debris initiation processes. To the traditional type of shear strength was added the effect of pore water pressure and pore air pressure and a type of discrimination was proposed to judge whether loose material

started or not. The First typical formula on initial discrimination of debris flow and erosion rate (equation 7) (Jun-Du, et al., 2021) :

EQUATION 7: $$K = \frac{(\sigma - Uw) * tg\emptyset + AC}{T + Gsin\beta}$$

Where A is the basal area of interface; G is gravity of loose material; T is the shear force of flow; β is the slope; σ is the total normal stress; Uw is the pore water pressure; C is the cohesion of loose material and Ø is the internal friction angle

The basic idea of this type (table 3) is that with the continuous inflow of rainfall the matrix aspiration of the loose material decreases as the water content increases and the result is the reduction of the shear strength. When the loose material is saturated and the shear strength is less than the tangential stress produced by the flow and gravity then a debris flow will occur (Jun-Du, et al., 2021). After saturation, the possibility of liquefaction and conversion of the material into debris flow may increase sharply, but soil saturation is not necessary for the existence of debris flow (Iverson & Vallance, 2001). Because the above have some limitations, some researchers have proposed the so-called pulp generation theory and the soft-base phenomenon of landslide conversion into debris flow (Jun-Du, et al., 2021). Two landslide liquefaction mechanisms have been proposed which are converted into debris flow by Iverson et.al (1997a) and Iverson and Vallance (2001) (Iverson , et al., 1997) (Iverson & Vallance, 2001).

One mechanism was that liquefaction happened in a soil mass with little cohesiveness when the pore water pressure reached the value of total normal stress, i.e. the effective stress decreased to zero. The other mechanism was that, in order to liquefy a cohesive soil mass, it was necessary to diminish the cohesive force via vibration in addition to maintaining a high level of pore water pressure. The fundamental reason of a landslide evolving into a debris flow was an increase in pore water pressure, which was primarily produced by soil contraction and continuous water delivery. However, earthquakes or movement on a rocky slope were the primary causes of soil mass vibration, that is, the conversion of kinetic energy into heat energy of soil particles. The author realized the mathematical simulation of the entire process of landslide debris flow and reproduced the beginning processes under the two liquefaction mechanisms in solid model tests using the Coulomb grain flow equation (Iverson, 1997b) (Iverson, 1997b).

1.5.2 Debris Flow starting from a Gully or Chanel

This phenomenon refers to the onset and movement of debris flow that occurs in streams or canal beds. It is formed either by the corrosion of the bed materials or by the entrapment of collapsing materials of the bank caused by continuous lateral corrosion. It has great diversity in material sources and growth forms and the growth environment has a lower requirement for canal slope due to the effect of water flow. Therefore, research on the onset of gully debris flow provides a strong basis for the relationships between

discharge, channel slope, and grain composition of loose materials. The critical discharge is thought to increase as the particle size increases (Jun-Du, et al., 2021):

EQUATION 8: $\quad q = Cd^{1.5}$

Where q is the minimum surface discharge per unit width; d is the specific particle size and; C is an empirical coefficient

However, it has been pointed out that the dynamic energy provided by the slope of the channel must also be considered taken into account. If the slope of the channel is small and the particle size is large, then motion of the bed load can develop in case the discharge is large. The empirical relationship between the critical slope and the median diameter of loose materials in the debris flow process formed by flow cleaning has been established (Jun-Du, et al., 2021).

EQUATION 9: $\quad Jc = 0.024d50^{2/3}$

Where, Jc is the critical slope for debris flow initiation; d_{50} is the median particle size of loose material

By placing an almost homogeneous layer of gravel in the pipeline with an inclination of 12 to 20 °, Gregoretti and Fontana (2008) conducted an experiment and summarized the rule of critical evacuation of the onset of stream debris flow under different particle sizes and inclination conditions (Cregoretti & Dalla Fontana, 2008). The result was used to estimate the critical discharge of debris flow events caused by erosion in 6 catchments in the Dolomites of Italy.

EQUATION 10: $\quad q = \dfrac{0.78d_M^{1.5}}{\tan(\theta)^{1.27}}$

Where d_M is the mean grain size of the debris material; Θ is the bed slope and; Q is the minimum surface discharge per unit width

In addition to the process research represented by the above achievements, that is, summarizing empirical or semi empirical relationships through solid model experiments, researchers also tried to further expand their knowledge from mechanical or energy level (Jun-Du, et al., 2021).

EQUATION 11: $\quad E_c = \gamma_s \, C_{vd} J > 0.01$

Where C_{vd} is the volumetric concentration of pebble in the mixed flow front; J is the slope; γ_s is the bulk density of solid; E_c is the critical energy for debris flow initiation from solid particles

EQUATION 12: $\quad F = [\dfrac{C*\rho_s - p_f}{(C*p_s - p_f + \rho_f \quad 1+1)} / k] \, \tan\text{Øs} / \tan\beta$

Where c* is the volumetric concentration of solids; ρ_s is the fluid density; K is related to the ratio solid depth and flow height; Øs is the effective static angle of internal friction and β is the slope angle

Takahashi (1978) developed a model to calculate the critical slope of the gully debris flow based on Bagnold's granular flow theory. The assumption was that in an infinite slope of the ravine the loose material after being soaked by the flowing water reached a state of saturation and then failure and flow of debris due to the excessive shear stress occurred (Takahashi, 1978). Blijenberg (2007) provided the safety factor version of the model as he applied it to the Alps in southern France (Blijenberg, 2007). The results of the model were conservative because even in cases where only extreme rainfall could provoke debris to flow, the cases would still be considered unsafe (CUI, et al., 2017).

It was pointed out that the loose materials of this model can be rinsed from the water flow before the failure. Therefore, there was an overestimation of the critical slope. Models based on the granular flow theory were considered unsuitable for gully debris flows because the debris flow process was far from equilibrium (Iverson & Vallance, 2001) (Jun-Du, et al., 2021).

A discontinuous feature exhibited by gully debris flows looks like a wave because loose materials erode and drift (Iverson & Ouyang, 2015). At the front, the eroded materials are collected, which due to the collision of the particles give energy so that the front can move in the channel with a gentle or even reverse slope. Erosion and entrainment are important factors in the development of stream debris flow. Studies have shown that there is usually an increase in the scouring depth of the riverbed as the canal slope, flow depth, discharge, basal shear stress, front water content and particle size increase (Theule , et al., 2015) (Haas & Woerkom, 2016). In addition, the theoretical analysis showed that when the density of the mixed layer was distinct from that of the riverbed layer then during the entrainment process volume changes in the eroded material and pore water pressure may affect the rate crawling as a result of feedback effect (Iverson, 2005). Eroded material is more likely to be swept away by runoff because it has low cohesion (McGuire, et al., 2017). Before the riverbed materials are converted into debris flow, there must be material exchange, energy transfer and rheology during the erosion, deposition and entrainment processes. However, corrosion and entrainment phenomena are considered uniform when calculating the erosion or entrainment rate even though they are two different phenomena (Iverson & Ouyang, 2015).

The relationship between the drag rate and the process of super concentrated flow being converted to fragment flow using arithmetic models has been demonstrated through several studies. These models according to the specific rheological law and the theory of continuity were usually presented in the form of a single-phase / two-phase depth-medium / integral model that connects the type of drag rate. (Gregoretti, et al., 2019) (Gregoretti & Dalla Fontana , 2007) (Zhou, et al., 2019) (Stancanelli, et al., 2015).

1.6 Deposition and morphology of debris flow

In order to be able to delimit and understand the area that can become endangered by a debris flow, the mechanisms of its deposition and its morphology must have been understood. As already mentioned, debris flows are catastrophic in nature causing great damage. Therefore, it is important to understand their deposition and their morphology for mitigation. In practice, debris flows are accelerated in a channel and the coarse-grained materials of which it is composed, as they move, are separated. This means that the coarse material moves forward and is followed by a saturated body of fine material. The flow head is thicker than the body and the tip of the flow. Near the head of the flow, the sediment deposits lose momentum causing the sediments to be removed from the flowing debris to form lateral mounds, which are a lateral levee on the flow. Where the coarse material is deposited, the lateral levees are steeper (Johnson, et al., 2012) (Zhou, et al., 2018). As the deposition process takes place in transient surges, the kinetic energy of the flow is diffused through longitudinal and lateral propagation (Zhou, et al., 2018).

According to the experiment conducted, Zhou et.al, it is concluded that when the mixture has a low water content its mobility is low. In addition, the lateral mounds are less visible as the particle size separation was less. In contrast, mixtures with higher water content had more pronounced lateral mounds. Moreover, when there is high water content, the flow heads are driven further along the outflow plane within the boundaries of the lateral levees. The advancing flow head and lateral levees are thicker than the central channels (Zhou, et al., 2018).

CHAPTER 2

2.1 Slope Failure and stability analysis

The elements that influence slope stability are numerous, and nearly all of them are linked. Meteorological occurrences (or rather, the consequences generated by them) are the most important of those, both as predisposing variables and, more importantly, as triggering factors. Rainfall has a wide range of effects on landslides, depending on the size, kinematics, and type of material involved. Shallow landslides are usually caused by short, severe storms, whereas most deep-seated landslides are caused by long-term variations in yearly rainfall over several years. There is no exact correlation between rainfall and landslides such as rock falls because they appear to be more sensitive to other factors such as chemical–mechanical weathering of the rock mass and temperature fluctuations above the freezing point (Sandersen, et al., 1996): only late spring and summer rockfalls can be linked to rainfall. Based on the foregoing, it is concluded that no crucial rainfall conditions exist for every type of landslide (Aleotti, 2004).

The failure of natural or artificial slopes manifests itself in the form of a landslide. As already referred to, landslides are the movements of soil and rock masses, which take place on natural surfaces with steep slopes and on the slopes of ditches, under the influence of gravity, which exceeds the frictional resistance for downward movement (Μπούνου, 2012). The term landslide includes the entire range of slope failures, such as landslides, caps and falls, while the term landslide includes only the rapidly occurring movements of soil masses (Μπούνου, 2012). Landslides occur on account of the shear failure of the soil, along a surface in the soil mass, due to the equation of the total available shear strength with the imposed, natural or exogenous shear stresses. In all rock and terrain slope stability solutions, the general equilibrium condition is that the holding forces or torques must be greater than those of the slip.

The safety factor is defined as the ratio of the forces that resist sliding and are due to the shear strength of the ground, to the corresponding forces that contribute to the instability of the slope causing it to slip (Λουπασάκης, 2013-2014) (Μπούνου, 2012). Thus, the safety factor is equal to the ratio of the shear strength of the soil to the shear stress that affects it. It is used to provide a design margin relative to the theoretical design capacity in order to allow uncertainty in the design process. The principle of marginal equilibrium is intended to examine the conditions prevailing on a slope under conditions of marginal equilibrium, i.e. SF=1 (Λουπασάκης, 2013-2014). If the safety factor is equal to the unit then the slope is in a state of marginal equilibrium. When the safety factor becomes less than the unit, then the slope fails (Highland & Bobrowsky, 2008). The stability of the slope increases, as there is an increase in the safety factor above the unit as there is an increase in the shear strength of the ground. A slope is considered ideally stable when the safety factor ranges from 1.4 to 1.5. Higher prices than these in constructions are at risk of instability. There is the calculation of immediate and long-term stability (Μπούνου, 2012).

The safety factor is determined by the following methods (Μπούνου, 2012):

1. Empirical method where geotechnical engineers based on history, experience, regulations select the appropriate factors that are highly valued to address slope stability

2. Conventional analysis such as the marginal equilibrium method where it is considered that the ground is in a state of failure adopting a continuous sliding surface with the failure criterion prevailing along its entire length and

3. Numerical methods where they are mostly used in solving geotechnical problems. A key factor is the analysis and simulation of complex geometric problems and field conditions, such as the presence of faults, simulation of excavation and support phases, effect of pore pressure, etc.

For the calculation of the immediate stability, the parameters of the shear strength are calculated, under unstable conditions, and the changes in the water pressure of the pores are ignored. On the other hand, for the calculation of long-term stability, the parameters of shear strength are calculated, under dripping conditions or under non-dripping conditions, where the pore water pressures are recorded (Λουπασάκης, 2013-2014). In addition, coherence refers to the gravitational forces exerted between the soil grains so that the strength of a soil material is proportional to that of solids. Cohesion in soil materials depends on the water content, density and plasticity of the soil. Internal friction is expressed by the angle of mass deposition of the soil material and its magnitude depends on the vertical load on the slip surface.

2.1.1 Forms of failure

Fall failure: occurs when sections of rocky material or hard soil material peel off abruptly from a steep slope and then fall freely into the gap or bounce and slam on the slope. These detachments appear on steep slopes and are the result of cooling-heating of the soil, soil disturbance after an earthquake, soil saturation in water due to rainfall and weakening of the soil due to the increase in the size of the roots of the vegetation (Μπούνου, 2012).

Failure tilting: refers to the overturning or alternation of soil layers or loose sections of rock, from a steep slope. The material rotates over a central point forward. The center point is located below the center of gravity of the segment with the lowest point. Prerequisite for this failure are the dense, steeply intersecting discontinuities, which slope away from the slope surface (U.S. Army corps of engineers, 1994).

Fall and tilting: failures differ in the breaking mechanism but are a warning of a larger failure. These two types of failures begin with the separation of the layers towards the free surface of the slope or the excavation surface due to the weight of the suspended volume where the instantaneous separation occurs or due to environmental processes, which compose the gradual separation of the layers (Abramson, et al., 2002).

Slip failure: Refers to a tumor that slides along a single discontinuity. A basic condition for its appearance is that the line of discontinuity is parallel to the slope and the slope of the sliding surface is less

than the slope and greater than the angle of friction. When the slip is flat then the coherence is equal to 0 (c=0) (Μπούνου, 2012).

Failure wedge: this failure describes to rock slopes. The wedge is formed by two levels of discontinuities and occurs when they intersect almost perpendicularly in the direction of the slope and incline towards its plane. The basic precondition here is that the intersection of the planes of the discontinuities passes through the level of the main front of the slope so that the detachment of the wedge-shaped piece can be done (U.S. Army corps of engineers, 1994).

Circular failure: This concerns the slopes, in strongly decomposed rocks. It generally refers to formations with low coherence or formations, which are penetrated by groups of dense discontinuities. The failing material moves on a circular or curved failure surface (Μπούνου, 2012).

Depending on the area affected by the failure surface, circular failure is classified into three categories (Abramson, et al., 2002).

1. Face failure: In this category, the arc of the ruptured surface meets the slope above its foot. This happens in case the slope angle is large and the ground near the foot has high strength.

2. Foot failure: Here the arch of the ruptured surface meets the slope at its foot.

3. Base failure: Here the arc of the ruptured surface passes under the foot of the slope and at its base. This happens when the slope angle is small and the ground beneath its base is softer and more plastic than it is above its base.

2.1.2 Factors influencing the stability of slopes

Landslide damage is due to increased soil sensitivity to stability because of overexploitation of natural resources, deforestation, and the development of urbanization. In addition, areas that are not inhabited, such as mountains, are used as places of entertainment, thus increasing the problem. Another important factor is the climate change and extreme weather conditions. The slope failures are due to natural and man-made factors and can have adverse effects on the economy due to the destruction of settlements and technical works. Thus, two categories affect the stability of the slopes, namely the natural and the artificial.

Physical agents are classified into five categories (Washington, 1984).

1. Geologic/Geomorphic factors: Specific soil containing weak or soft rock composition, undesirable structure and adverse bedding sequences is predisposed for the movement of soil mass. The types of rocks that are weaker are a result of severe weather conditions and the relative strength of the material. There is a possibility sedimentary, as volcanoclastic rocks will turn into clay-rich soils due to high rainfall, and they are prone to soil creep and earthflows.

Rock structures are an important factor for the stability of natural slopes. Descending levels downhill between some sedimentary and volcanic rocks of different capacity or deterioration, as well as

joints and cracks oriented in the same direction, may prevent vertical and root penetration, thus acting as potential levels (Washington, 1984).The bedding whether it is horizontal or cross-linked can act as a natural support and help with stability.

Fracture zones contain broken or deformed rocks, which result from the stresses exerted. Their weakness is enhanced by water penetration and chemical corrosion. In general, low cohesion formations move more easily downwards than rock formations. In addition, the arrangement of the soil layer or discontinuity with respect to the orientation of the slope and the degree of fragmentation of the material affect the potential for failure.

2. Slope shape: Slope inclination is an important feature in determining the distribution of water in unstable soils. Groundwater is dispersed when the slopes are convex and tend to be more stable than concave slopes, where the latter collect groundwater in small areas of the slope. After failure, the cavities are filled with localized sloughing around the headwall soil creep, and movement of organic debris and surficial material from above (Washington, 1984). Therefore, the soil with depressions tends to be thicker and thus increases the chance of failure. Recurrence of failure occurs when cavities are overloaded with mineral and organic debris in combination with storms and melting snow. The frequency of these is tens to hundreds of years depending on the filling rates and the processes that take place in specific locations.

3. Soil properties: Shear strength (s) describes the resistance of the soil to failure. It is considered a function of the normal stress on the slip surface (p), cohesion (c') and internal angle of friction. The unit weight and density of the soil in moisture content, soil depth and slope are affected by stress. At the failure surface, the pore water pressure reduces the normal voltage to an effective normal voltage acting as a buoyancy. In addition, an important factor for the stability of cohesive soils is the effect of clay mineralogy. However, the mineralogical and chemical properties are not solely responsible for slope failures but act in conjunction with other factors that strongly affect slope stability (Washington, 1984).

4. Hydrological factors: Rainfall and snowmelt significantly affect the hydrological processes, the rate of water entering the mantle, its rate of transmission as well as evapotranspiration. When water penetrates the soil layers of a slope, the internal friction and cohesion are reduced and finally the shear strength of the materials and, therefore, their slip resistance. The same is true of groundwater aquifers. They enter through cracks in the layers of a slope resulting in the reduction of the active voltage and the degradation of the shear strength (Μπούνου, 2012).

5. Seismicity: Strong ground vibrations disrupt and cause loosening of soil materials resulting in soil failure (Μπούνου, 2012). The factors on which the induction of landslides due to vibrations depends are the slip masses, the vegetation, the land use, the orientation of the possible failures in relation to the epicenter of the earthquake, the direction of the seismic propagation of the waves, its magnitude seismic depth, seismic wave attenuation and aftershock distribution (Washington, 1984).

6. Vegetative factors: Plants are also a factor in the stability of the slopes. They contribute to stability because their roots add strength to the soil by anchoring it vertically through the mantle of the soil. However, this mechanism only works in fine soils (Washington, 1984). Finally, the temperature can cause the rock to crumble through contraction-expansion. As the temperature changes from hot to cold, the strength of the formations decreases.

Artificial Agents are classified into the following categories (Μπούνου, 2012):

The construction of phase, through excavations in the natural ground at an angle, by filling over the surface of the natural terrain at an angle, by strengthening surfaces, keeping the upper levels with retaining walls, changing the level of the aquifer, interrupts the natural cycle of change in nature. Therefore, the stability of a slope is likely to be affected by anthropogenic short-term or permanent changes.

1. Construction activities: A slope can lead to states of instability and failure because the slope of the ground surface and the geometry of the slope are changed through earthmoving processes in the context of trenching.

2. Additional loading (embankments, other infrastructure): When additional loads occur near the slope, the forces for landslides increase.

3. Abrupt reduction of aquifer / tank level: When the level of the aquifer decreases sharply, the pores cannot relieve the pressures that exist resulting in the reduction of the shear strength and thus a failure occurs.

4. Vegetation cover: It is known that hydrophilic trees have deep roots and can retain soil materials by limiting the action of water. Consequently, forested areas, which are continuously deforested, lead to failure. It is important that the cracks in the rock formations increase due to the intense erosion but also the extensive tree cover at an inappropriate slope.

In conclusion, the natural slopes, if deemed necessary, should be strengthened. Safety in combination with quality and economy should be considered. In order for this process to take place, the geological characteristics of the study area, the location of the groundwater, the seismic activity must be considered, in order to be able to prevent and deal with the failures that may occur (Μπούνου, 2012).

2.2 Characteristics and failure mechanisms of debris flow

Debris flows consist of fine-grained and coarse-grained materials in which there is a variable amount of water. The resulting mixtures flow under the influence of gravity downwards as a thick mass. They are very destructive because they cause intense erosion in the soil on which they flow. As the sediment charge increases, so does their erosive capacity. Their speed is directly related to the intensity of the risk. Debris flows can reach extremely fast speeds as the density and rapid movement of materials lead to a mass with significant energy (WLI, 1995) (Winter, et al., 2005). Debris flows are easy to identify in the field. Usually when a tilt failure is reported it means the source area on the side slope of a stream channel. Slope failure is referred to as a physical shallow slide or rockslide or man-made filling failure. The streambed is unstable, especially when there is extreme discharge. The characteristics of the area where a debris flow occurs are the steep slope, many loose materials, water and vegetation (Calligaris & Zini, 2012). Sometimes a kind of landslide starts at a fast speed where as it moves downwards a mass motion is produced which resembling a flow. Saturated materials can increase the volume and therefore saturation, too. In many cases, debris flows enter existing flow channels and continue to flow. The characteristics of debris flows, however, vary when debris and water are added during the flow and thus there are chances of changes in the nature of the flow. It has been observed that debris flows in surges or pulses of materials, which separate the flow. This means that changes are made in the characteristics of the liquid. In addition, flow transformations along a path are frequent as a function of changing hydraulic conditions as well as the distance from their source (Skilodimou & Bathrellos, n.d.). A debris flow path is divided into initiation zone, transport zone and deposition zone.

The initiation zone is a ground failure at the top of a slope or at the top of a torrent, stream, and so on. This instability can have the character of a shallow landslide in debris, which is transformed into a debris layer. Furthermore, it may be a failure of a man-made embankment or a natural rock slide.

There are cases of high flow so the debris flow starts directly through the riverbed. In general, a large morphological slope from 20° to 45° characterizes the ignition area of the waste stream (36% to about 100%).When the slopes have a smaller soil slope then there is not enough dynamic energy to start the failure of the granular soil. Slopes, which are characterized by a steeper slope, have a ground cover that is thin or discontinuous enough for the presence of slipperiness. The volume of the initial slip varies, that is, a few tens of cubic meters is enough to start a large debris flow. Otherwise, a runoff could be the final release phase of a major landslide or rock fall (Λέκκας, et al., 2015).
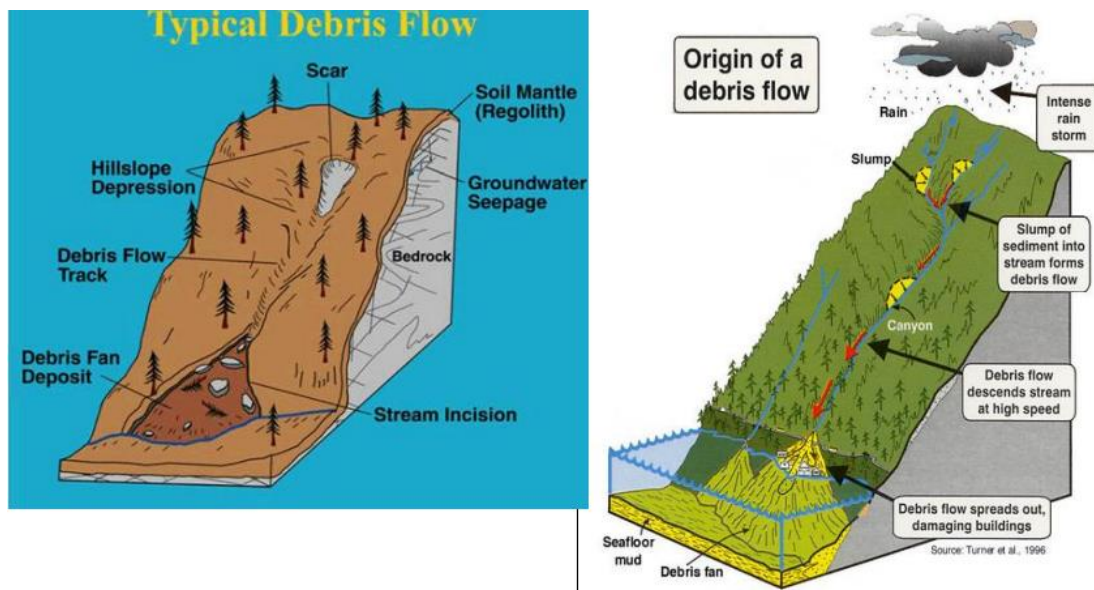
The front part swells as it carries most of the boulders while the back part contains more water and the grain sizes are obviously smaller compared to the front part. These characteristics are given so far by further studies such as Schlumberger (1882), Blackwelder (1928), Sharp & Nobles (1953), Curry (1966) and Johnson (1970), which give similar results. They show differences in the distribution and concentration of the grains and in the shape of the passage path such as width, inclination, and so on. Therefore, they present a great variety in their velocities. The observed velocities are between 0.5 m s $^{-1}$ and 20 m s $^{-1}$. In addition, the volume densities vary from case to case. The densities reported are from 1400 kgm^{-3} to 2530 kgm^{-3} and these are equivalent to a solid material volume concentration of from about 25% to 70 or 80% respectively. Debris flows are often referred to as mudflows but as can be seen the normal debris flow contains a smaller amount of fine particles. The results of mechanical analysis of sediment samples showed that less than 20% of the pieces are thinner than the size of the mud and only a few percent are thinner than the clay while on the other hand huge stones are more often transported.

A geographical feature is the alluvial cone or debris cone, which is created by deposition at the mouth of a canyon. There are cases where the material does not spread across the width of the cone or the valley. In these cases the distal end of the deposit retains its lobed shape. Based on the available data, the occurrence of debris flows occurs in sedimentary beds in mountainous areas where their slopes are steep from 15° and rest on plains or gorges whose slopes are larger than 300. However, the fine particles have the ability to transport in flat positions as a suspended load (Takahashi, 1981).

2.3 Elimination of weak mattresses and possible failure zones

The stability of the slope increases if there is a reduction in weight from the head and extension of the toe, thus reducing its inclination. If, for example, 4% of the sliding volume is removed from the head to the foot of the slope, then there is a 10% increase in slope stability. Care should be taken to remove the material from the head so as not to upset the balance in this part and not to spread the phenomenon of failure. Smoothing of failure areas must be designed at the same time as the slope is drained, so that excavation materials can be placed at the foot of the slope for stability. In terrestrial formations, the maximum slope is generally set at 2: 1 (height to base) (Μπούνου, 2012).

2.3.1 Construction of support structures or other supports

The construction of the support works aims to increase the stability of the slopes or to stabilize the landslides. Their construction cost is high because these constructions accept large loads. Some of these support structures will be mentioned just below.

Retaining walls are usually used to stabilize slopes when cutting or filling is required and there is insufficient space or right of passage except for slope. Retaining walls are structures that are made at the base of the slope as their foundation is made in depth depending on the sliding surface. In general, they are distinguished into rigid and flexible (Abramson, et al., 2002). Rigid retaining walls are made of reinforced or non-reinforced concrete structures. Their shape and properties vary depending on the loads they are to be subjected to. On the other hand, flexible retaining walls withstand retreats because they tolerate large lateral loads before deformation and failure. Their cost compared to rigid retaining walls is lower and they include the wire boxes, the reinforced ground walls and the pile walls. The advantage of the application of the wire boxes is that they contribute to the drainage of the soil due to their structure and, ensuring low pore pressures and therefore low ground pushes (Μπούνου, 2012). In cases where the failures are deep, the drilling of injected piles with a diameter of 1.5 meters in a row is chosen as a stabilization method, to create a wall, which rests at a great depth and below the sliding surface of the slope but also for the best support of the pile. This method is chosen in difficult support conditions due to the high cost of construction (Abramson, et al., 2002).

2.3.1.1 Soil Reinforcement

As for incoherent soils, in order to achieve stabilization and increase cohesion, some techniques are applied that will be mentioned below (Abramson, et al., 2002) (Μπούνου, 2012).

2.3.1.2 Reinforcement with cement injections

In this case, grout is pressed from cement, water or other chemical admixtures in order to fill the weakness zones on the slopes. It is one of the techniques of mechanical stabilization of the slope but the drilling of the concrete injection holes should be done deeper than the point where the weakness of the ground has appeared in order to achieve better possible results (Abramson, et al., 2002).

2.3.1.3 Reinforcement with anchors

It concerns soil reinforcements with nails for its stabilization. The reinforcements are made in different ways depending on the soil conditions (Μπούνου, 2012).

Passive nails: The use of passive materials is applied since the opening around the rock receives significant shear or tensile stresses. They are applied in rocky and cohesive soils. The stages of their installation process are the drilling, installation and anchoring by injection of cement grout of steel or metal perforated bars Φ25-35mm or metal pipes and they resist the stresses resulting from the movements of the slopes (Σοφιανός, 2015).

In addition, the surface reinforcement and smoothing helps to stabilize the surface to be drilled, having a reinforced structural mesh and a layer of shotcrete up to 15 cm thick. The reinforcement of incoherent soils is carried out with self-drilling anchors, where they form the drilling stem and remain within the soil mass (Μπούνου, 2012).

 However, in case of unsafe soil mass, the reinforcement is done by drilling prestressed anchors. These consist of long ropes. For their prestressing after anchoring, a stress distribution beam is made of reinforced steel or reinforced concrete (Σοφιανός, 2015) (Μπούνου, 2012).

There are temporary anchors that operate for less than 2 years and permanent anchors operating throughout the life of a structure.

The parts that make up the anchors are:

- the anchored part, which is the part of the anchor that ensures the anchoring to the ground by means of the cement injection.

- the free part, which is the part in which the reinforcement extends freely during prestressing,

and,

- the anchor, which is the mechanical part that ensures the application of the prestressing force (Μπούνου, 2012) (Σοφιανός, 2015).

CHAPTER 3

3.1 Landslides in Greece

Greece has undergone great geophysical development due to the orogenic cycle. Many geotectonic zones or areas are distinguished based on fundamental differences in lithology and structural evolution. These zones have an elongate shape that coincides with the main mountain ranges, representing distinct tectonic units. In places, these zones are separated by major thrust boundaries or transitional belts (Koukis, et al., 2005).

In the eastern Greece, the age of some lithological formations range from the Paleozoic to recent, including metamorphic and older or juvenile igneous rocks. The western and central Greece is mainly composed of the external geotectonic zones. They are characterized by the presence of strong E-W tangential tectonic movements. As a result, W-ward ductile thrusting and intense folding and fracturing of the alpine formations is observed. Post-alpine Neogene sediments were deposited into trenches in response to neotectonic activity. A fundamental factor of a landslide ,is the weakness of the lithological formations of the outer zones. The landslides that occurred in the area are directly related to the active tectonics of the ongoing faulted grabens. Heavy rains and earthquakes are responsible for such instability phenomena, contributing to the shearing, and erosion of the alpine basement rocks and the post-alpine sediments.

A landslide hazard map of the Greek area was established by koukis et.al (2005), regarding the number of phenomena per 100 square kilometers. The map shows that most of such landslides events are concentrated in the Pindos mountain range in the northern and western Peloponnese as well as in Pieria, Pelion, Evia, western mainland Greece and Crete (Koukis, et al., 2005).
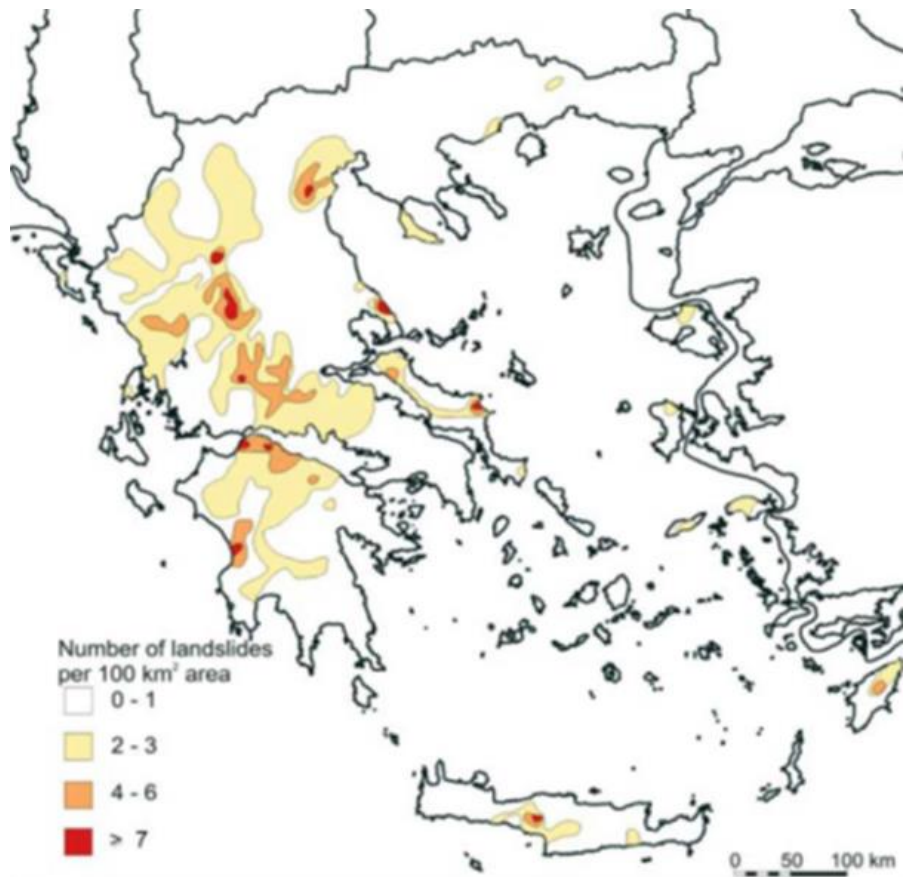
FIGURE 6 MAP OF LANDSLIDE DANGER ZONES IN GREECE (KOUKIS, ET AL., 2005)
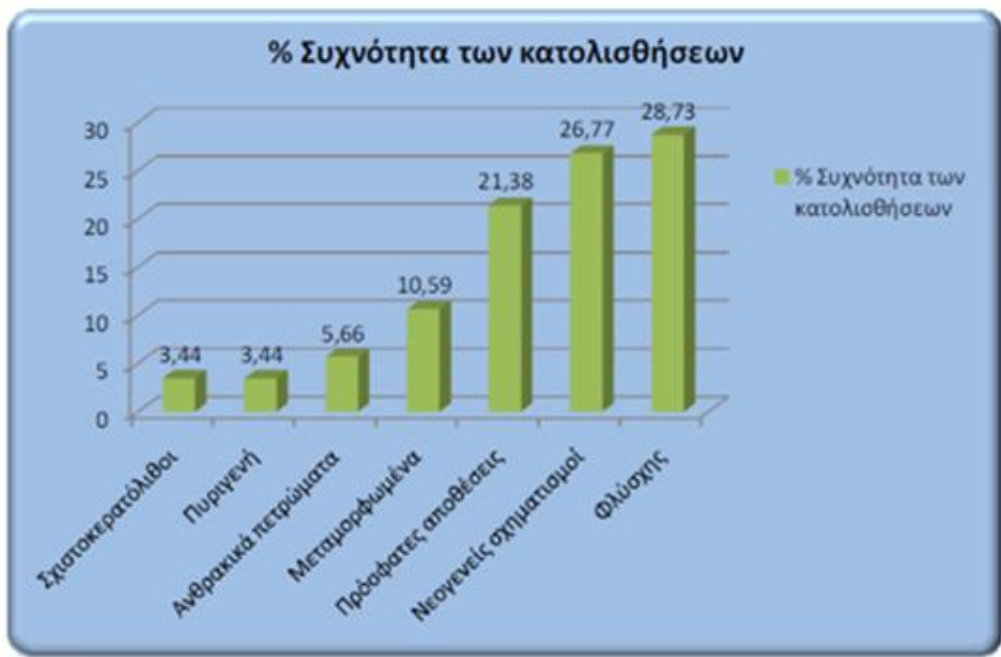
3.2 Study Area

The study area is located in western Attica and more. Specifically, in the eastern and southeastern foothills of Mount Patera of the central Greece. Within an area of 3,808 km^2, Attica is the most densely inhabited region. Many industrial entities, such as ,factories, shipyards, and landfills, may be found in western Attica. This industrial zone is included in Thriasio Plateau area covering a total range of 812.95 km^2 (Vallas et al. 2018). The area of Mandra is located in the western part of the Attica prefecture with an area of 426.2 square kilometers and a total population reaching 17,885 inhabitants (Diakakis, et al., 2019). Generally, the city is located at the top of an alluvial fan. From the western sideof the Thriassio plain, two streams are joined together to form a main stream that runs into the Gulf of Elefsina. To the west ,Mount Patera with an altitude of 1016 meters found, while to the north and east ,the Parnitha mountain of 1413 meters altitude and the 468 meters Egaleo mount are observed, respectively. Environmental pressures have insensately due to the strong land changes such as the existence of industries and urbanization. As a result, the number of floods has been increased. There was no appropriate flood protection and drainage collection plan in the area.

More specifically, in November 2017 a great disaster affected the Mandra city due to a catastrophic flood. Mandra is located 40 kilometers west of Athens with about 13,000 inhabitants and belongs to the industrial cities that has shown a significant increase in recent decades (Vallas et al. 2018). Furthermore, the plain is crossed by two highways, built parallel to the coastline (Diakakis, et al., 2019).
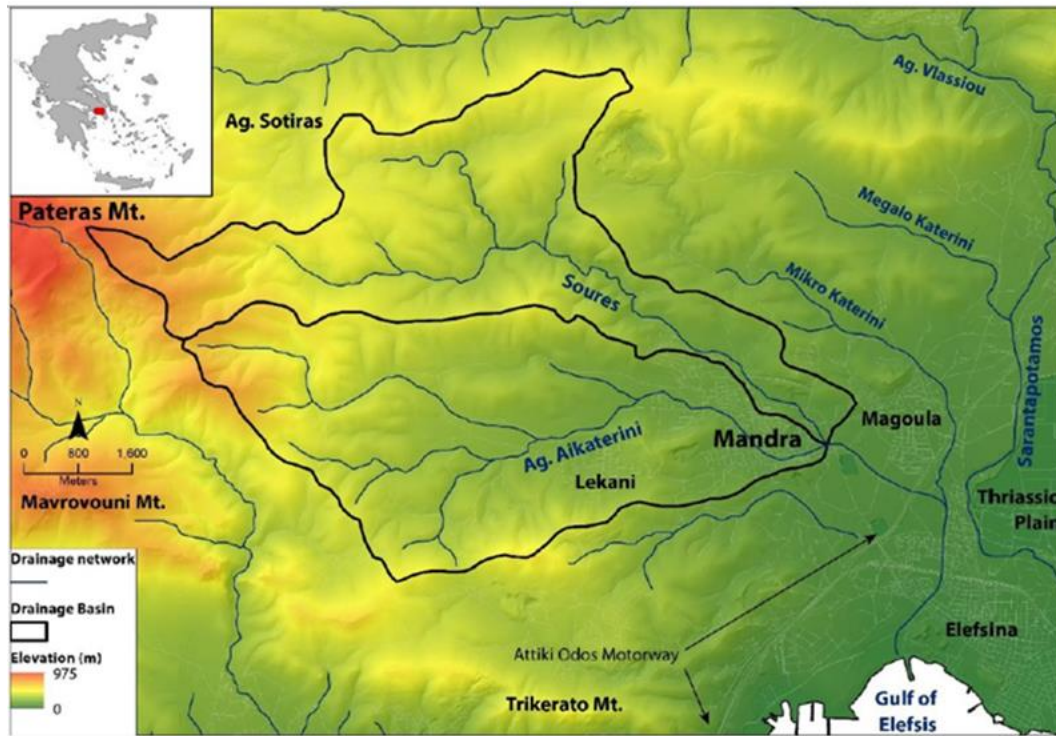
FIGURE 8 THE CATCHMENTS OF THE TWO TRIBUTARIES, SOURES AND AGIA AIKATERINI, ON THE EASTERN FOOTHILLS OF PATERAS MT. ARE SHOWN ON A MAP OF THE RESEARCH REGION. THE AREA'S ROAD NETWORK IS REPRESENTED BY GREY LINES (DIAKAKIS, ET AL., 2019)

3.3 Geomorphological features

Because of its proximity to Mount Pateras, the geomorphological features of the landscape in the surrounding area is mostly flat, with a semi-mountainous aspect to the west. The catchment area looks to comprise 75 km^2, with an average altitude of 246 meters and a 15% slope. In this area, the river has a dendritic form and flows to the east approaching the plain of Thriasio just below the Mandra. There it suddenly turns southward and to the gulf of Eleusis because of the effect of the Saradapotamos deposits. Most rivers in West Attica have little or no water most of the time (Diakakis, et al., 2019).

The morphological slopes often prevail, especially inside the watercourses of the torrents Soures and Agia Aikaterini, are between 10% and 50%, with minor sections indicating higher values in the mountains and near some riverbeds. West of Mandra city, a wide plain is developed in the Agia Aikaterini valley, where quaternary deposits of greater width and thickness emerge. However, in the Soures valley, the same plain is characterized by a steeper morphology and significant erosion.
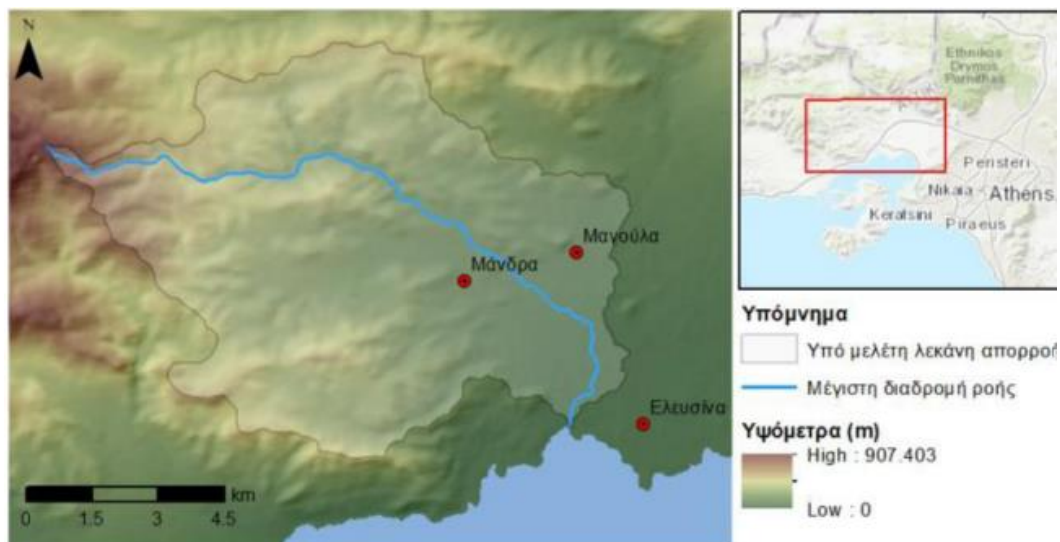
FIGURE 9 HORIZON OF THE CATCHMENT AREA'S GREATEST FLOW PATH (FLOODHUB, 2018)
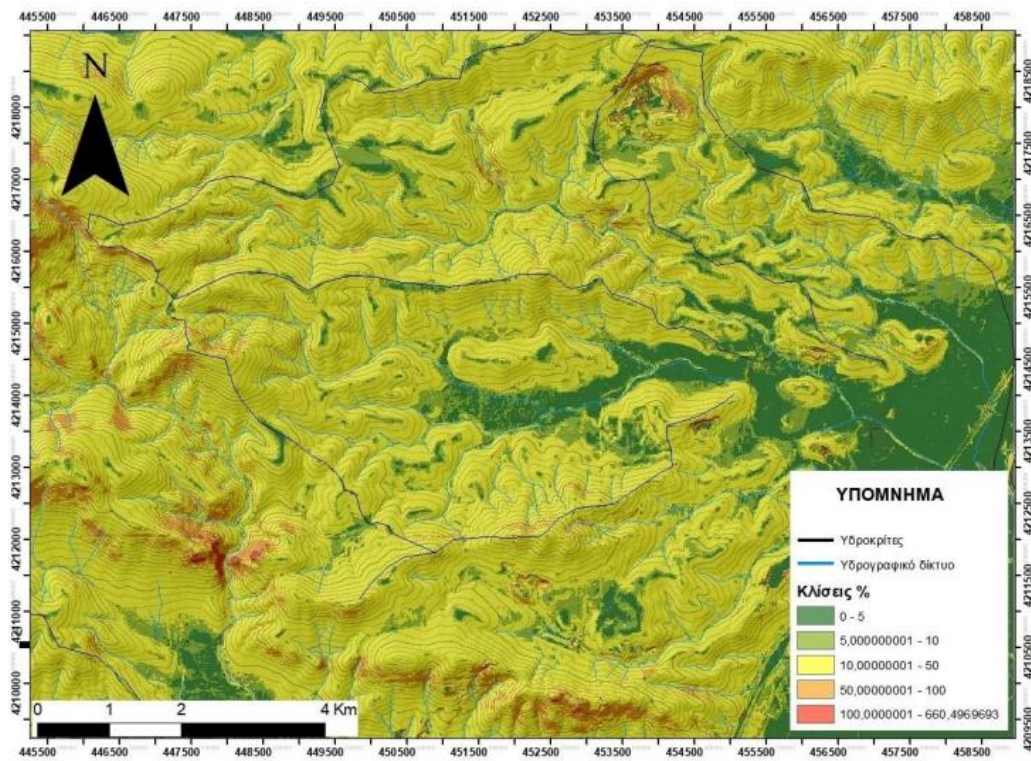
FIGURE 10 SLOPES OF THE RESEARCH AREA ON A MAP. SLOPES OF MORE THAN TEN PERCENT ARE COMMON IN THE SURROUNDING AREA. THE PLACES WHERE THE SLOPE DROPS DRAMATICALLY (0-5 PERCENT) CORRELATE TO THE AREAS WHERE FLOOD WATERS ARE RELEASED AND TRANSPORTED MATERIAL DEPOSITS DEVELOP (ΘΕΟΔΩΡΊΔΟΥ & ΚΑΛΟΎΣΗΣ, 2019)

3.4 Geological characteristics

Middle-Upper Triassic limestones and dolomitic limestones of the sub-Pelagonian Unit dominate in the Mandra area. These formations are fractured and karstified, with bauxites occurences. The Pelagonian zone is also represented by clay shales, sandstones, and keratolites. Along the riverbeds,both the geological bedrocks and Pleistocene-Holocene loose sediments are observed.

The following geological formations can be found in the surrounding area (Θεοδωρίδου & Καλούσης, 2019):

Quaternary

Holocene

Modern alluvial deposits (Al): consisting of loose unbound materials, clay-sandy materials, cobblestones within streams. In small inland basins these materials are more fine-grained and locally found terra rossa.

Debris cones and slope debris (Sc, cs): unconsolidated or low-consistency materials of slate, gravel, sand and clay, developed in the Slope Mountains.

Pleistocene

Debris cones, slope debris (Pt.sc, cs): comprising of older debris torrents, alluvial materials that include slats, gravel, cobbles, sand and clays, with local coatings of clay-marl sandy material, brown in color. Strong is occasionally observed.

Alpine Formations

Pelagonian Zone

Extraction limestones (Cenomanian-Senonian) (K.k) (transgressional Cenomanian-Senonian limestones) : they are thin-layered at the base and medium-thick-layered, locally marly, covered with inconsistent layers of iron-nickel and bauxite deposits towards the upper stratigraphic levels. They inconsistently transcend with   the   Cemonian-Turonian   limestones   or   older   pre-Cretaceous   formations. Iron-nickel deposits (Fn): Lenticular-layered deposits that are inconsistent with the Pre-Cretaceous limestones but to the Upper Cretaceous limestones. Nickel content is low.

Bauxite Deposits (B) : They are found at the base of Cenomanian limestones having a lenticular-layered form unrelated to the pre-Cretaceous carbonate rocks.

Limestones, Dolomitic limestones, Dolomites (Upper Triasic –Lower Jurassic) (Ts-Ji.k) : Thin-interlayer limestones that include flint layers and tubers. Locally they contain thin layers of clay slate. Limestones, Dolomitic limestones, Dolomites (Middle Triasic –Lower Jurassic) (Tm-Ji.k): Medium-thick to laminated limestones, often dolomitized crystalline limestones and dolomites, strongly fragmented. Limestones, Dolomitic limestones, Dolomites (Middle-Upper Triassic) (Tm.k,d): Limestones massive to thick layered locally crystalline, strongly fragmented. In their lower part, the dolomites predominate.

Phyllites and Sandstones (Low-Middle Triasic) (Tm.ph) : Phyllites and sandstones with conglomerate. Limestone and dolomite layers are found as well as eruptive rocks accompanied by tuffites. Limestones, Cherts, sandstones, slates, volcanic tofites (Tr)

Arkose , greywacke και clayey slates (Neopaleozoic – Middle Triassic) (P): Arkose, greywacke and clayey slates alternate with phyllites and quarzitic conglomerate.

Clayey slates and sandstones (Upper Carboniferous -Permian) (C-P): Clayey slates and sandstones alternating either with greywacke or with conglomerate with lenticular layers of limestone. Locally, they are weakly metamorphosed.

ΥΠΟΜΝΗΜΑ

ΤΕΤΑΡΤΟΓΕΝΕΣ
ΟΛΟΚΑΙΝΟ

al — Σύγχρονες αλλουβιακές αποθέσεις αποτελούμενες από χαλαρά ασύνδετα υλικά, αργιλοαμμώδη υλικά, κροκαλολατύπες στις ζώνες κοίτες των ρεμάτων. Σε μικρές εσωτερικές λεκάνες τα υλικά αυτά είναι πιο λεπτόκοκκα και τοπικά συναντάται terra rossa.

sc,cs — Κώνοι κορημάτων και πλευρικά κορήματα ασύνδετα ή μικρής συνεκτικότητας υλικά από λατύπες, χαλίκια, άμμο και αργίλους, που αναπτύσσονται στις παρυφές των ορεινών όγκων.

ΠΛΕΙΣΤΟΚΑΙΝΟ

Pl.sc,cs — Κώνοι κορημάτων, πλευρικά κορήματα. Συνίσταται από παλαιότερα κορήματα, ριπίδια χειμάρρων, προσχωσιγενή υλικά που αποτελούνται από λατύπες, χαλίκια, κροκάλες, άμμο και αργίλους, με ενστρώσεις κατά τόπους αργιλομαργαϊκού αμμούχου υλικού, καστανέρυθρου χρώματος. Κατά τόπους παρατηρείται ισχυρή συγκόλληση

ΑΛΠΙΚΟΙ ΣΧΗΜΑΤΙΣΜΟΙ
ΠΕΛΑΓΟΝΙΚΗ ΖΩΝΗ

Kk — Ασβεστόλιθοι επικλύσεως (Κενομάνιο - Σενώνιο)
Στη βάση τους είναι λεπτοστρωματώδεις και προς τα ανώτερα στρώματα μεσο - παχυστρωματώδεις, τοπικά μαργαϊκοί και καλύπτουν τοπικά με ασυμφωνία σε ασυμφωνία σιδηρονικελιούχων και βωξιτικών κοιτασμάτων. Υπέρκεινται ασύμφωνα των κενομάνιων-τουρώνιων ασβεστόλιθων ή παλαιότερων προανωκρητιδικών σχηματισμών.

Tm.J.k — Σιδηρονικελιούχα κοιτάσματα
Κοιτάσματα φακοειδούς - στρωματοειδούς μορφής που υπέρκεινται ασύμφωνα των προανωκρητιδικών ασβεστόλιθων και υπόκεινται σύμφωνα των ανωκρητιδικών ασβεστόλιθων. Η περιεκτικότητα σε Νικέλιο είναι χαμηλή.

Tm.k.o — Βωξιτικά κοιτάσματα
Συναντώνται στη βάση των κενομάνιων ασβεστόλιθων με φακοειδή - στρωματοειδή μορφή και βρίσκονται ασύμφωνα στα προανωκρητιδικά ανθρακικά πετρώματα.

Tm.J.k — Ασβεστόλιθοι, δολομιτικοί ασβεστόλιθοι, δολομίτες (Αν.Τριαδικό - Κ.Ιουρασικό)
Ασβεστόλιθοι λεπτο - μεσοστρωματώδεις που περιλείουν ενστρώσεις και κονδύλους πυριτόλιθων. Τοπικά περιέχουν λεπτά στρώματα αργιλικού σχιστόλιθου.

Tm.J.k — Ασβεστόλιθοι, δολομιτικοί ασβεστόλιθοι, δολομίτες (Μ.Τριαδικό - Κ.Ιουρασικό)
Ασβεστόλιθοι μεσο-παχυστρωματώδεις έως και άστρωτοι, συχνά δολομιτωμένοι κρυσταλλικοί ασβεστόλιθοι και δολομίτες, έντονα κερματισμένοι.

Tm.k,d — Ασβεστόλιθοι, δολομιτικοί ασβεστόλιθοι, δολομίτες (Μ.-Αν.Τριαδικό)
Ασβεστόλιθοι άστρωτοι έως παχυστρωματώδεις τοπικά κρυσταλλικοί, έντονα κερματισμένοι.
Στο κατώτερο τμήμα τους επικρατούν οι δολομίτες.

Tm.ph — Φυλλίτες και ψαμμίτες (Κ.-Μ.Τριαδικό)
Φυλλίτες και ψαμμίτες με παρεμβολές κροκαλολατυποπαγών. Συναντώνται ενστρώσεις ασβεστόλιθων και δολομιτών καθώς και σώματα εκρηξιγενών πετρωμάτων που συνοδεύονται από τοφφίτες.

Tr — Ασβεστόλιθοι, κερατόλιθοι, ψαμμίτες, σχιστόλιθοι, ηφαιστειακοί τόφφοι

p-Pz — Αρκόζες, γρασσοβάκες και αργιλικοί σχιστόλιθοι (Νεοπαλαιοζωικό - Μ.Τριαδικο)
Αρκόζες, γρασσοβάκες και αργιλικοί σχιστόλιθοι σε εναλλαγές με φυλλίτες και χαλαζιακή κροκαλοπαγή.

C-P — Αργιλικοί σχιστόλιθοι και ψαμμίτες (Αν.Λιθανθρακοφόρο - Πέρμιο)
Αργιλικοί σχιστόλιθοι και ψαμμίτες που εναλλάσσονται με γρασσοβάκες και κατά θέσεις με κροκαλοπαγή με φακοειδείς ενστρώσεις ασβεστόλιθων. Τοπικά παρουσιάζουν ασθενή μεταμόρφωση.

——— Όριο γεωλογικών σχηματισμών
— — — Πιθανό ή καλυμμένο γεωλογικό όριο
═══ Ρήγμα ορατό και πιθανή προέκτασή του

⌣ Λεκάνη απορροής

FIGURE 11 GEOLOGICAL MAP OF MANDRA - NEA PERAMOS(ΓΕΩΛΟΓΙΚΟΙ ΧΑΡΤΕΣ ΙΓΜΕ, ΦΥΛΛΑ ΕΡΥΘΡΑΙ, ΑΘΗΝΑ – ΕΛΕΥΣΙΣ)

Indicatively, this E-W oriented ridge of 975 meters, consists of Middle to Upper Triassic limestones, dolomitic limestones and dolomites of the Sub-Pelagonian zone. It should be mentioned that these limestones are united karstified , forming irregular brown-red bauxites. The Mt.Pateras is characterized by a steep relief, draining by ephemeral torrents. Thus, a steep topography is developed due to an interaction between the uplifted basement rocks, valley and landslide erosion on the hillslopes (Diakakis, et al., 2019).

FIGURE 12 QUATERNARY RIVER-WINTER DEPOSITS ALONG THE RIVERBED OF AGIA AIKATERINI (ΘΕΟΔΩΡΊΔΟΥ & ΚΑΛΌΥΣΗΣ, 2019)

FIGURE 13 MESOZOIC STRATIFIED-THICKENED DOLOMITIC LIMESTONES DISCOVERED IN THE KATSIMIDI RIVERBED DURING THE FLOOD (ΘΕΟΔΩΡΊΔΟΥ & ΚΑΛΌΥΣΗΣ, 2019)

3.5 Tectonic evolution

Attica is made of huge first class tectonic horses. The Geraneia, Kithairon, Parnitha, and Penteli faults can be found running E-W. These structures are limited to ruptured zones, in which smaller tectonic horses or ditches of 2nd, 3rd order appear. Therefore the wider area shows great fragmentation with two main groups striking, NE-SW and NW-SE to WNW-ESE. These structure directly affect the normal runoff of the hydrographic networks, creating radial, centripetal and rectangular shapes. Parnitha, Kithairon, and Patera are the ruptures related to the research region. On the east side of Parnitha and on the west side of Pastra (part of Kithairon), the Parnitha fault-block has upward movements. In the case of Parnitha, the rotation is counterclockwise around the NE-SW axis, with the eastern half having the maximum elevation, while the northwestern part the minimum. Due to tectonic processes, the Thriasios plain and the Asopos basin have developed fissures in the southwest and northeast, respectively. In the case of Pastra, the rotation is clockwise around a NE-SW direction axis, with the western half having the highest elevation and the eastern part the lowest. Patera fracture has a complex kinematics that include upward clockwise rotational movements around NW-SE and NE-SW directed axis . In the SW, the mountain range is uplifted, forming the Megara basin's ruptured zone, while in the NE, forms the ruptured zone on the eastern Gulf of Corinth (Θεοδωρίδου & Καλούσης, 2019).
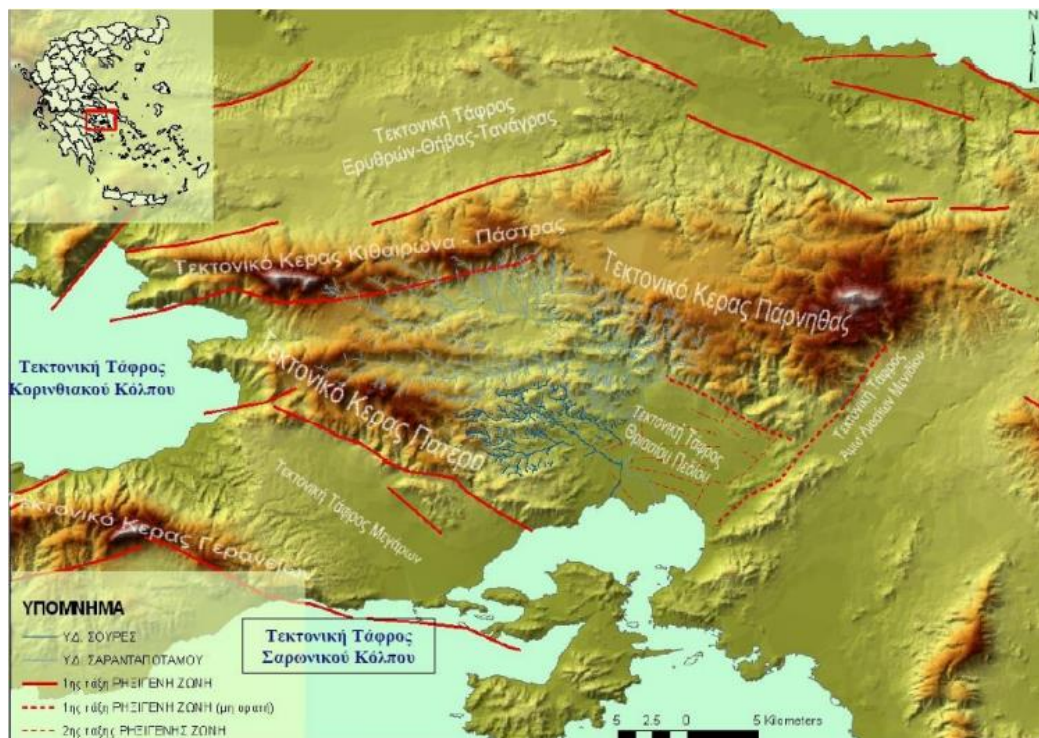
FIGURE 15 TECTONIC HORNS AND DITCHES (ΘΕΟΔΩΡΊΔΟΥ & ΚΑΛΟΎΣΗΣ, 2019)

The distribution of morphological elements (morphological slopes, discontinuities), the deep erosion at the edges of the cracks, the distribution of the stages and forms of surface erosion of the carbonates, the geographical and altitude distribution of the Cretaceous strata all point to a strong tectonic character (Θεοδωρίδου & Καλούσης, 2019).

3.6 Hydrogeology

The study region exhibits a wide range of water permeability in geological formations. Water permeates through the tributaries of limestones, making them water permeable. Semi-permeable Holocene and Pleistocene sediments, display selective water permeability in certain areas, depending on the percentage of coarse and detailed components of the sediments. Impermeable rocks include clay shales, sandstones, and keratolites, in which water cannot find a way to dive but instead,it flows superficially (Diakakis, et al., 2019) (Diakakis, et al., 2019).

As it has been noted (Georgakopoulos,2009) , in the two basins (Soures and Agia Aikaterini), the macro-permeable-karst Mesozoic limestones , cover a total area of 76%, while the semi-permeable Quaternary and the impermeable formations do not exceed the 24% and 1% respectively.
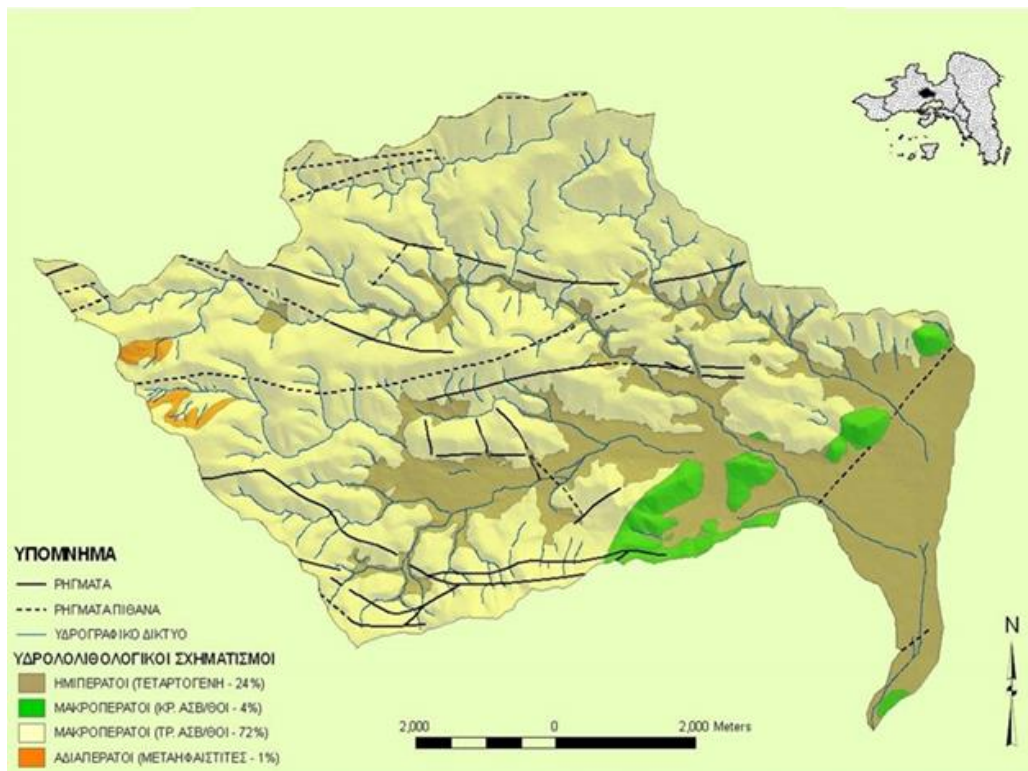
FIGURE 16 GEOLOGICAL - HYDROLITHOLOGICAL MAP OF THE SOURES TORRENT BASIN (ΘΕΟΔΩΡΊΔΟΥ & ΚΑΛΟΎΣΗΣ, 2019)

3.7 The Mandra's Basins

In Mandra city, there are two separate catchments. The first is the stream of Agia Aikaterini, which ends up in the central part of Mandra and the second is the Soures stream, that passes through the northeastern outskirts of the city. These two streams are concentrated below the urban area of Mandra.

Then, they are diverted to Sarandapotamos, the latter of wich flows east into the Gulf of Eleusis and is the largest river (Soulios, et al., 2018).

The Mandra hydrological basin has an area of 65 km^2. The hydrographic network of the area is sparse with small coefficients of branching, density and frequency because of limestone occurences. On account of the intense interventions that have prevailed in recent years, the area is intensively flooded (Ερμίδης, 2018).

The stream of Agia Aikaterini covers an area of is 23.3Km^2. Its average altitude is h=270m with the highest point at 659m and the lowest at 80m. Its maximum thalweg is 9.8 km long. The Soures stream covers an area of 18.2 Km^2. Its average altitude is 305m, the highest point at 772m and the lowest at 80m. Its maximum thalweg is 11.6 km long (Soulios, et al., 2018).

The two streams share many similarities and differences as well. More particularly, the common features are (Soulios, et al., 2018):

- the two streams have a ephemeral flow and torrent behavior

- Manifested in both changes in the hydrographic network, that is, deepening or widening in the downstream part of their riverbed, which means, there was an increase of the riverbed due to deposits

Finally, they both have a similar geological composition. However, the ratio of quaternary and clay material is larger in Agia Ekaterini than in Soures

On the other hand, the following differences were observed (Soulios, et al., 2018):

- The Soures basin has a higher slope value at 19.6% than the Agia Aikaterini basin, which is 16.7%. This has a consequence on the water speed and therefore on the corrosion and transport capacity to be higher in the Soures basin

-The Soures basin has a maximum seawater equal to 11.6 km and the concentration time is estimated at 2 hours and 52 minutes. The basin of Agia Aikaterini has a maximum thalweg of 9.8 km and the collection time is estimated at 2 hours and 58 minutes. The velocity of the surface waters in the Soures basin was higher. Meaning more corrosion and transport

- Therefore, the upper part of the Soures stream is very corrosive, transporting coarse-grained material, such as cobblestones, gravel, sand or even boulders. The stream of Agia Aikaterini carried suspended materials, mainly clay, and mud was deposited in the urban fabric, flooding the wider area

CHAPTER 4

4.1 Flood elements

In general, the concentration time of a catchment area indicates the time lag with which the peak of the runoff occurs relative to the time of the rainfall initiation in the catchment area. The concentration time is obtained from the analysis of pairs of watermarks and hydrographs at the outlet of the basin. In this case, empirical methods have been used to calculate the expected floods. Empirical methods are used when there are no systematic, reliable, long-term flow data. In Greece, the methods used to calculate the concentration time of a hydrological basin are the ones of Giandotti, Kirpich and the Passini. One of the most well-known empirical method, is the so-called rational as mentioned in Giandotti (Soulios, et al., 2018).

This method can be applied if the runoff rate or the total overflow rate is known (Grimaldi, et al., 2012) (Kaufman de ALMEIDA, et al., 2014) (Soulios, et al., 2018). This rate is not about the annual runoff average but the percentage of rain that flows out and reaches the outlet basin during flooding. This factor is usually calculated with estimates in which an average value of 0.65 (65%) is adopted. In the case study, 70% was considered a suitable value, which corresponds to a return period of 100 years, due to the intensity of the rainfall, the geological composition and the duration of the rainfall (Soulios, et al., 2018). It was calculated that the time of gathering in Agia Aikaterini according to Giandotti's formula is tc= 2 hours and 58 minutes. This means that for a flood with a maximum flow rate for the respective rainfall intensity, the rainfall should last 2 hours and 58 minutes. The flood discharge for a T= 10-year return period will be $q=10^6$ m^3/s and for its occurrence, precipitation of Pc= 23.40 mm/h is required for tc=2 hours and 58 minutes (Soulios, et al., 2018).

For the calculation of the corresponding rainfall intensity, the original equation (as it was initially proposed for the rational method) was applied as follows (Soulios, et al., 2018):

EQUATION 13: $Pi = (30logT + 15)t_c - 0,6$

Where Pi= rainfall intensity (mm/h); T= return period (10, 100, 1000 years etc); t_c= time of concentration

Various methodologies have been proposed to calculate the intensity of rainfall in Greece (Koutsoyiannis, 2004). The results of the methods as well as the method applied in the work of Soulios et.al are related. For a 100-year flood return period, that is T = 100 years, the flood discharge will be q = 177 m^3/s with a corresponding rainfall intensity Pc = 39.50 mm/h. In addition, for a flood with a return period T = 100 years then q = 248 m^3/s and a rainfall intensity Pi = 54.7 mm/h (Soulios, et al., 2018).

The flood that took place in the area of Mandra is regarded as flash flood. This type of flood is very dangerous because it is characterized by heavy rainfall with a small spatial distribution in a short period of time and creates a flood event that people are unprepared for. Therefore, it is difficult for taking reactions in such situation. It is important to be mentioned that bad weather conditions were observed in the Mount

Pateras and not in the city of Mandra. The mountain consists of steep slopes and this contributed to the worsening of the phenomenon because of a concentration of flowing water, which was subsequently directed to the lowland areas of Mandra with great momentum (Ανδριόπουλος, 2020). These formed debris flows concern well-classified low plasticity materials. The reasons for the debris formation vary from erosion processes, such as weather conditions, volcanic activity, glacier transport to even anthropogenic activity such as piles of materials from mines. These contain a significant percentage of organic matter, as, for example, tree trunks, plants or soil horizons and, depending on the proportions of sludge, are divided into derbis flows or mud flows (Hungr, et al., 2001). The key element of debris flows is the presence of a channel. Based on Hungr et al (1984) a maximum depth-to-depth ratio of 1 to 5 was proposed to move the material in an almost flat slope channel, which is influenced by geomorphological factors that define its branch in the hydrographic network and the direction of the material as well. In the case of a study, the canal pre-existed but was clogged. Initially, with the onset of runoff, the presence of water increased with the lateral boundaries helping to enlarge the depth of the channel. In cluster flows in terms of classification is that large clusters come to the surface of the flow and thus form opposite granulometry (Costa & Fleisher, 1984). This when combined with the strong vertical slope velocity leads to classification along an accumulation of the large fraction of the deposit near the channel outlet (Iverson , et al., 1997). Thus, the maximum expansion of the debris flows could reach 40 times greater than that of an extreme flood (Hungr, 2000) . Once they reach the maximum deposition of the canal then the lateral expansion begins while from the exit of the canal small fractions or mudflows escape, as in the area of Mandra.
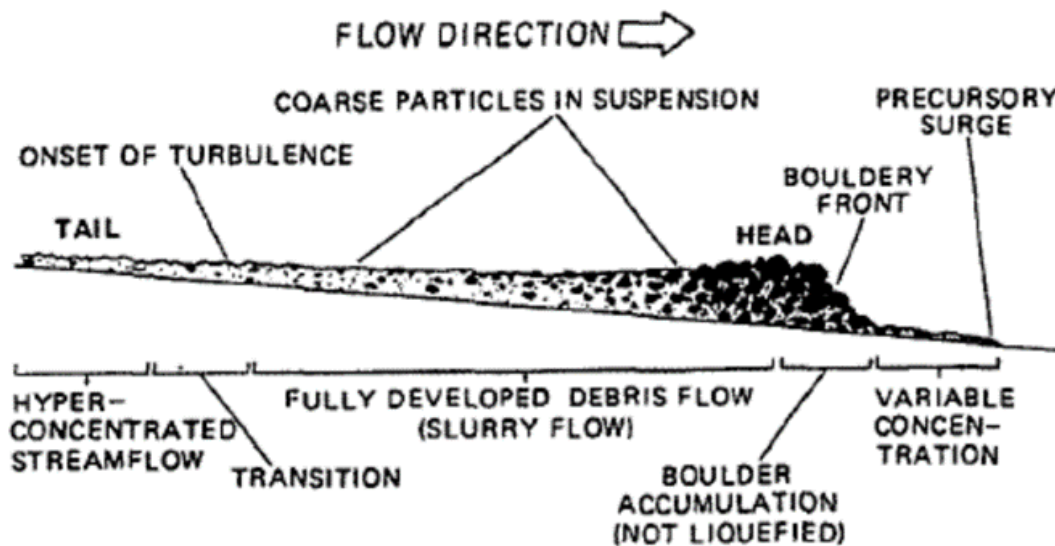
FIGURE 17 CLASSIFICATION OF DEBRIS FLOW (HUNGR, ET AL., 2001)

The delimitation of the flood phenomenon became upstream and downstream of the city of Mandra, the dimension of which is 4.03km where it extends between the slopes of the hills of Mount Patera, 5 km before the Mandra city of and the exit of the basin. The flooded area in its western part consists of two elongated ends along the Soures stream to the north and the torrents of Agia Aikaterini to the south. First on the northwest Mandra these two legs were merged, without exchanging large amounts of water at the highest level of the flood. Then, merger then took place on the southeast side of the city because the water was morphologically allowed to expand into the wider area. However, the construction of the Attiki Odos highway hampered the flood water and thus it was drained through two openings of the highway. The flooded area had expanded from about 350 meters upstream of Mandra city, to 1500 meters upstream of the E94 motorway (Diakakis, et al., 2019).
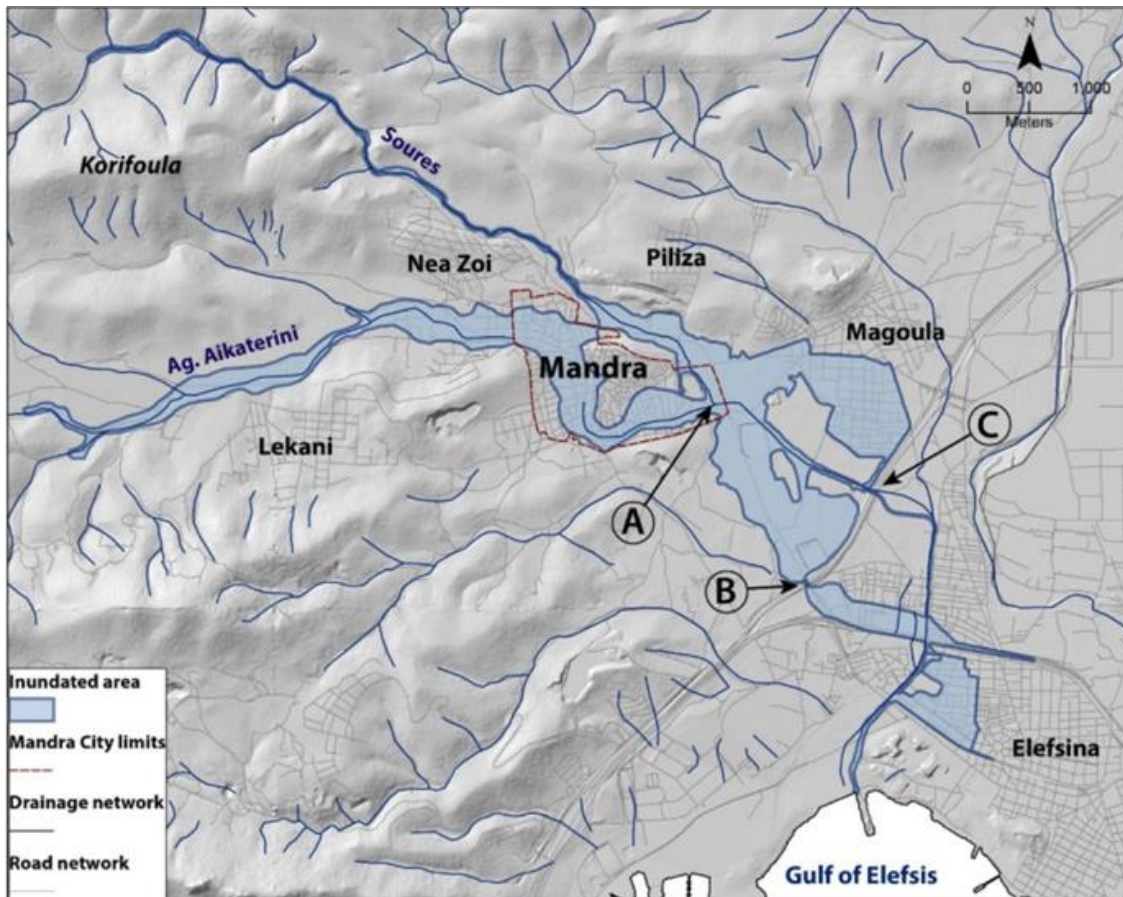
FIGURE 18 MAXIMUM FLOOD AREA IN THE PEN AREA ON NOVEMBER 15, 2017 (DIAKAKIS, ET AL., 2019)

The damage was huge due to the capacity of the flood as volumes grater than> 1m^3 were transported over very long distances. Since Holocene and Upper Pleistocene deposits existed, the erosion was more intense and the bedrock (e.g limestone) in the riverbed was affected. From the spatial distribution of the damages it seems that, the effects were not the same in the wider area. In the upstream parts of the

Mandra, area the deposits seemed to be more intense in the agricultural areas because the urban area functioned as a large-scale trap of coarse-grained sediment. Specifically, in the upstream part of Agia Aikaterini, geomorphological effects as well as gutters and deposits of 1-3 cm boulders were ascertained from the field observations. In contrast to the western and northwestern part of the area, the deposit records of the transported material consisted of grains the size of gravel up to small boulders 60 to 70 cm (Diakakis, et al., 2019).
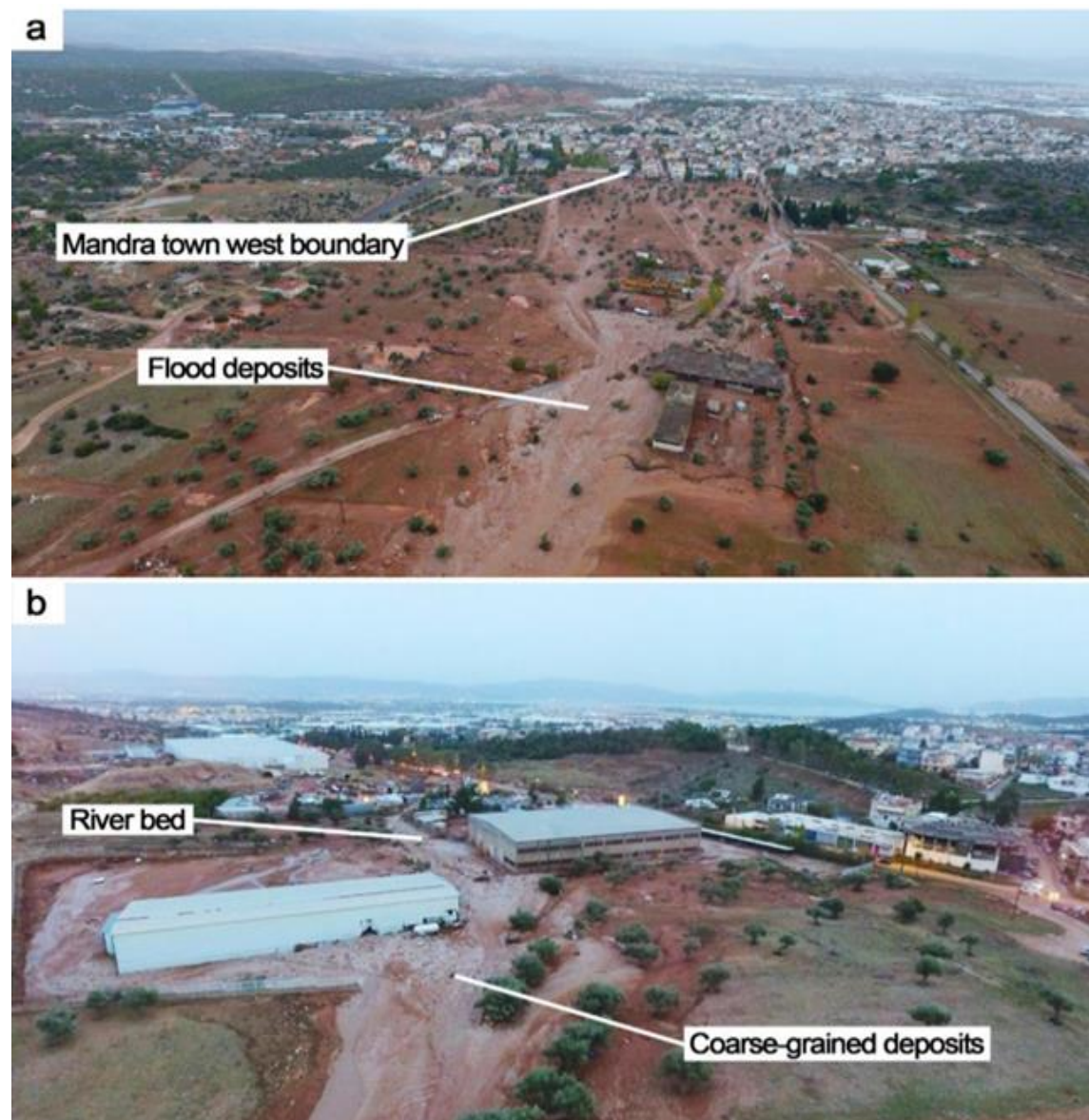
FIGURE 19 DOWNLOADS FROM UAS THAT PRESENTS DEPOSITED MATERIAL (MAINLY COARSE-GRAINED) JUST ABOVE THE CITY LIMITS OF MANDRA IN BOTH CASE (A) OF AGIA AIKATERINI AND (B) OF SOURA. BOTH SHOTS LOOK DOWNSTREAM (DIAKAKIS, ET AL., 2019)

The spatial distribution of the storm where the maximum rainfall was observed in an area bordered by the northern part of the Soures basin to the north, with total rainfall ranging from 154.6mm to 164mm. In the south, in the rest of the Soures basin and almost in the whole Agia Aikaterini basin , the corresponding amount of rain was 138.4mm to 154.7mm. The total rainfall lasted about 7 hours and so can be categorized, marginally, as a flood (Soulios, et al., 2018).
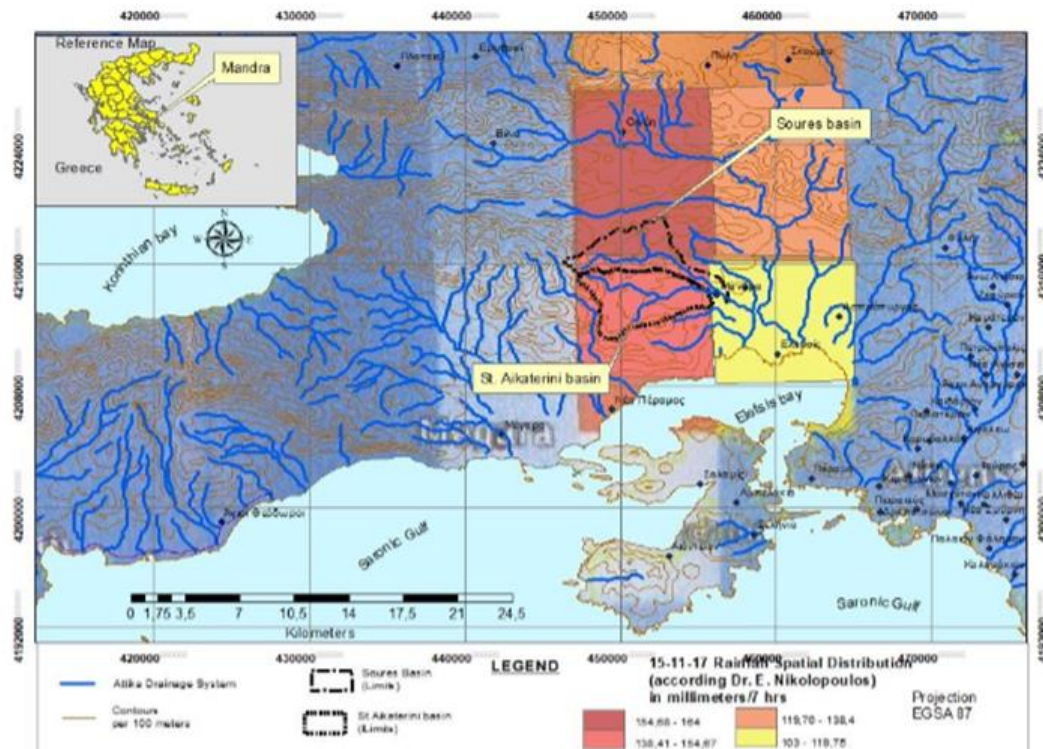
FIGURE 20 THE SPATIAL DISTRIBUTION OF RAINFALL IN THE AREA OF MOUNT PATERA FOR 14-15 / 11/2017 (SOULIOS, ET AL., 2018)

The following diagram shows the time distribution and maximum rainfall heights. At night towards the morning of 15-11-2017, a maximum intensity of 47mm / h is seen, but for a limited period of about one hour, while for a continuous period of three hours, from 05:00 to 08:00, the average rainfall intensity was about 39-40mm / h. As already mentioned, these values refer to a 100-year return period. Therefore, the corresponding flood discharge was calculated equal to 180 m^3/s and 140 m^3/s for the Agia Aikaterini and Soures basins, respectively (Soulios, et al., 2018).

4.2 Climatic Conditions-Rainfall Data

The National Meteorological Service from the nearby station of Elefsina provides the annual precipitation average. This corresponds to 373 mm with 59 mm for the month of November. The catastrophic flood was caused by an intense storm, which took place between November 14, 2017 at 23.00 pm, and November 15, 2017 at 12.00 pm.Most of this storm recorded within six hours between 01.00 and 07.00, indicating a very short duration and an extremely spatially located rainfall (Diakakis, et al., 2019).

In addition, the University of Connecticut studied NASA satellite imagery assessing the spatio-temporal evolution of the storm from November 14 to 15, 2017. Here, reference is made to the amount of water contained in the cloud that caused the storm. It is not certain that this entire amount has reached the soil surface but its effects are justified if considered that the amount of rain is of the same order of magnitude (Soulios, et al., 2018).

The data from the National Observatory of Athens from the use of the X band of the multi meter radar (XPOL) showed that the wind speed was around 15 ms-1, which means that it was moderate to high with direction towards the flood area. An algorithm estimated that the rainfall reached close to 300, locally

between 15.00 on 14 November 2017 and 15.00 on 15 November 2017, in an area focused on the streams of Agia Aikaterini and Soures with direction N-S and dimensions 18 km length and 4 km width. According to the estimates from XPOL, the average rainfall of the basin was between 153 and 194 mm. The total accumulation was 41 km / h and the maximum intensity 57 km / h for the streams Agia Aikaterini and Soures respectively (Diakakis, et al., 2019).
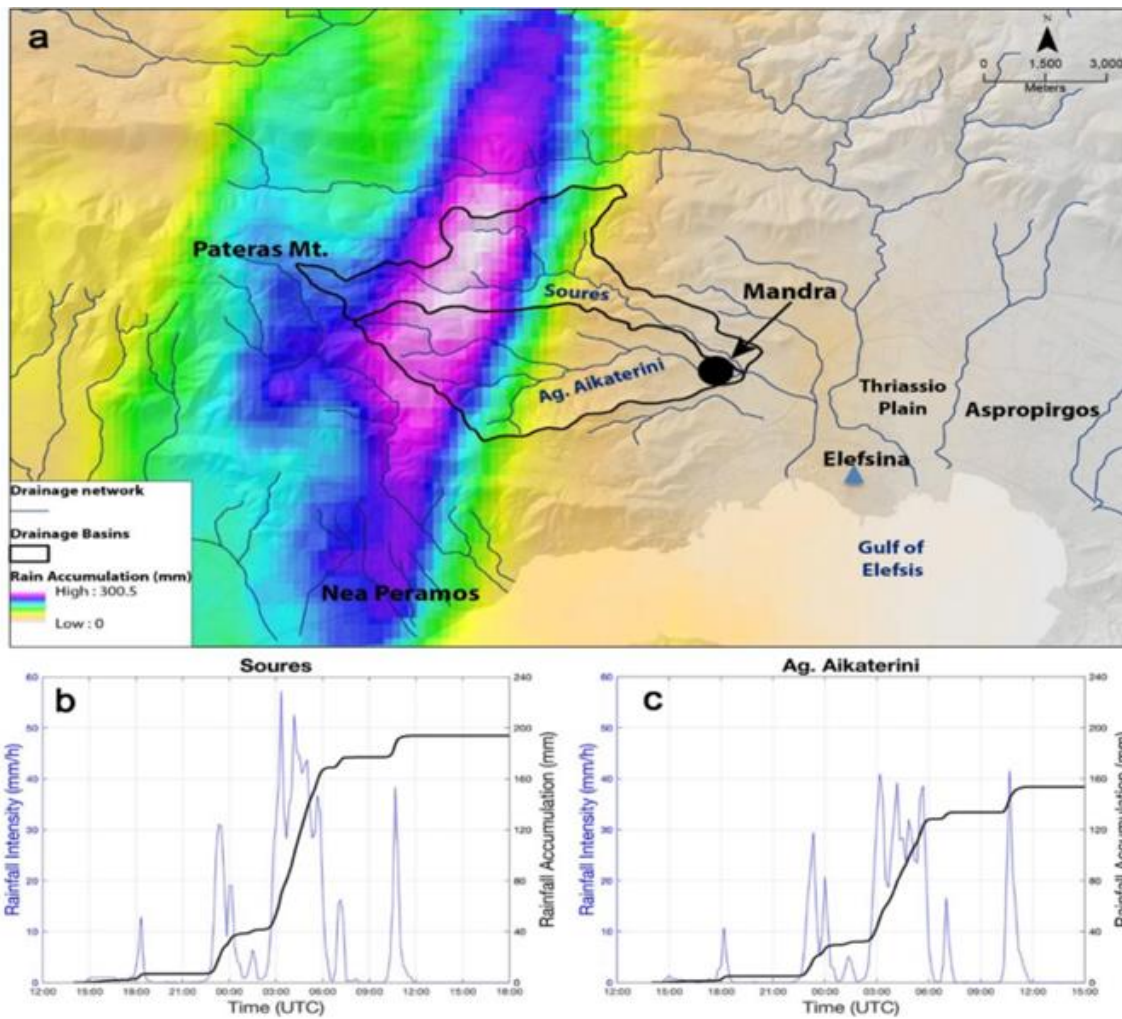
FIGURE 22 (A) RAINFALL ACCUMULATION MAP OF THE STORM EVENT OVER THE TWO CATCHMENT AREAS, TOGETHER WITH THE AVERAGE RAINFALL TIME SERIES IN THE CATCHMENT AREAS (INTENSITY AND ACCUMULATION) (B) SOURES AND (C) AGIA AIKATERINI. NOTE THAT THE START / END TIME SHOWN IN THE GRAPHS (B, C) CORRESPONDS TO NOVEMBER 14, 12:00 TO NOVEMBER 15, 15:00 UTC (DIAKAKIS, ET AL., 2019)

The maximum rainfall was observed in an area limited by the northern part of the Soures river basin to the north with the total rainfall ranging from 154.6 to 164 mm. To the south, in the rest of the Sources basin and in almost all of Agia Ekaterini basin, the corresponding height of the rain was 138.4 to 154.7 mm (Soulios, et al., 2018).

4.3. Debris flow and floods

The distribution of phenomena in the area developed where there was the maximum cumulative rainfall and slightly downstream, to the south (Koulouriotiko stream) and east (Soures and Agia Aikaterini) of Mount Pateras.
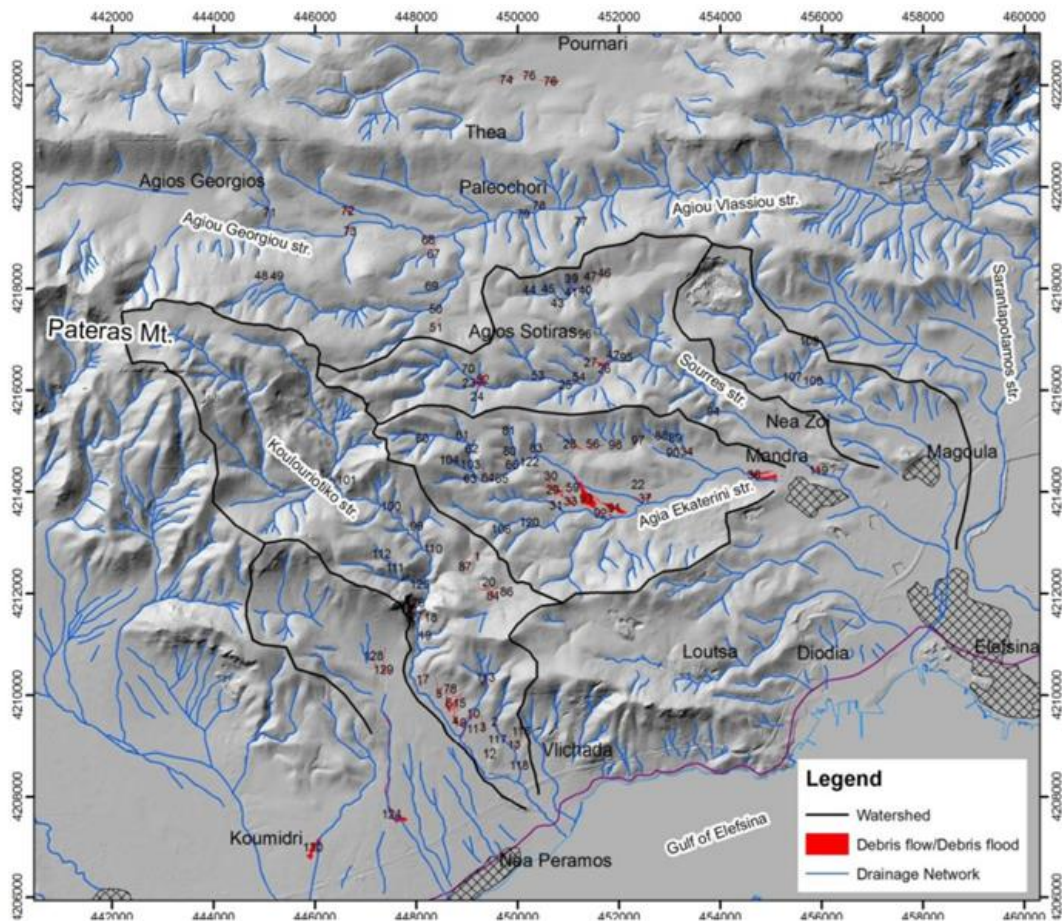
FIGURE 23 LOCATIONS OF MAPPED OCCURRENCES OF EROSION AND DEPOSITION IN THE FORM OF FLOW OR FLOOD OF DEBRIS IN THE AREA AFFECTED BY THE FLOODS OF NOVEMBER 15, 2017. MOST AND MOST INTENSE PHENOMENA ARE LOCATED IN THE BASINS OF THE STREAMS OF AGIA AIKATERINI, SOURES, KOULOURIOTIKO AND AGIOS GEORGIOS (ΓΡΑΜΜΈΝΟΥ, 2021)

In the Soures and Agia Aikaterini basins, 84 places / areas of manifestation of discrete flows / flood peaks were observed and mapped, in classes ranging from class 1 to class 5, according to the classification depending on the area.

The majority of the phenomena belong to the classes 2 (38 places, 45.2%) and 3 (33 places, 39.3%), while the phenomena in the classes 4 (7 places, 8.3%) and 5 (2 places, 2.4) were less but more impressive. %). Both places of class 5 belong to the basin of Agia Aikaterini, to the gulf of Agios Ioannis in the stream Katsimidi, and to the plain area immediately upstream of the city of Mandra.
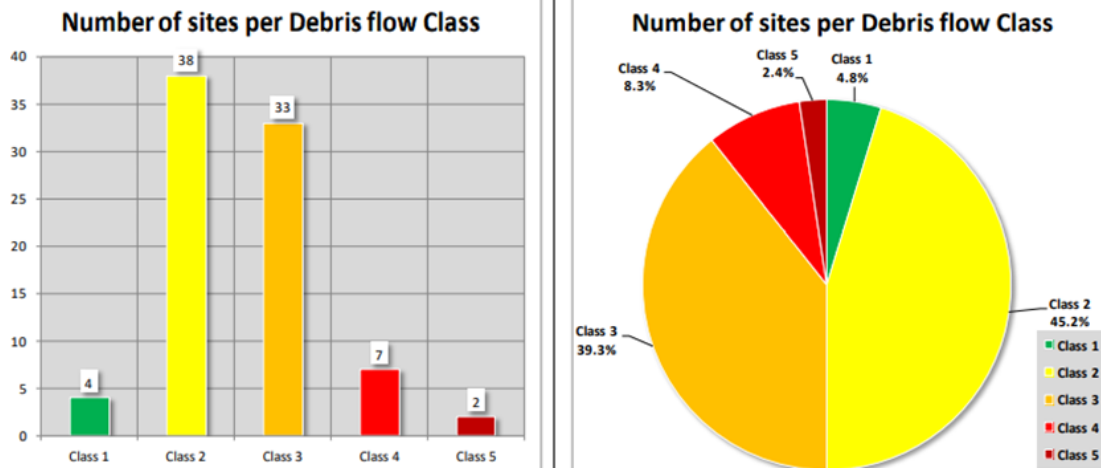
FIGURE 25 NUMBER (LEFT) AND PERCENTAGE (RIGHT) OF PLACES WITH FLOW / FLOOD OF SEDIMENTS IN TOTAL IN THE BASINS OF AGIA AIKATERINI AND SOURES (ΓΡΑΜΜΈΝΟΥ, 2021)

Comparatively, it can be mentioned that the number of places is slightly larger in the basin of Agia Aikaterini than in Soures, while per class the torrent Soures is superior only in class 3, but it has no phenomenon of class 5. Similarly, the total area of Agia Aikaterini basin is much superior in the 2nd, 4th and 5th classes than Soures. However, the opposite case is observed in the 3rd class.
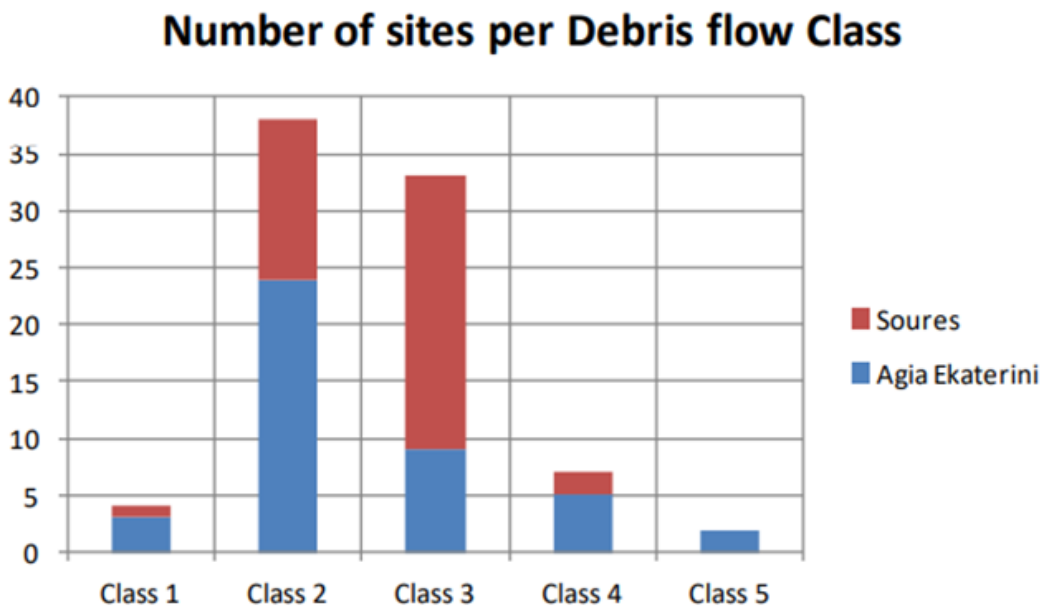
FIGURE 26 NUMBER OF DEBRIS FLOW / FLOOD SITES IN THE SOURES AND AGIA AIKATERINI BASINS (ΓΡΑΜΜΈΝΟΥ, 2021)

Number of debris flow sites per basin

41
49%

43
51%

Agia Ekaterini
Soures
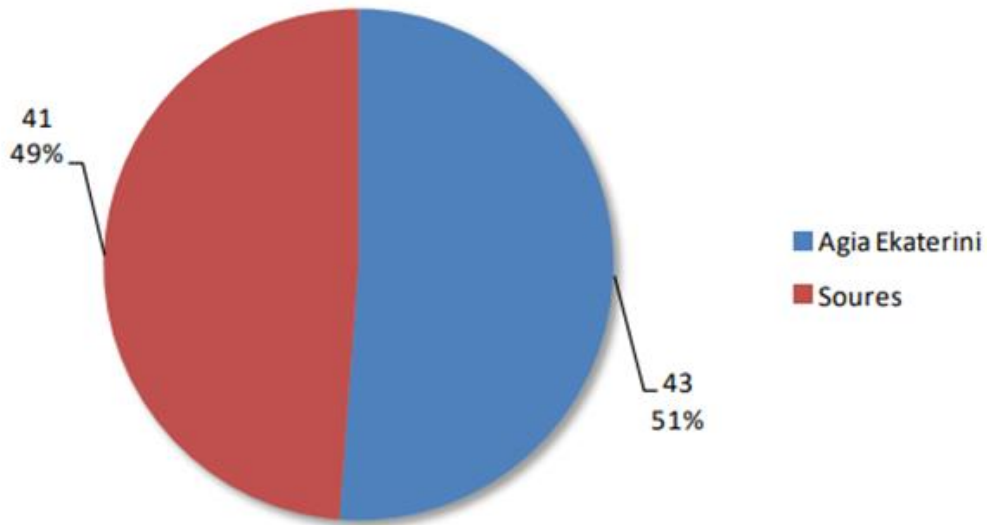
FIGURE 27 PERCENTAGE OF NUMBER OF FLOW / FLOOD SITES IN THE SOURES AND AGIA AIKATERINI BASINS (ΓΡΑΜΜΈΝΟΥ, 2021)

Total area of sites per Debris flow Class

Soures
Agia Ekaterini
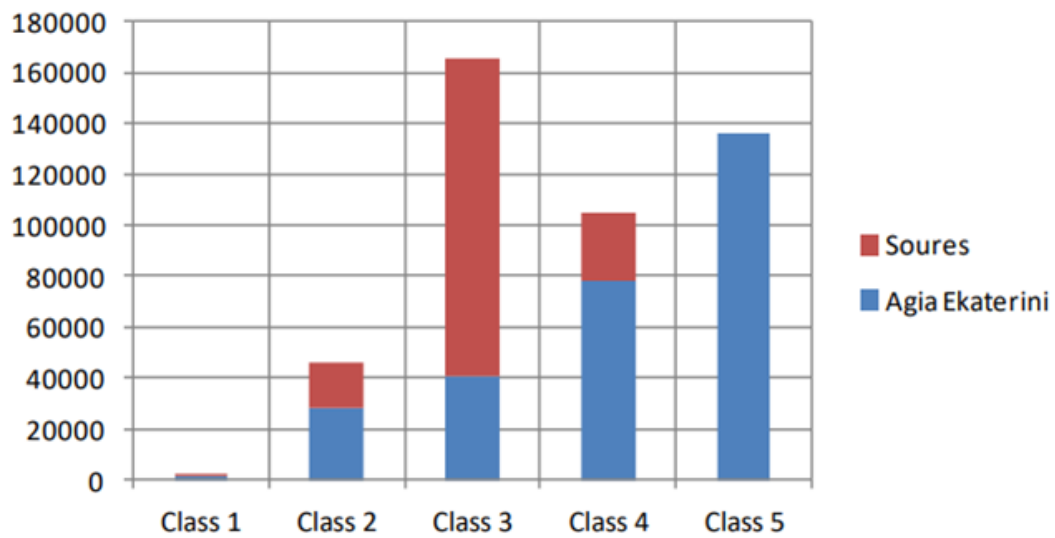
FIGURE 28 EXTENT OF RIDGE FLOW / FLOOD SITES IN THE SOURES AND AGIA AIKATERINI BASINS (ΓΡΑΜΜΈΝΟΥ, 2021)
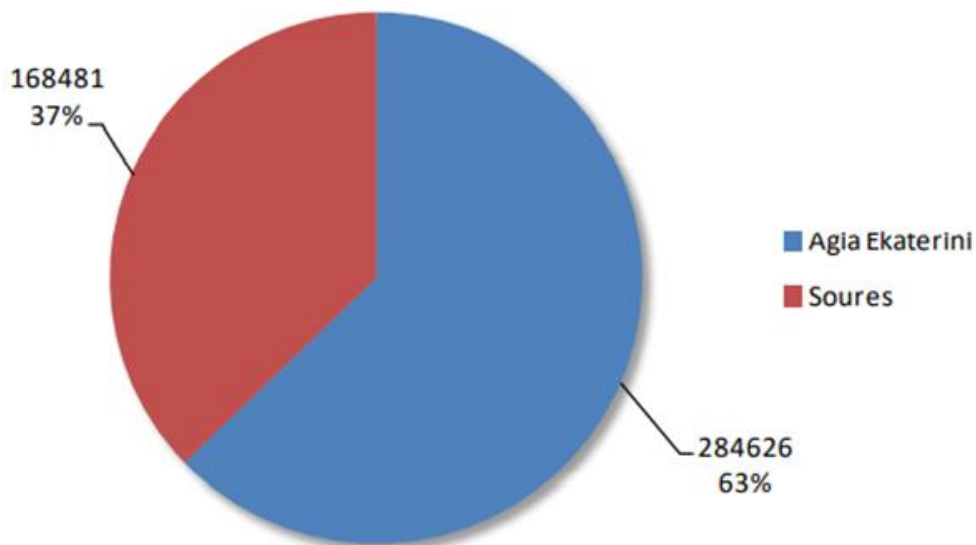
FIGURE 29 PERCENTAGE OF AREAS OF FLOW / FLOOD PEAK LOCATIONS IN THE SOURES AND AGIA AIKATERINI BASINS (ΓΡΑΜΜΈΝΟΥ, 2021)

The ignition zone of the phenomena mostly included (Γραμμένου, 2021):

1.   first class branches with large morphological slopes, with or without forest cover,

2.   areas with poor vegetation or deforestation, either in parent rock or in sloping deposits and thin mantle soil,

3.   higher-order riverbeds along which runoff enters areas with significantly lower slopes.

The debris flow deposition zone was mostly in various recipients, in the following categories (Γραμμένου, 2021):

1.   in higher order branches,

2.   in areas where the slope of the morphology is drastically reduced,

3.   in areas upstream of artificial barriers (buildings, masonry fences, etc.)

4.   in areas with increased vegetation or forest cover.

The following images are typical cases inside and outside the Soures and Agia Aikaterini basins where the cases of ignition and deposition appear, especially in combination with the above maps.

FIGURE 30 SATELLITE IMAGE BEFORE (14-10-2017, ABOVE), AFTER (31-08-2018, MIDDLE) AND WITH DIGITIZED THE MAIN EROSION AND DEPOSITION AREA (BELOW), IN BRANCHES THAT CONTRIBUTE TO THE KOULOURIOTIKO STREAM (ΓΡΑΜΜΈΝΟΥ, 2021)

FIGURE 31 SATELLITE IMAGE BEFORE (14-10-2017, ABOVE), AFTER (09-08-2018, MIDDLE) AND WITH DIGITIZED THE MAIN EROSION AND DEPOSITION AREA (BELOW) IN KORAKOREMA, WHICH CONTRIBUTES TO THE SOURES STREAM (ΓΡΑΜΜΈΝΟΥ, 2021)

FIGURE 32 SATELLITE IMAGE BEFORE (14-10-2017, ABOVE), AFTER (31-08-2018, MIDDLE) AND WITH DIGITIZED THE MAIN EROSION AND DEPOSITION AREA (BELOW), WEST OF THE AGIOS IOANNIS RIPPLE

4.4 Particle size analysis

According to Andriopoulos (2020), a particle size analysis was performed in cartographic, recent flood deposits or waste flows in the area of Mandra, more specifically in the stream of Agia Aikaterini, where the sampling sites were Agios Ioannis and Katsimidi. The data were obtained through SMEA (Unmanned Aerial Vehicle Systems) and by ground means, aiming at the granulometric analysis of small fractions.

On October 11, 2019, sampling took place in the area of Mandra in the very morning hours with favorable weather conditions. Since there was no rain for the last 6-8 hours, the ground was dry. The sampling points were divided into two places, with the first being in the area of Agios Ioannis, in the streambed east of the church and with the second one in the Katsimidi area north of the first, both places located northeast of the Mandra city. In the first place, 7-point shots were taken with SMEA with the center only the meter, at 1m, 3m, 5m, 10m, 15m, 20m, and 30m height from the surface. Photos were taken in a terrestrial way at a height of less than one meter. In addition, another 11 shots were taken along the metric strip, ie perpendicular to the streambed, at a height of 5m and there were 90 shots by predetermined flight, which were converted into an orthomosaic (orthophoto map). Then, in the second position, 8 point shots were taken with SMEA with the center as the monometer, 2 shots were taken at 1m, and from one shot at 3m, 5m, 10m, 15m, 20m and 30m height from the surface. The photographs taken were on the ground at a height of less than 1 meter (Ανδριόπουλος, 2020).

According to Andriopoulos, an analysis position was chosen for the position of Agios Ioannis for the fine-grained, one for the medium-grained and two for the coarse-grained. It seems that there is a wide range of prices as the particle sizes range from 10mm to 30mm. Regarding, the shooting results at different heights are almost the same except for shooting at 3 meters, where the values exceed 95%. In addition, as a comparison of ground medium (> 1m) and SMEA (1m) the detection is exactly the same (Ανδριόπουλος, 2020).

For the analysis of the selected medium grained fractions, shots were taken via SMEA from 3, 5 and 10m. There is a greater granulometric value variation of the medium grained as they range from 15 mm to 135 mm. From different shots at different altitudes, the results are almost the same (Ανδριόπουλος, 2020). For the selected coarse-grained fraction, the first position was taken via SMEA from 15m and 20m, as well as from an orthophoto map clipping. The shots of the second position were made through SMEA, from 15m, and from an orthophoto map. Therefore, the variation of the granulometric values in the coarse grains ranges from 35mm to 735mm, meaning that slightly smaller than 1m 3 block-dimensions. There is a satisfactory match of the results from the same height but different source (Ανδριόπουλος, 2020).

 In Katsimidi, one analysis site was selected for the fine-grained, one for the medium-grained and one for the coarse-grained. For the analysis of the selected fine grain, as in Agios Ioannis, in the shots there is not a large range of values because the particle sizes range from 10mm to 30mm. Therefore, the results from the shots from different heights are almost the same except for the shot from 1m where more than 80% of higher values can be seen. On the other hand, the results of the ground mean (> 1 m) and SmieA

(3m), are the same. Sample analysis of the selected medium grained fraction, were performed via SMEA, from 3m and 5m respectively. There is a remarkable greater variation in the particle size values with the medium grains ranging from 15mm to 100mm. The results from shooting at different heights are largely the same, except for a difference of a few millimeters at high values above 90% (Ανδριόπουλος, 2020).

For the analysis of the coarse grained fraction, shots were taken via SMEA, from 10m and 20m respectively. In coarse grains the range of particle size ranges from 20mm to 650mm. The results from different heights are satisfactory towards their identification. Studying the analysis area, the irregularities of the curves are expected, as large particle size fluctuations are observed, with obvious large blocks (Ανδριόπουλος, 2020).

There are no major differences in any granding class. The averages of the granulometry fractions calculated at the site of Agios Ioannis are higher than those at Katsimidi, with the coarse grains mainly being higher. This can be confirmed because the site of Agios Ioannis is a typical example of debris flows, where fluid has been mixed with large quantities of corroded and transported material. The phenomenon that took place was extreme as its consequences. The studied samples were a mixture of Holocene / Pleistocene deposits and limestone bedrock. The erosion caused by the flood was so severe that mostly angular fragments are observed instead of rounded cobbles.The possible porosity created by corrosion in combination with the color changes (brown, white) of the sample create a difficult case (Ανδριόπουλος, 2020).

CHAPTER 5

5.1 Model of debris flow entrainment

5.1.1 Digital Elevation Model

An accurate digital elevation model is required for a valid numerical calculation. The resolution of digital elevation models is often specified by government mapping agencies. Highly accurate elevation models (about 0.5 m) can be obtained by airborne laser scanning or digital photogrammetry, especially in most European countries (Christen, et al., 2012). Bühler et al (2011) (Bühler, et al., 2011) have shown that elevation models with low spatial resolution (on the order of 25 m or more) can miss important terrain features, while elevation models that are too accurate (on the order of 1 m or less)can lead to long computation times and even incorrect simulation results. The best spatial resolution for the elevation model depends on both the procedure and the case. For example, in snow avalanche studies, a computational resolution of 5 m is often chosen (even if the elevation model is more accurate) because the snowpack smooths high-frequency terrain waves. The software system must therefore provide the ability to sample digital elevation models to the appropriate resolution for the process being modelled (Bartelt, et al., 2013) (Christen, et al., 2012).

5.1.2 Process Model and Model Parameters

The selection of model parameters remains one of the fundamental challenges for numerical computations in the field of natural hazards. Any process model needs a set of well-tested model parameters to simulate events with statistical confidence (Christen, et al., 2012). Process models based on physical principles, i.e., computer models controlled by parameters that map directly to terrain features and material properties, are of great benefit. This is rarely the case in natural hazards research, where models for snow avalanches, debris flows, and rock fall all require few but empirical parameters that vary from case to case (Berger, et al., 2011) (Christen, et al., 2012). This severely limits the scope of numerical software. Clearly, a numerical model cannot have too many parameters, as this, critically, limits user confidence and increases the possibility of applying incorrect values. Model continuity is another important factor in engineering practice. Otherwise, simulations have to be recalculated, leading to uncertainties and possibly legal problems (Christen, et al., 2012).

5.1.3 Numerical Solution

Today's computing capabilities and advances in software development are changing the way natural hazard problems are solved. However, many different applications require time and resources to learn and use efficiently. Hastily performed simulations without adequate sensitivity analyzes and parameter studies are not uncommon in practice. This may be in part due to the fact that many different programs must be mastered in order to perform an analysis efficiently. If it were possible to use the same software package for the analysis of different natural hazards, this effort could be minimized and, more

importantly, the risk of errors due to insufficient knowledge of the different software products could be reduced (Christen, et al., 2012).

5.1.4 Visualization

Engineers visualize dangers using a number of tools, including maps, pictures, 2D and 3D simulation results, XY plots, terrain profiles, and animations. Georeferenced data must be able to be imported and exported, and simulation results must be able to be overlain. This is essential for reporting, for the presentation of results to local and state agencies, and the ease of interpretation of simulation results by experts. The Visualization of the calculation results makes the numerical calculations transparent and easier to be undterstood by non-experts. The software must be able to export the results to other tools such as ArcGIS or GRASS for further processing of the data (Christen, et al., 2012).
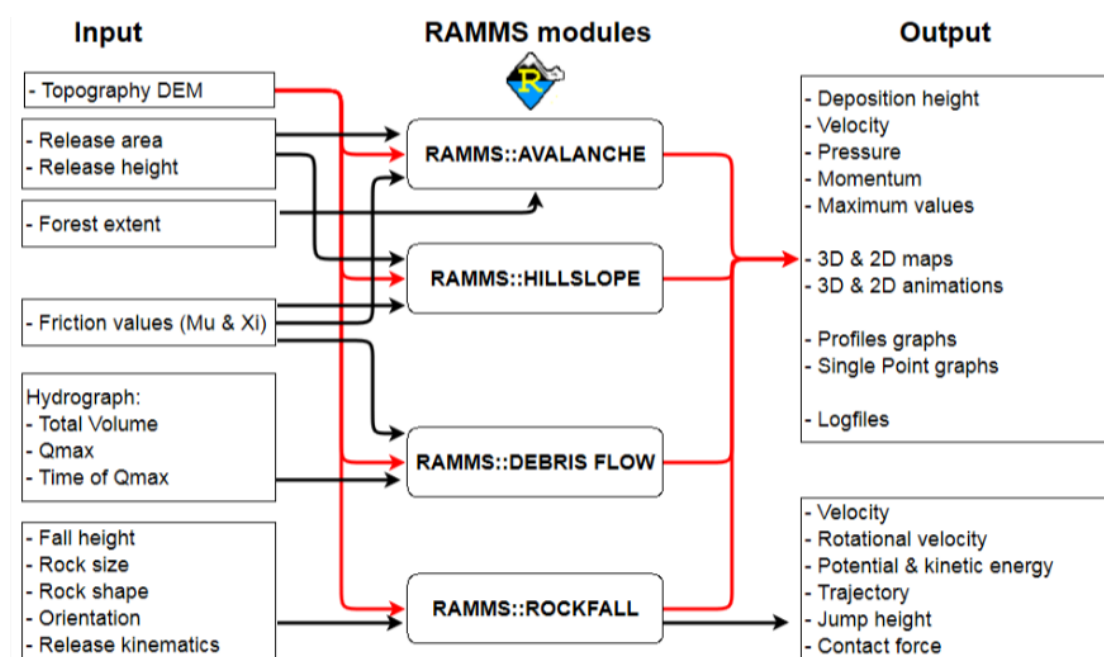
FIGURE 33 RAMMS PROJECT WORKFLOW SHOWING BOTH THE SPECIFIC AND UNIFIED INPUT AND OUTPUT FUNCTIONS FOR THE UNIFIED RAMMS MODULES (CHRISTEN, ET AL., 2012)

5.2 RAMMS::DEBRIS FLOW

RAMMS (Rapid Mass Movements) is a package that combines three-dimensional processing module for snow avalanches, debris flows, and rock falls with a protection module (forest, dams, and other structures) and a visualization module, into a single tool. The RAMMS debris-flow model is based on two-dimensional depth averaged shallow-water equations for granular flows in three dimensions, as determined by the coordinates of the digital elevation model's topographic surface in a Cartesian coordinate system (x, y, z), and at time (t) (Bartelt, et al., 2013) (Frank, et al., 2017) . The field variables flow height H (x, y, t) and flow velocity U are included in the mass balance equation (x, y, t)

EQUATION 14: $Q(x, y, t) = \partial t H + \partial x (H U x) + \partial y (H U y)$

Where Q(x, y, t) is the mass production source term and Ux and Uy are the depth-averaged velocities in the horizontal directions x and y, respectively (Christen, et al., 2010).

The depth-averaged momentum balance equations take into consideration the momentum conservation in both x and y directions:

EQUATION 15: $Sgx - Sfx = \partial t (H U x) + \partial x (C x H U^2 x + g_z K_{\frac{a}{p}} \frac{H^2}{2})$

EQUATION 16: $Sgy - Sf_y = \partial t (H U y) + \partial x (H U x U y) + \partial y (C y H U_y^2 + g_{2 k_{a|P}} \frac{H^2}{2})$

When using the standard Voellmy–Salm friction approach, the earth pressure coefficient ka/p is normally set to 1, cx and cy represent topographical coefficients determined from the digital elevation model, the effective gravitational acceleration is Sg, while the frictional deceleration in the x and y directions is Sf (Christen, et al., 2010). The Voellmy friction relation is used to calculate the flow's frictional deceleration (Salm, et al., 1990)Sf, which specifies the dry-Coulomb term (friction coefficient) scaling with normal stress and viscous or turbulent friction (coefficient) based on flow velocity U (Bartelt, et al., 2013) (Christen, et al., 2010)

EQUATION 17: $S_f = \mu * \rho * H g \cos(\varphi) + \frac{\rho g U^2}{\xi}$

Where is the overflowing surface's typical tension, The normal stress on the spilled surface is Hgcos(ɸ), where g is the gravitational acceleration, the slope angle, and the normal stress.

The resistance of the solid phase (the term containing) which influences the deceleration behavior of a more slowly moving flow can be described as the tangent of the effective internal friction angle of the flow material. For a faster flowing flow, the viscous or turbulent fluid phase (the word includes) has more resistance (Bartelt, et al., 2013).

The module RAMMS:: DEBRIS FLOW was developed to simulate the runout of debris flows in complex terrain (Graf & McArdell, 2011). The module can also be used to calculate impact pressures and flow heights for sizing engineering remedies. A second-order numerical solution of the depth-averaged

equations of motion for granular flows is at the heart of the program. Model results are produced and visualized on three-dimensional elevation data, just like the avalanche module.

Either a single or multiple block runoff areas or define a hydrograph can be chosen that allows the user to specify runoff and velocity as a function of time. RAMMS:: DEBRIS FLOW neglects erosion and entrainment at the moment, but algorithms to "inflate" are under development (Berger, et al., 2011). The model uses the two-parameter Voellmy fluid model (Voellmy, 1955) to describe the rheology of flowing debris, which has been useful in modelling debris flows. The Voellmy model describes the frictional behavior of the flow process based on Coulomb friction (μ) and velocity-squared turbulent friction (ξ). To calibrate the Voellmy model, users typically simulate well-documented historical events and determine the best-fitting parameter sets, applied in subsequent analyses. The ability to modify topography to include deposits from a previously modelled flood wave allows users to evaluate the influence of multiple flood waves on debris flow runout.

As for the input hydrograph, either measurements or estimates of discharge can be used, to shorten the computation time (as the area of the computational domain can be reduced) or increase the grid resolution by starting the model at a point below the initiation zone, e.g., at the apex of the fan (Christen, et al., 2012).

Project and Scenarios

For a certain area of interest, a project is defined. One or more scripts for analysis can be created within this. It is possible to calculate each possibility. As a result, each project situation has its own set of parameters. For each scenario, the topographic data that will be entered are going to be the same. The other input parameters, such as the release area, calculation area, calculation grid analysis, expiration time, and time step, might be different (Bartelt, et al., 2013).

Based on field data, potential model limitations, and past modeling experience with the RAMMS debris-flow model, the type of initial release mechanism, block release (e.g., landslide), or input hydrograph, can be determined. Depending on the representative debris flow , the simulation's starting conditions can be chosen. Discriminating the non-channeled and channeled debris flows is important. Hill flows or shallow landslides are examples of non-channeled flow streams, whereas channel runoff flows occur when material follows the torrent channel. A release area with a set initial depth is beneficial for tiny flow streams without piping, while a hydrograph may be more appropriate for flow streams with flow. It is useful to create a release region with a particular initial depth for small flow streams without pipe, but a hydrograph may be more suited for flow streams with flow. The simulation findings are heavily influenced by the release sites and depths. Hydrograph simulations have the similar behavior. To map release areas, reference data such as pictures, GPS measurements, or field maps should be used, and measured or well-estimated input data should be used to generate discharge hydrographs (Bartelt, et al., 2013).

In the RAMMS Run Simulation window the calculation settings could be changed, such as the output name, simulation grid resolution, simulation time (end), time step, and so on. Before the simulations begin, it is recommended that you specify some preferences to manipulate the files easier. The workplace, as well as the area of relief data, maps, and orthophotos, are all defined by preferences. When you create a new project, RAMMS will automatically open the georeferenced data if the path to maps and image files is appropriately configured in the options (Bartelt, et al., 2013).

Input Hydrograph

It is desirable to utilize an input hydrograph to model channelized debris flows. This, however, necessitates information of the volume of material (discharge) flowing past a specific point. There are two possibilities for a RAMMS simulation with a hydrograph. Whether the discharge at different times at a given site is known, for example, by measured flow heights and matching channel cross sections, or whether the estimated total volume may be utilized in conjunction with empirical relationships between total volume and maximum discharge (Bartelt, et al., 2013).

Field measurements of debris flow parameters are beyond the scope of this manual; however, if debris flow activity in a catchment is regular, constructing a monitoring station may provide extra information for RAMMS calibration. When the monitoring data is simplified, many debris flows have a basic triangular wave-like structure (Bartelt, et al., 2013).
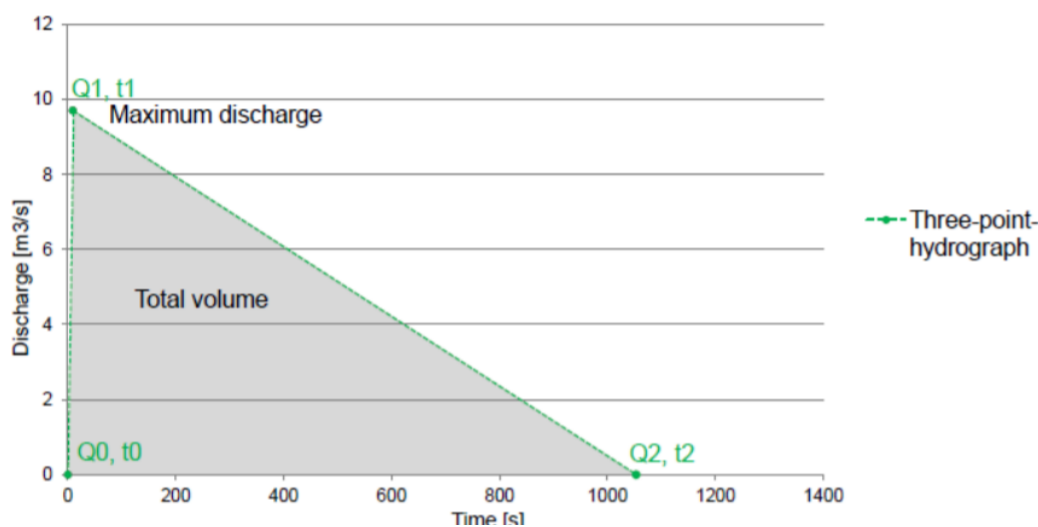
FIGURE 34 TOTAL VOLUME OF DEBRIS FLOW ON A THREE-POINT HYDROGRAPH (BARTELT, ET AL., 2013)

The maximal debris flow discharge (Q) and corresponding time (t1), as well as the end time (t2), can be computed using a well-estimated total volume (e.g. field data). A three-point hydrograph computation is what it is called. Four points often describe discharge hydrographs in nature. After the maximum discharge, however, a three-point hydrograph results in somewhat higher flow heights and velocities. If the detailed

discharge hydrograph is unknown, a three-point hydrograph can be used. Users should examine the sensitivity of model outputs to the form of the input hydrograph in essential applications, such as when preparing different scenarios as a foundation for danger maps (Bartelt, et al., 2013).
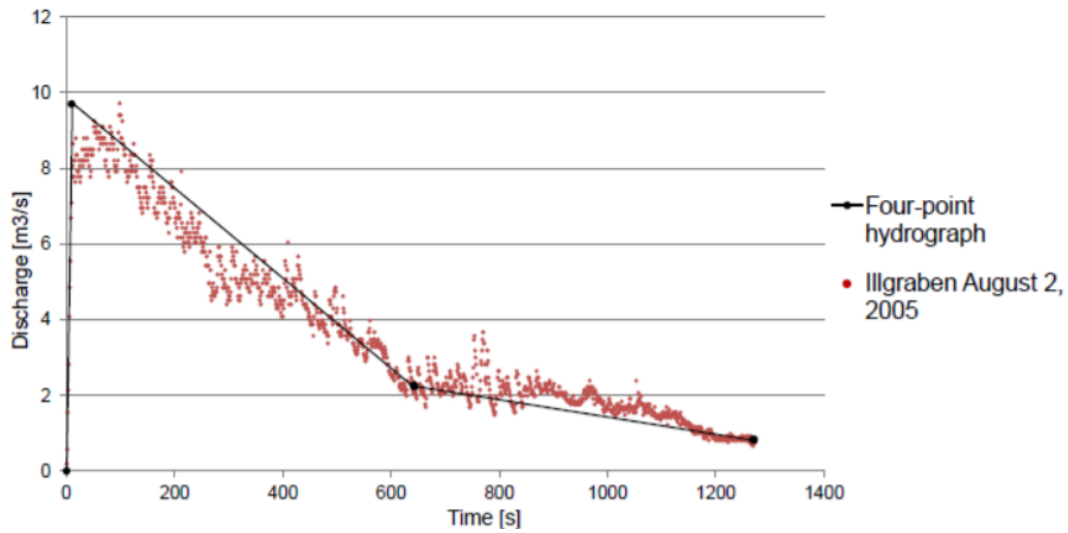
FIGURE 35 FOUR-POINT HYDROGRAPH INDICATING DISCHARGE VALUES OF AN EVENT, ILLGRABEN, VALAIS, SWITZERLAND, AUGUST 2, 2005 (BARTELT, ET AL., 2013)
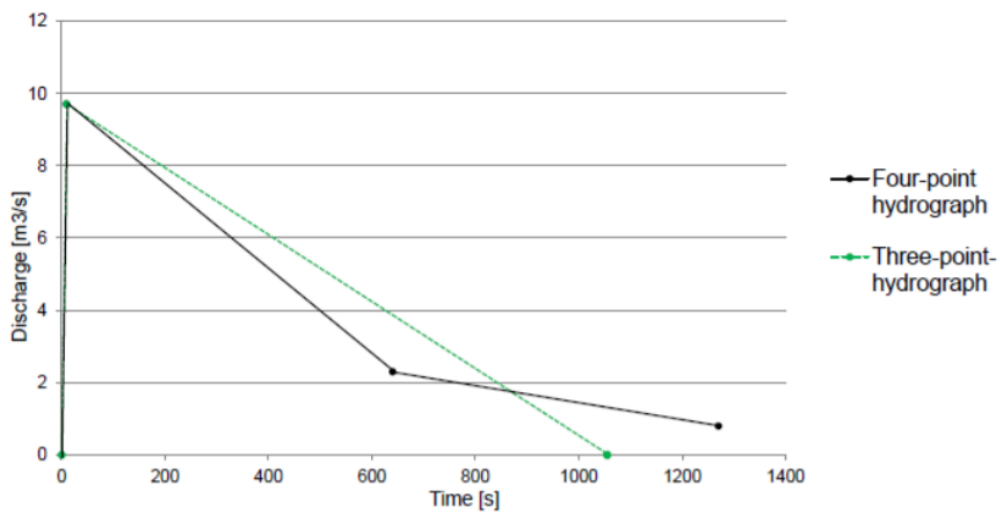
FIGURE 36 COMPARISON OF A THREE-POINT AND A FOUR-POINT HYDROGRAPH FOR THE SAME TOTAL VOLUME DISCHARGE DATA (BARTELT, ET AL., 2013)

The RAMMS model has been used extensively throughout Europe (particularly in the Alpine region), with applications in South America and Asia also being considered. Furthermore, RAMMS was used to predict very tiny debris flows (i.e. 1,000 m^3 or less) to extreme debris flows with magnitudes exceeding a few of million m^3. In most situations, the simulation resolution was very high, especially when substantial debris flow magnitudes were involved, with resolution ranging from less than 0.5 m to 20 or 30 m. The resolution was usually between 2 and 5 meters in most circumstances. The Voellmy-fluid friction parameters also encompassed a wide range of values. Only a few case studies employed the parameters above the line connecting the end points: ($\mu = 0$, $\xi = 1,400$ m/s^2) ($\mu = 0.65$, $\xi = 0$ m/s^2). They stayed generally within the parameters suggested by Scheidl et al. (2013) as typical for debris flows. The Dry-Coulomb type friction parameter (Mu) was measured and ranged from less than 0.001 to 0.7. This parameter's value was usually around 0.1 or 0.2. The viscous-turbulent friction parameter (X$_i$) was measured in millimeters per second and ranged from 10 to 2,000 millimeters per second. Its most common value was between 200 and 500 m/s^2.

With increasing the magnitude of the debris flow reduces slightly and increases slightly, respectively. However, no significant link was discovered. The RAMMS model has been utilized for a number of purposes, including modeling of glacial lake outburst floods, as shown in the table 9 (Miko ˇs & Bezak, 2021).

CHAPTER 6

6.1 Method and Materials

In 2017, a disastrous incident occurred in the Mandra district of Attica, which began with severe and brief rainfall and finished with a stream of debris. As a result, the proper research teams visited the area and collected various data. The gathered information included rainfall amounts and, as a result, debris flows and disaster-related mortality. Based on the collected data, maps and diagrams were created that analyze the spatial distribution of rainfall, the distribution of flow time, climatic data, erosion and sediment deposition sites, etc.

A high-intensity convective storm, exacerbated by orographic effects, dumped up to 300 mm in 13 hours in the Agia Aikaterini and Soures catchments at the foothills of Mt. Pateras in Western Attica, with 153 and 194 mm of basin-average total accumulation in the Agia Aikaterini and Soures catchments, respectively. Observations from NOA's high-resolution XPOL radar enabled the collection and study of the flash flood triggering storm's space-time variability, which would have been impossible to see with existing in-situ sensors as they were all located well beyond the event's core.

In two small ephemeral catchments drained by the two tributaries of the Soures stream, the storm generated a swift and severe response. In compared to the catchment area of the two torrents, the flood generated inundation of notable depth (up to 4.2 m) and extent (4.03 km^2) (42.33 km^2). The unit peak discharge in both basins was around 9–10 m^3/s/km^2, which is within the range of values reported for past extreme flash flood events. Significant consequences were recorded over the flooded area, with 24 fatalities, but with varying degrees of diversity, spatial distribution, and typology among the many contexts (rural, urban, and industrial) that were impacted. The 2017 flood was a highly rare event (in the range of centuries, if not more) in the area, according to all available evidence, including meteorological, botanical, and geomorphological data. More research should be done in order to accurately identify the event's return period (Diakakis, et al., 2019).

The slope-conveyance method has traditionally been used to assess discharge (Gaume & Borga, 2008). The Gauckler-Manning type was used to conduct surveys at the intersections of Soures and Agia Aikaterini, assuming a consistent flow (Manning, 1891). A comprehensive Digital Surface Model (DSM) with a resolution of 2.7cm was constructed in these two places using the Structure from Motion technique (SfM). The detailed DSM was utilized to extract a vertical cross section and determine the cross sectional area and wetted perimeter. The Cowan (1956) method was utilized to determine the Manning n coefficient using the Arcement and Schneider (1989) and Phillips and Tadayon (2006) approaches (Andreadakis, et al., 2018). Flood extent was calculated from color photos by digitizing the borders at the contrasting land surface / water boundary, thanks to the high quality of the imagery and video. High water marks such as: (a) lines of dried mud on surfaces, (b) leaves / pine straw stuck on various places (e.g. tree limbs), (c) seed lines, (d) wrack / debris lines, and so on were measured systematically at various parts of the flooded area, with an emphasis on the town of Mandra, where high water marks such as: (a) lines of dried mud on surfaces, (b)

leaves / pine straw stuck on various places (e The IDW algorithm was used to interpolate point values inside the inundated area after the maximum water level was recorded at point locations using the HWMs identification (Andreadakis, et al., 2018).

In the present work, the pre-existing data and results were considered to simulate the debris flows in the program Rapid Mass Movement Simulation (RAMMS). Existing requirements included whether this program's simulation of debris flows will be represented by modest deviations from existing maps. A hydrograph was used where the necessary parameters are the total volume (Vol), the maximum discharge (Q_{max}), the time (t_1) at which the maximum discharge occurs and the velocity (v). Giandotti's and Manning's formula were used to calculate these parameters. The total runoff volume (V_{ol}), calculated by multiplying the rainfall height by the upstream area, and the velocity are common parameters in both calculations of both models.

Giandotti's equation (Grimaldi, et al., 2012)**:**

The general equation is:

EQUATION 18: $Tc = \frac{4\sqrt{A}+1.5L}{0.8\sqrt{H}}$

where Tc is the time of concentration (h); A the watershed area (km2); L the length of the main channel (km) ,and H the difference between the mean basin elevation and the outlet elevation (m).

Multiplying the rain's height by the area of the upstream basin yields the total volume of runoff. Furthermore, in all cases, the velocity remains constant. As a result, the maximum discharge equation is used to calculate the velocity equation.

Peak discharge is commonly calculated using morphological and hydrological factors from the watershed, according to Giandotti's method. The following is the formula for the equation (El-Hames, 2012):

EQUATION 19: $Q_P = \alpha R^b M^c$

Where R is a rainfall-related parameter that may reflect watershed moisture state; M is a catchment-related parameter, and a, b, and c are empirical constants that can be derived through calibration using specific data.

Giandotti's equation takes the effect of relief from the average height into consideration. Giandotti's equation takes into account the effect of relief from the average height since the two empirical connections utilize a different index to reflect the influence of relief on the basin's response time (Αντωνιάδη, 2016).

The slope-area measurement is the most commonly used indirect measurement technique for determining peak discharge, according to Manning's Method. The discharge is calculated using a uniform-flow equation that includes channel parameters, water-surface profiles, and aroughness or retardation coefficient (Bhattaral, et al., 2015).

The Manning equation is the most often used equation for calculating uniform open channel flow (Chow, 1955) (Fischenich, 2000)

EQUATION 20: $Q = \left(\frac{1.49}{n}\right) A \left(R_h^{\frac{2}{3}}\right) S^{1/2}$

Where Q denotes the volumetric flow rate going through the channel; A is the flow's cross-sectional area in feet squared normal to the flow direction; S is the channel's bottom slope in feet per foot (dimensionless); n the Manning Roughness coefficient is a dimensionless empirical constant; The hydraulic radius is R_h = A/P

For a constant flow rate of water through a channel with constant slope, size and shape, and roughness, uniform open channel flow (which is required for use of the Manning equation) occurs. For a constant flow rate of water through a pipe of constant diameter, surface roughness, and slope, uniform partially full pipe flow occurs. The water will flow at a constant depth under these conditions. The slope of the hydraulic grade line is denoted by S. Because the depth of flow is constant in uniform flow, the hydraulic grade line slope is the same as the liquid surface slope and the channel bottom slope. In the Manning equation, the channel bottom slope is usually utilized for S (Bengtson, 2017).

Given the approximations used in the derivation of this formula and the ambiguity around the value of n, it appears that carrying the numerical coefficient, 1.486, to more than three significant figures is not justified. A value of 1.49 is suggested as being sufficiently precise for practical use. It should be noted that a number of recent publications have justified the form and embraced the proposed value.

RESULTS

As straightforward step, the model was calibrated using local hydrograph data. During the calibration procedure, the interrupt settings remained consistent, with the values being the same as in the program guide. The hydrograph values used were not the same. These figures were calculated using the Manning and Giandotti methods. The Giandotti method required only one data entry, whereas the Manning model required four distinct calculations and four different data types. The purpose was to assess the outcomes based on the damage maps that had already been established.

	V (m³)	Q (m³/s)	Tp (s)	A (m²)	n	V (m/sec)	Height Maximum (m)	Pressure Maximum (kPa)	Velocity Maximum (m/s)
Giandotti	474.625	89.68	3.168	SfM		2.17	**1.03**	27.94	**3.74**
Manning	474.625	195.99	3.168		Sfm optical granulometry	4.76	1.04	27.75	**3.73**
Manning	474.625	127.0	3.168			3.08	1.06	27.87	**3.73**
Manning	474.625	357.82	3.168			8.69	1.09	27.54	3.71
Manning	474.625	231.87	3.168			5.63	**1.03**	27.98	**3.74**

*A results from structure for motion (Giandotti)
* n results from structure for motion and optical granulometry (Manning)

The hydrographic data entered into the software using the giandotti and manning formulas is shown in Table 10. The two formulas appear to have two same results of maximum height. Furthermore, the two formulas seem to have two identical values of maximum velocity and Manning's formula two identical values of maximum velocity as well. Besides, at maximum pressure all values have small deviations.
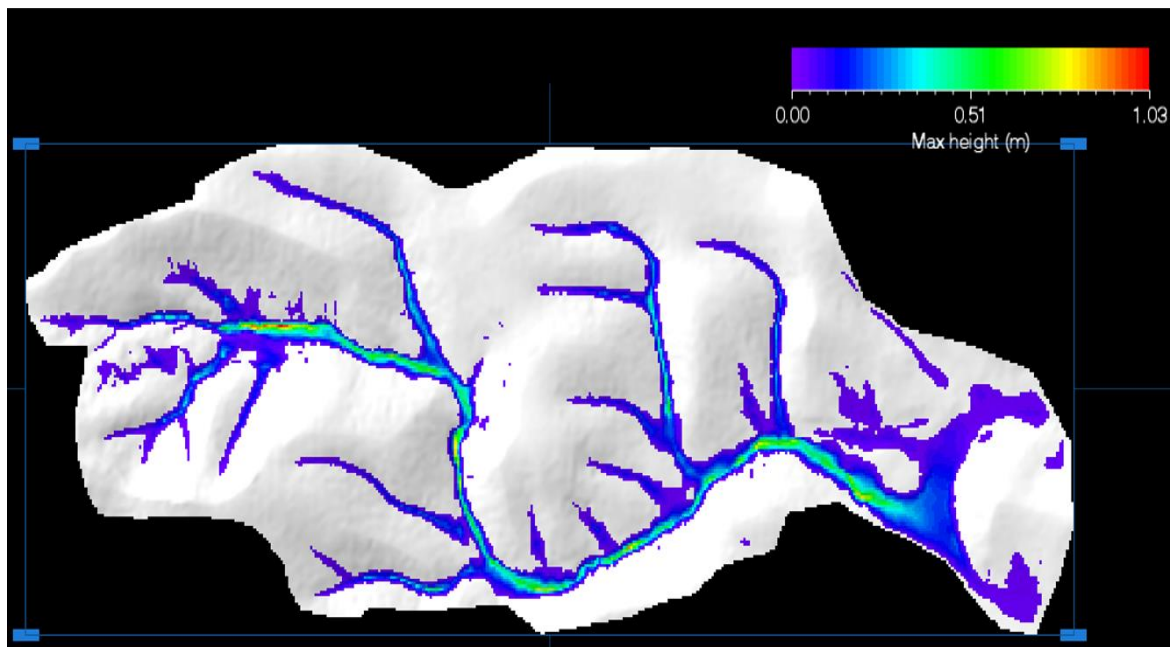
FIGURE 37 MAX HEIGHT- GIANDOTTI :V_{oL}(M^3)=474.625, Q_{MAX}(M^3/S)=89.68, T_P(S)=3.168, V(M/S)=2.17

The maximum height can be up to 1.03 meters depending on the scale and the entered data. Representative, low values appear to be highlighted by light purple to light blue colors,while, moderate ,and high values are depicted in green and yellow to red, respectively.
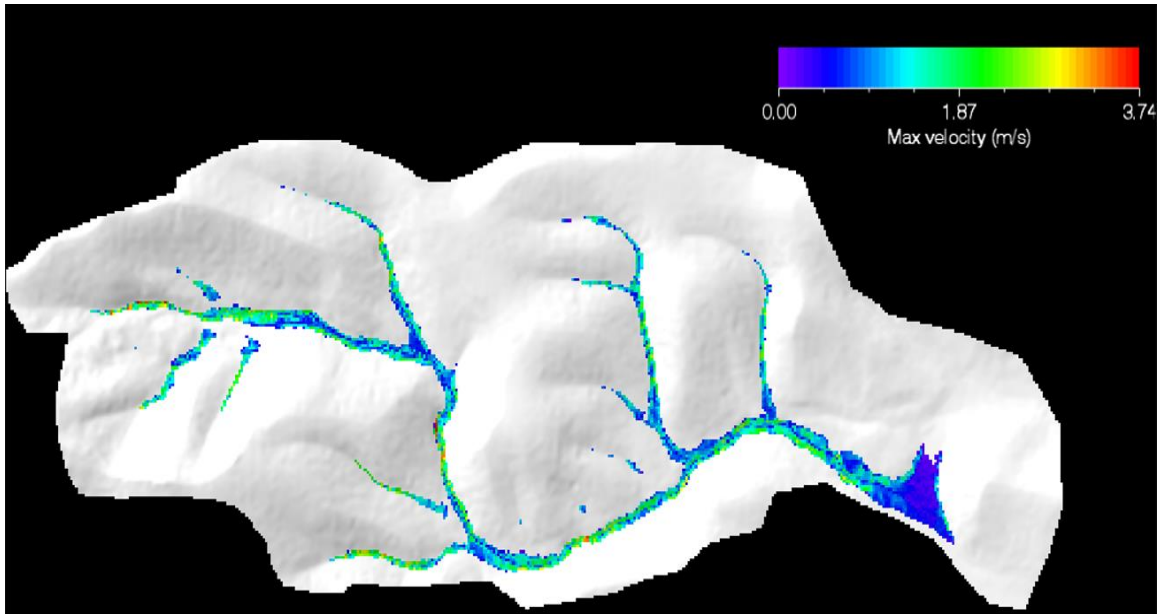
FIGURE 38 MAX VELOCITY- GIANDOTTI

Similarly, the colors of the scale are illustrated based on the entered data. Low values are represented by light purple with light blue color, middle and high values are depicted in green and yellow to red, respectively. It is reffered to the maximum velocity, which is 3.74 m/s. There is a big percentage of values ranging from 1 m/s to 2.5 m/s right from the beginning. In fact, there are low values in some locations where they are clearly visible when approaching Mandra city.
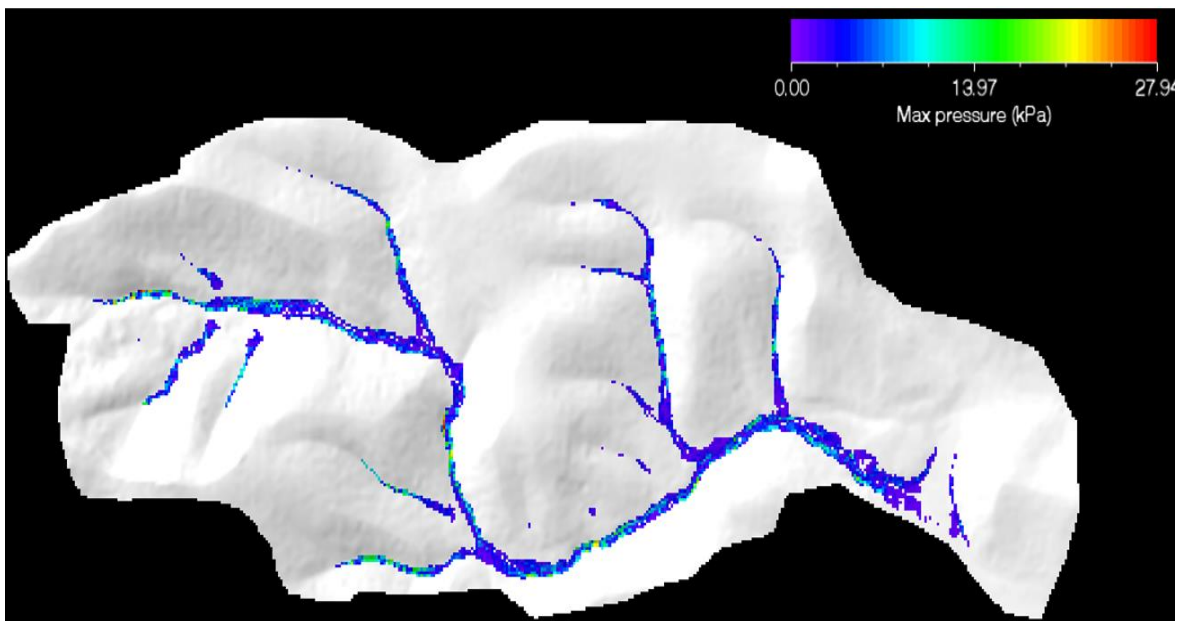
FIGURE 39 MAX PRESSURE- GIANDOTTI

The scale's colors reflect what has already been stated. The pressure hits its highest point of 27.94 kPa. The pressures are generally moderate, yet there are isolated areas with medium and high pressures. The pressure and velocity relationship is inversely proportional; the lower the pressure exerted by a fluid (liquid or gas), the higher its velocity.

The second scenario was created using the manning formula, and three separate sub-scenarios were created.
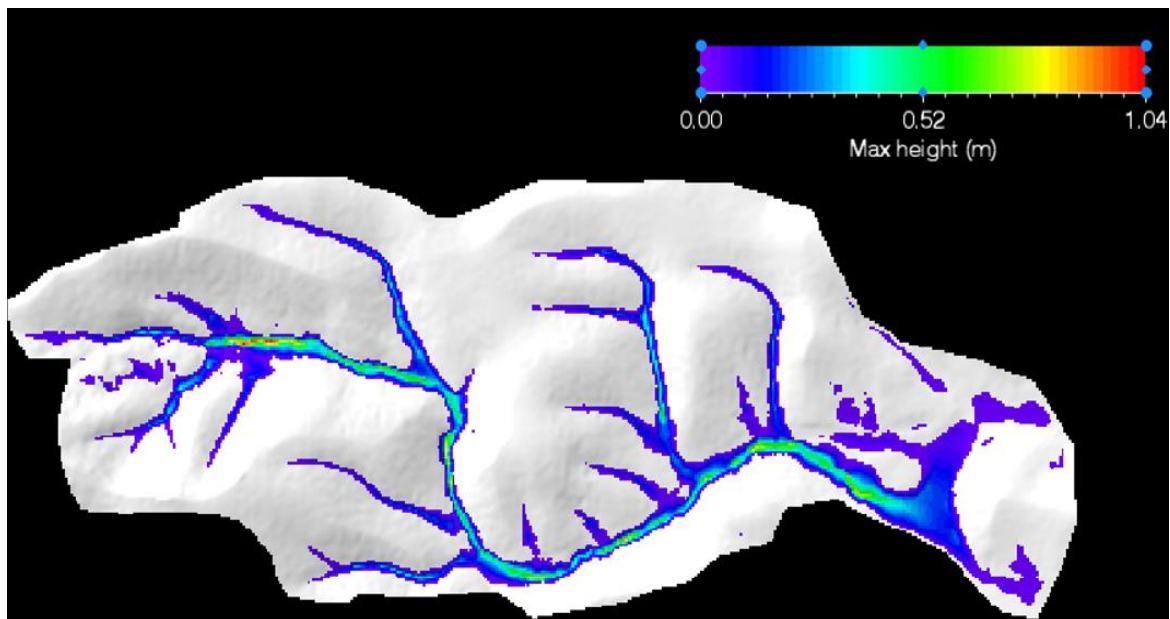
FIGURE 40 MAX HEIGHT - MANNING 1: $V_{OL}(M^3)$=474.625, $Q(M^3/S)$=195.99, $T_P(S)$=3.168, $V(M/S)$=4.76
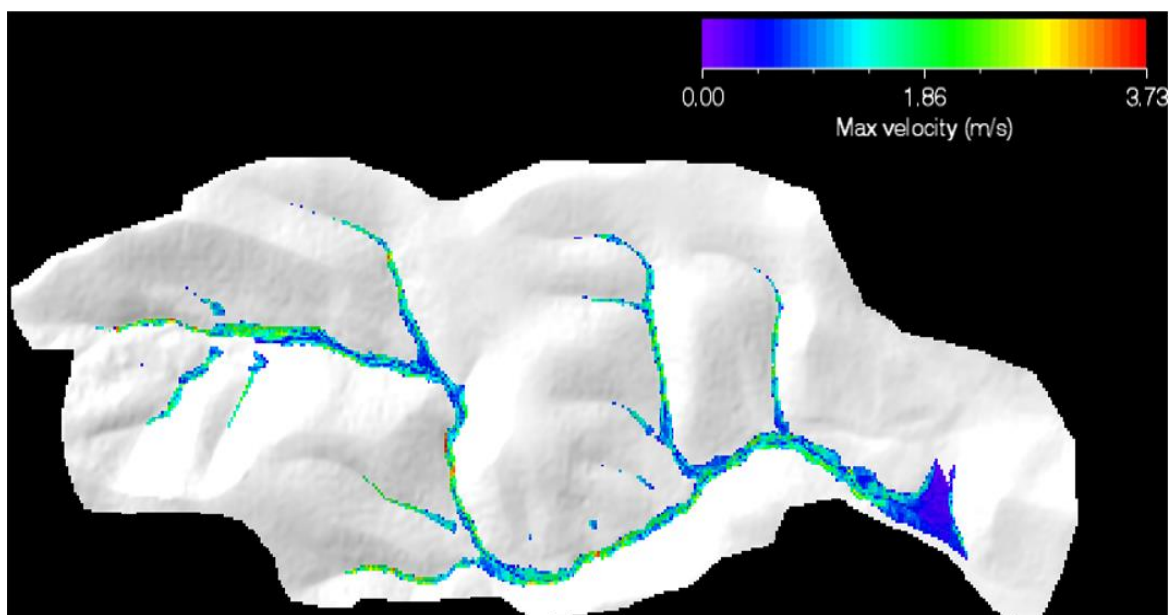
FIGURE 41 MAX VELOCITY- MANNING 1
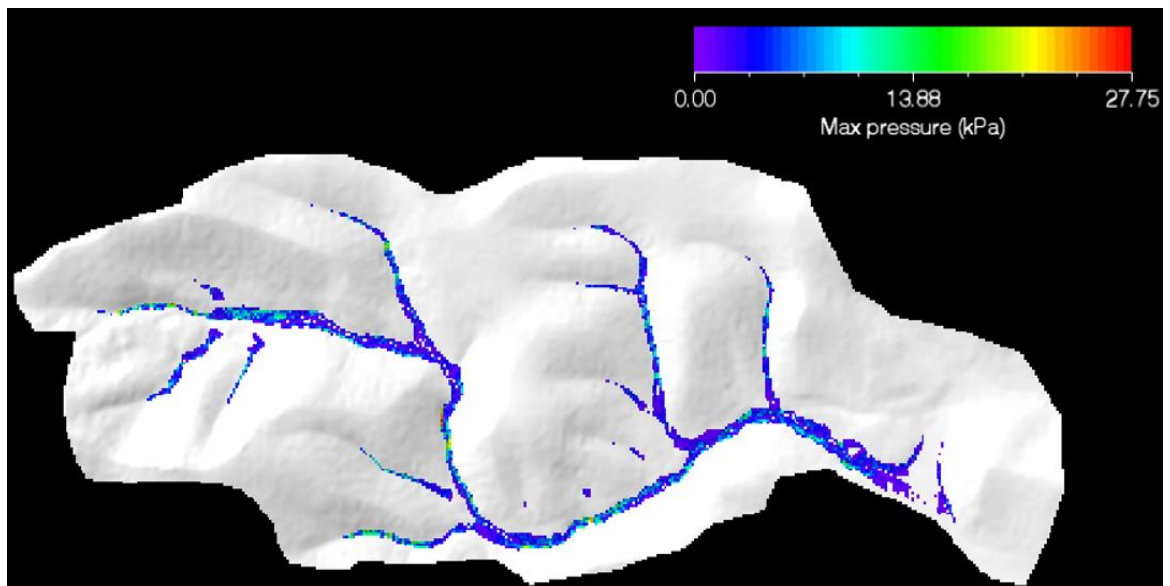
FIGURE 42 MAX PRESSURE- MANNING 1
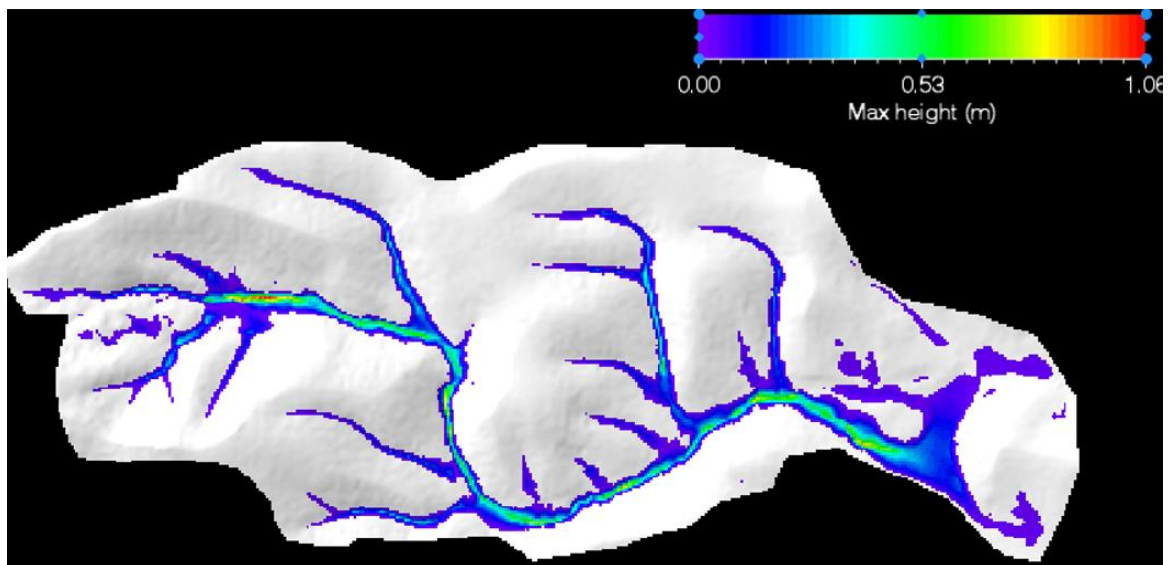
FIGURE 43 MAX HEIGHT- MANNING 2: $V_{OL}(M^3)$= 474.625, $Q_{MAX}(M^3/S)$=127, $T_P(S)$3.168, $V(M/S)$=3.08
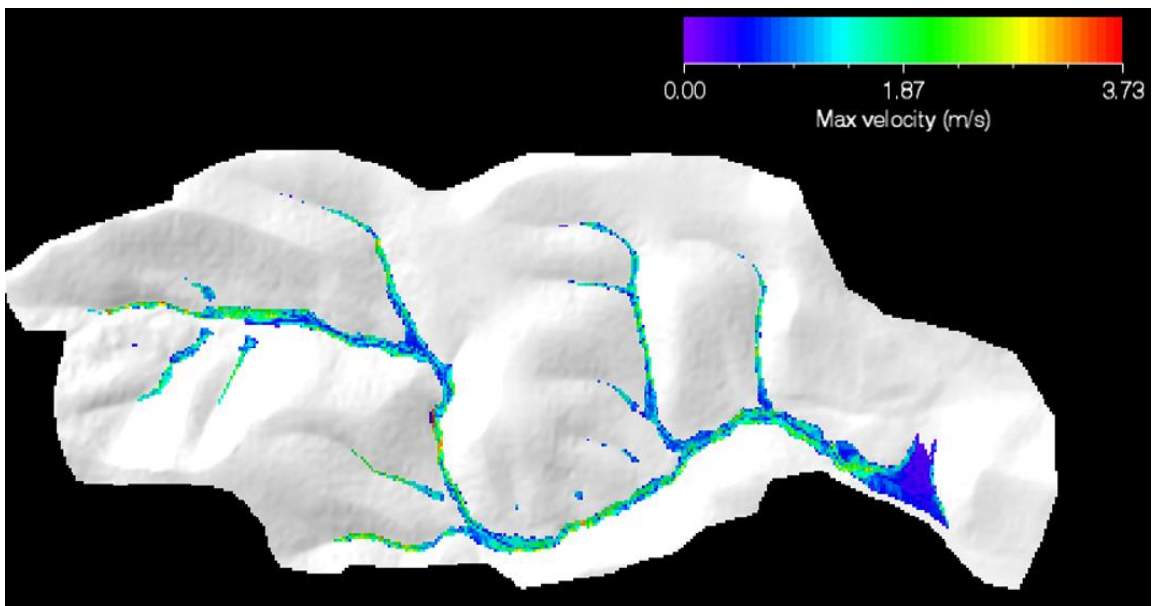
FIGURE 44 MAX VELOCITY- METHOD OF MANNING 2
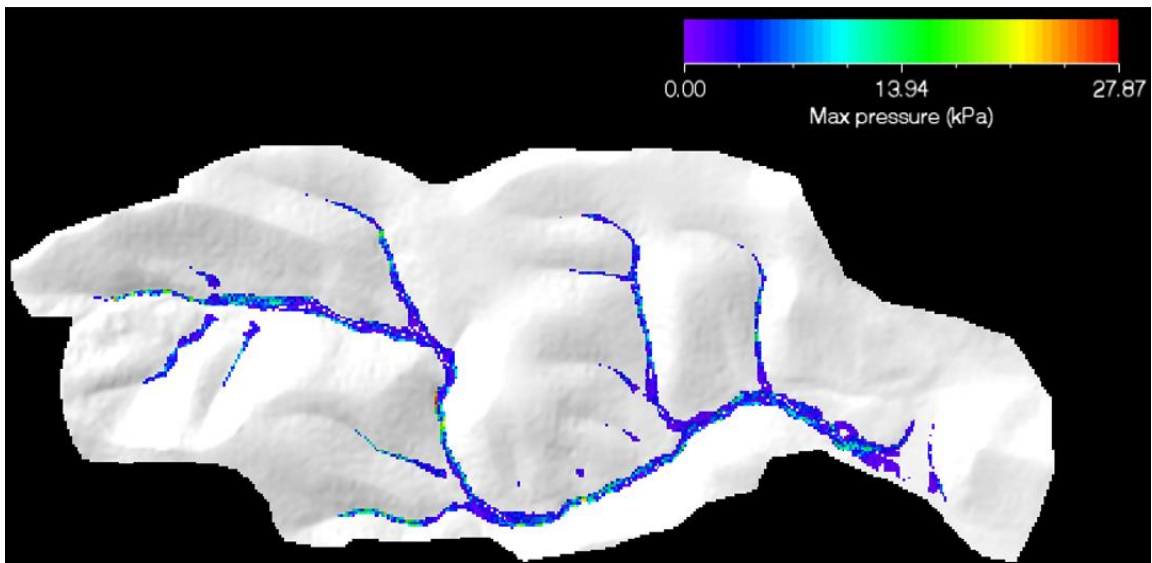
FIGURE 45 MAX PRESSURE-METHOD OF MANNING 2
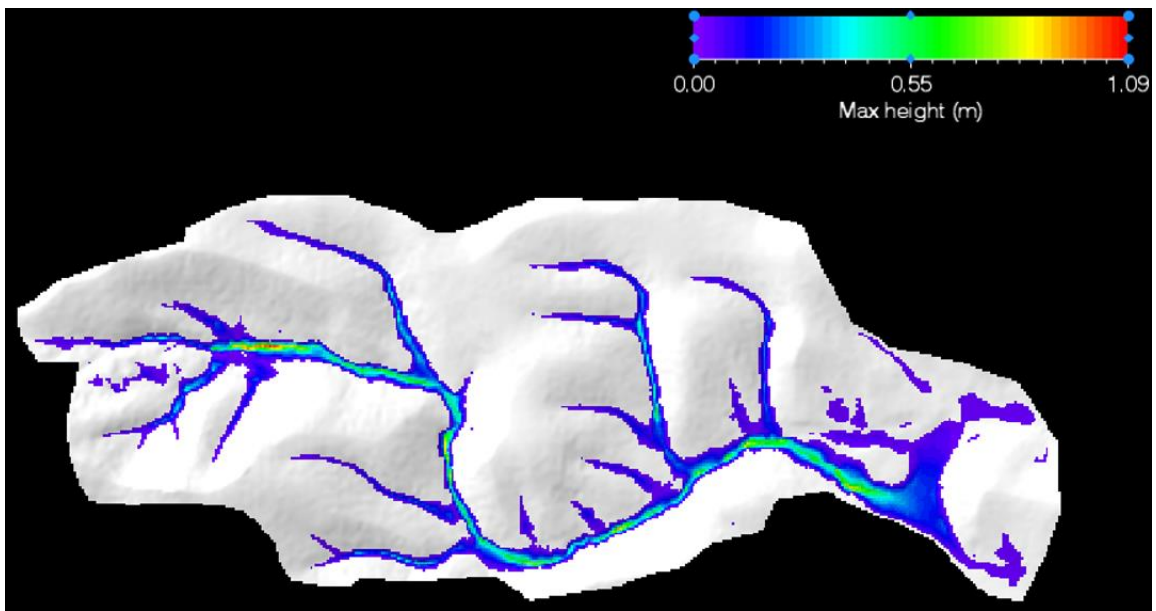
FIGURE 46 MAX HEIGHT-MANNING 3 : $V_{OL}(M^3)$=474.625, $Q_{MAX}(M^3/S)$=357.82, $T_P(S)$=3.168, $V(M/S)$=8.69
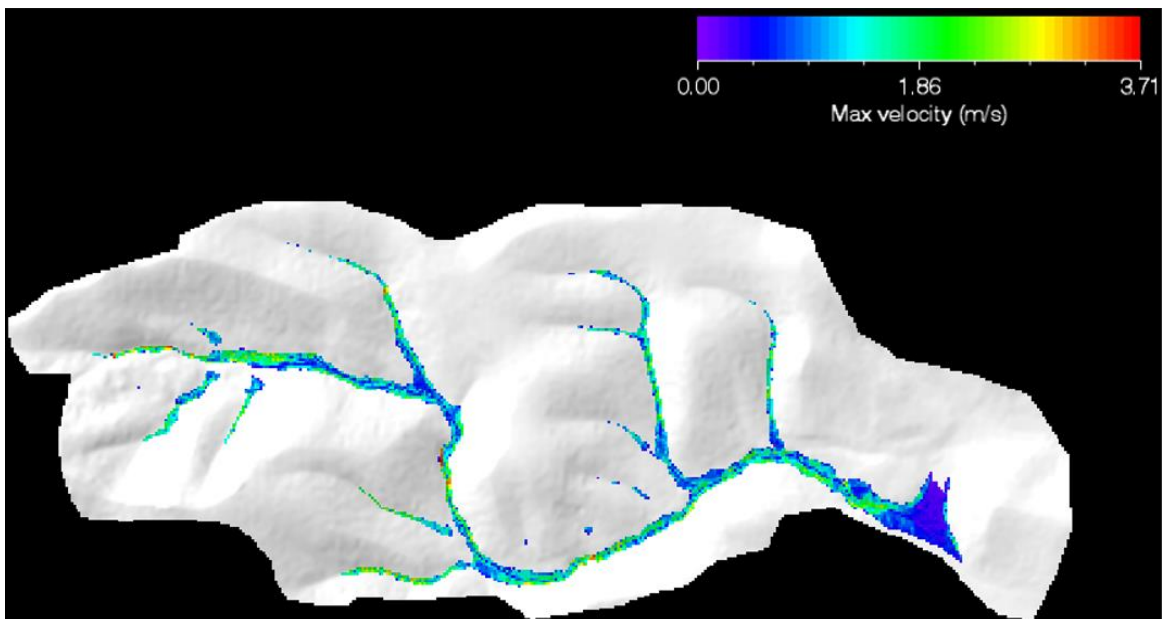
FIGURE 47 MAX VELOCITY- MANNING 3
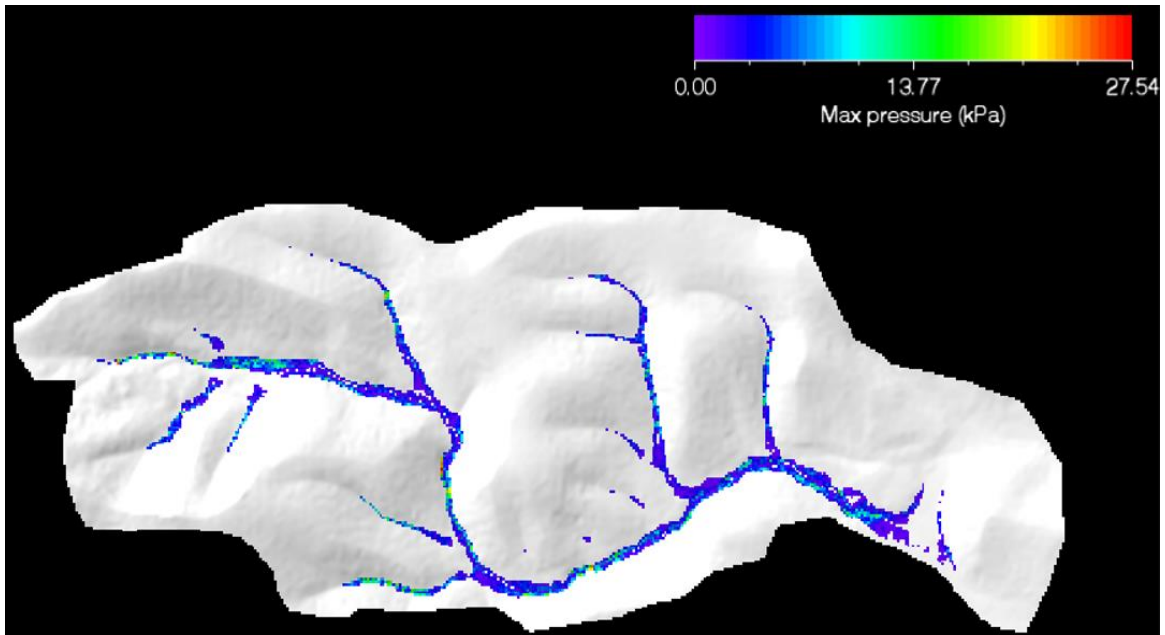
FIGURE 48 MAX PRESSURE- MANNING 3
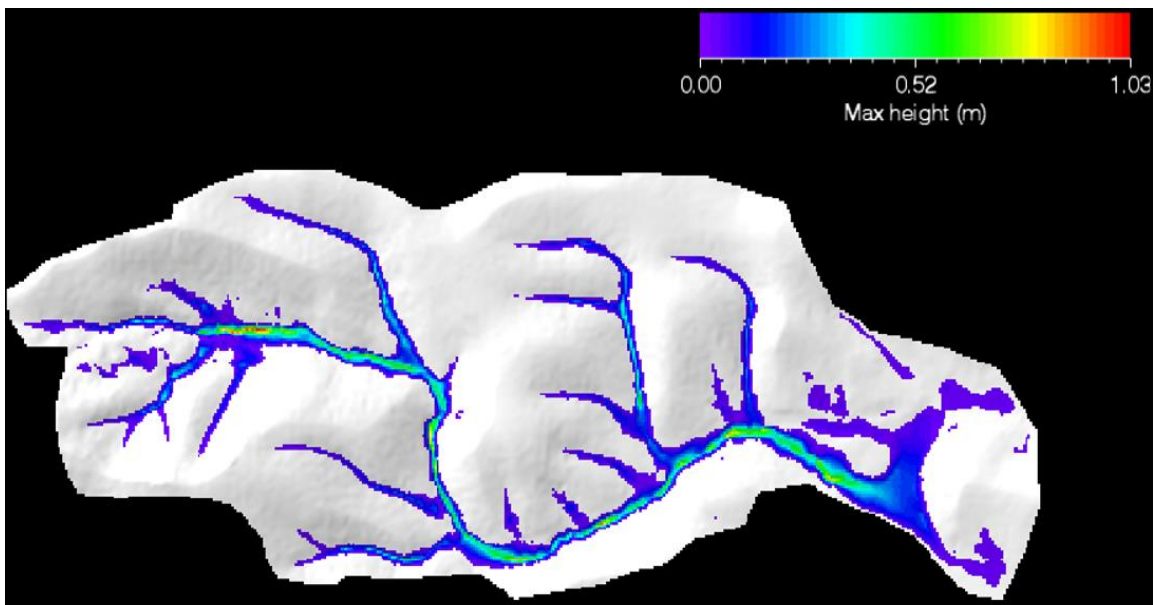
FIGURE 49 MAX HEIGHT- MANNING 4 : $V_{OL}(M^3)$=474.625, $Q_{MAX}(M^3/S)$=231.87, $T_P(S)$=3.168, $V(M/S)$=5.63
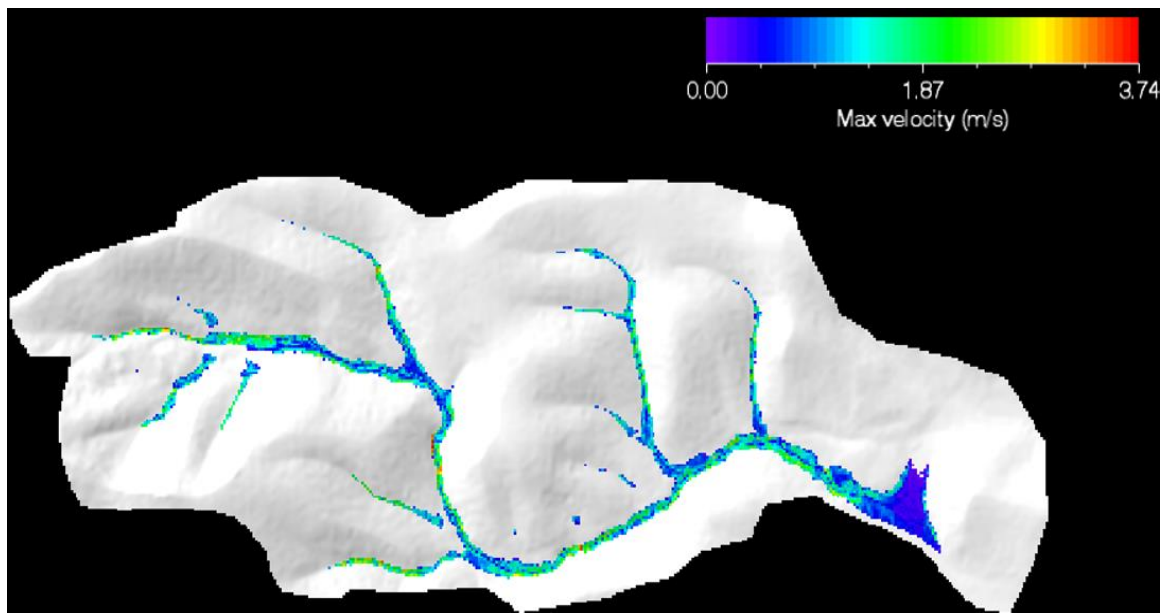
FIGURE 50 MAX VELOCITY- MANNING 4
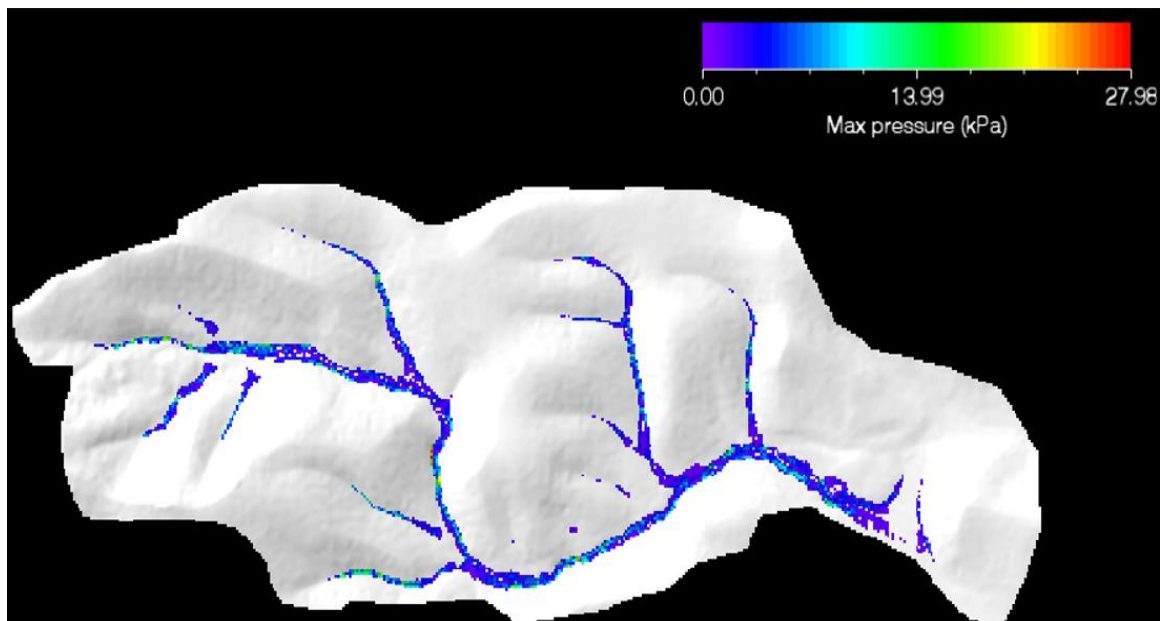
FIGURE 51 MAX PRESSURE- MANNING 4

The fundamental issue with the block release is that in comparison to field data, the initial flow depth, width, or length of the initial landslide can be unreasonably significant. Because most models do not account for entrainment along the channel course, users are forced to utilize unrealistically huge landslide volumes. The total debris-flow volume, which is normally measured in the deposition zone, is frequently employed as the initial landslide volume, obviating the possibility of channel-bed erosion and bulking (Frank,

et al., 2015). The RAMMS input hydrograph beginning condition was designed to help users avoid this difficulty by allowing them to specify a debris influx as a function of time at a lower location in the watershed (e.g., just above the fan apex) (Frank, et al., 2017).

By establishing a specified block release height based on a pre-defined release area, the block release volume may be determined. The model assumes that the landslide will fail instantly. Using an automatic mechanism in RAMMS, the initial landslide surface elevation is then set to the initial elevation of the land surface. In comparison to a landslide "block" positioned on top of the ground surface, the main advantage of this approach is that it hampers unrealistic lateral spreading of the initial landslide mass.

DISCUSSION & CONCLUSIONS

The present thesis examines the terrible flood that occurred in Mandra, in November 2017. Following the event's conclusion, measurements were taken using a plethora of techniques. The occurrence in the Agia Aikaterini stream has resulted in this scenario. Debris flows and floods developed in droves in the area that received the most rain, resulting in soil saturation. For this well-documented instance, the RAMMS program examined. The hydrograph was utilized as a calibration parameter, which is an objective evaluation of the model's performance, i.e., a reliability index that can indicate the results' accuracy.

The calibration of the two Voellmy friction coefficients, as well as the use of the Voellmy friction model as pointed out here in gravitational mass flow modeling (e.g. debris flows), is always necessary. The rheology of a debris flow, and hence the Voellmy friction coefficients, will vary based on the material composition (fluid-like or granular). Furthermore, friction is expected to increase as volume increases due to momentum loss during erosion processes. The inflow rates of the material can control the shape of the flowing body, and input hydrographs are based on field-measured discharge hydrographs or rebuilt using empirical correlations. It is thought that the hydrograph depicts more realistic initial conditions for channelized debris flows. Also, because the input hydrograph can be positioned further down the channel and the computation domains are smaller, input hydrograph simulations require less time to calculate. The simulations clearly show that the flow takes place in the same locations that were previously mapped in another study, as it can be seen in the graphic below. The areas where there was a lot of debris flow may be clearly seen. There are relatively slight differences between the Giandotti and Manning formula.
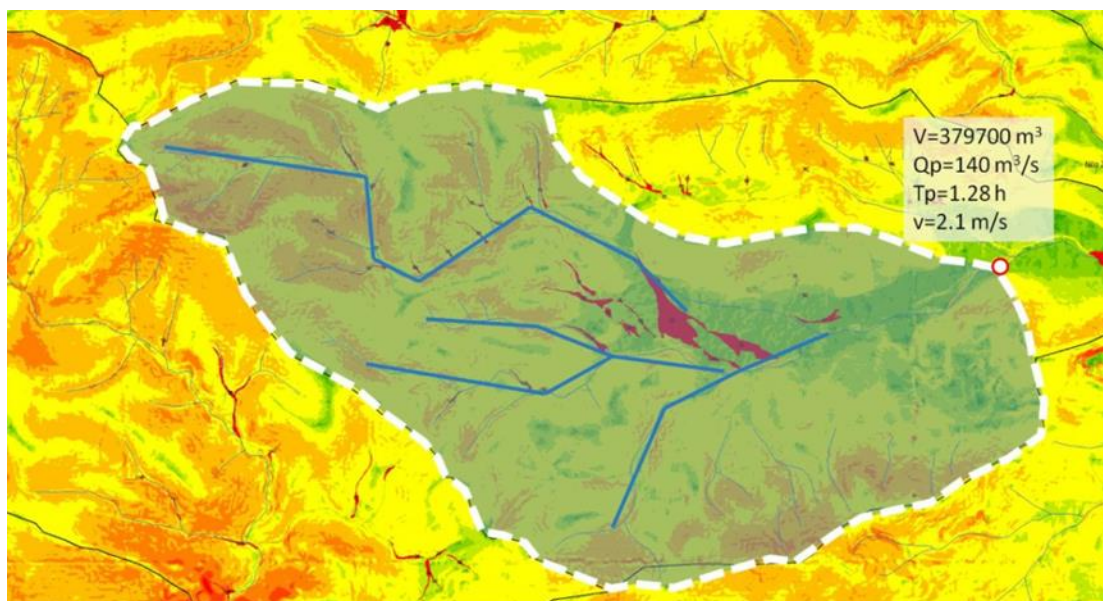
FIGURE 52 STREAM OF AGIA AIKATERINI

The Giandotti and Manning equations for hydraulic data are capable of modeling real debris flow events. Subsequently, enhancements are possible a hydrograph based on the used genuine discharge hydrographs. This simulation research included an evaluation and confirmation of how it is represented in

the program based on precedents. This includes flow parameters such as, maximum velocity and maximum pressure that have been measured and mapped. The new findings show that their simulation closely resembles previously published results. This includes the effect of the hydrograph on velocity, flow rate, and pressure over time. The debris flows movement and deposits seem to be very similar to what has been seen in the field. A hydrograph, or measurement of flow depth over time, demonstrates small changes in the Katsimidi stream. A discharge hydrograph with a volume of 474.265 m^3 was created. Based on what has been reported, the Voellmy friction coefficients (μ and ξ) are anticipated to be volume dependent and change as the volume increases. We expect that a larger volume will be required since a significant amount of momentum will be lost due to substantial re-working and entrainment of partially-dry sediment deposits (unusually, in comparison to general landslide literature assumptions). More field-based data on large-volume debris flows is required to examine the influence of volumes on the debris flow behavior of a and the selection of suitable Voellmy friction coefficients (Graf & McArdell, 2011).

The simulation appears to accurately depict the points of the area with the most significant debris deposition in this scenario. Furthermore, in our simulations, the entire 474.625m^3 volume is instantly released. We exclude that debris flows frequently occur in numerous smaller surges, and that material is entrained and accumulated as it goes down the channel, resulting in an increase in volume during the event. After a hydrograph was used, the material flowed in the area at a slower rate but for a longer period of time, and the discharges were chosen based on the projected duration of the event. However, it's likely that the Voellmy friction coefficients are volume dependent and will change as the volume increases. Good data are needed to choose the right Voellmy friction coefficients. The parameters of = 200m/s2 and = 0.25 have remained unchanged from the program guide in this example. When employing the RAMMS debris flow runout model without entrainment modeling, the most convincing modeled flow parameters (front travel time and hydrograph shape) can be obtained using Voellmy friction coefficients of = 200 m2s^{-1} and = 0.20 (Frank, et al., 2015). Flow velocity is affected by both features. Throughout the deceleration phase, has an inverse connection with velocity and exerts his effects after the peak velocity has been reached. The sensitivity of flow velocity to minimal, and a 100% change in the parameter causes velocities of 1-2 m/s at the fan apex (Simoni & Graf, 2012).

The turbulence parameter has a significant impact on the behavior of the simulated flow in the depositional area. In reality, the rate of deceleration rises as the flow slows down. Turbulence has been shown to have a complex impact. It offers exceptional velocity and acceleration/deceleration control over the flow. As a result, topographic effects are emphasized or decreased. There appears to be no sensitivity of the flow velocity in this case , it has a significant impact on peak flow velocity in a variety of channel reaches. Nonetheless, for full flow arrest, which is more sensitive to, the turbulence value is rarely essential. Turbulence is likely the most distinguishing aspect of a Voellmy rheology when contrasted to a macro-viscous Bingham-like rheology. In terms of flow height, the contribution of is insignificant during both transport and deposition (Simoni & Graf, 2012). According to Cesca et al (2008), in RAMMS simulations, the complete input solid volume is located in a limited area and is not timed. As a result, the debris flow is

released into a channel that is too tiny to accommodate the entire discharge. As a result, avulsion occurrences emerge along the channel, resulting in higher lateral spreading than previously seen (Cesca & D'Agostino, 2008).

According to additional research, the friction model affects the simulation of debris flows, where the coefficients of Voellmy friction must be adjusted according to the material composition of the flow, i.e. whether it is fluid or granular. Because these coefficients fluctuate for different volumes due to momentum loss during corrosion processes, friction is expected to increase with increasing volume. Because the hydrograph is assumed to mimic true starting conditions, these simulations benefit from faster processing times (Graf & McArdell, 2011) (Cesca & D'Agostino, 2008). According to Simoni et al (2012), the computer does a good job with the facts, and the model correctly forecasts a significant portion of the actual deposit (Simoni & Graf, 2012). The riverbed appears to follow the relief of the area normally, according to Theodoridou & Kalousis' research (Θεοδωρίδου & Καλούσης, 2019).
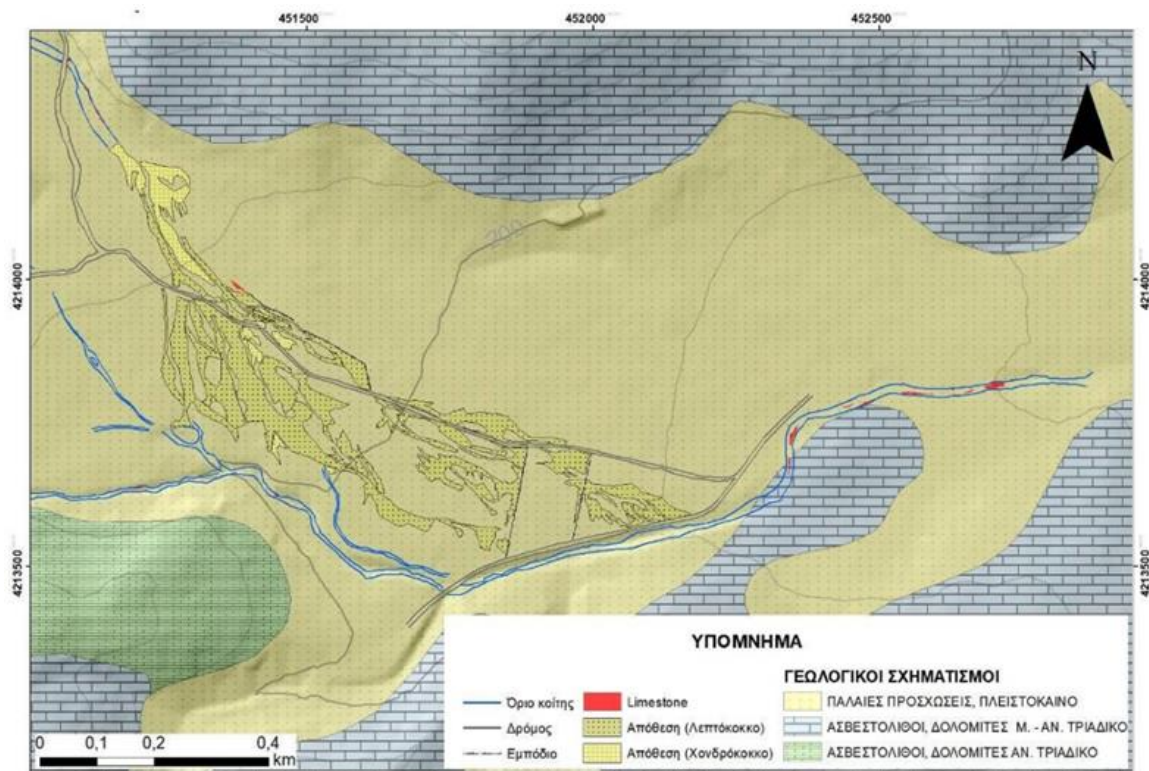
FIGURE 53 FLOOD DEPOSITS AND A NEWLY CONSTRUCTED RIVERBED ARE DEPICTED IN THIS ILLUSTRATION MAP (ΘΕΟΔΩΡΊΔΟΥ & ΚΑΛΟΎΣΗΣ, 2019)

The current widening values are of class x2-x5, indicating that despite being the average value of the erosionf rate, the riverbed's limits are still changing significantly. Wider spreading values are more common in subsidiary branches than in main branches. The peaks in the main branch that appear to follow a common direction from NW-SE to NNW-SSE appear to be linked. This course appears to be followed by the subsidiary branches as well. As a result, there is a pattern of maximum lateral erosion of riverbed boundaries in this direction, which may be due to the geodynamic regime of the area, which contains NW-SE direction faults (Θεοδωρίδου & Καλούσης, 2019).
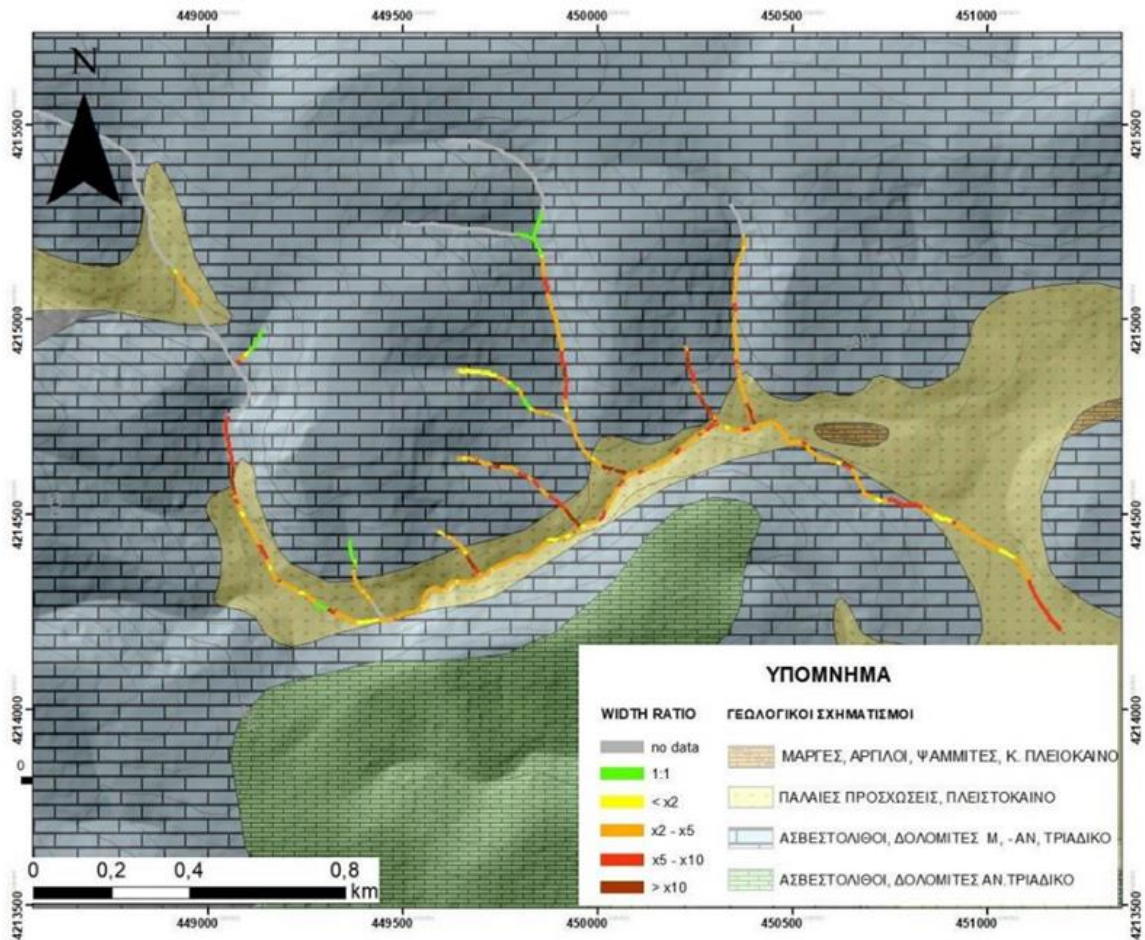
FIGURE 54 THE VARIATION IN THE WIDTH OF THE RIVERBED IS DEPICTED GRAPHICALLY ON A MAP (ΘΕΟΔΩΡΊΔΟΥ & ΚΑΛΟΎΣΗΣ, 2019)

The Katsimidi stream that emerges from the confined valley turns south and enters a morphologically flat terrain. In this place, the torrent's energy decreases, and the runoff's carrying capacity gradually decreases. This fact is not visible in the current work since the branch is cut short just before it reaches the low slopes of the area.

The following are the initial beds in the northern sub-basin of the stream Agia Aikaterini-Katsimidi, according to Theotis' research (Θεοτής, 2021).

Additional segments of the two streams in the vicinity were digitized and mapped in contrast to the old riverbeds (Θεοτής, 2021). According to the graphic, the program used in this study was able to display the riverbeds after the flood event based on the data entered.

FIGURE 56 A COMPARISON SHOT OF THE RIVERBEDS IS PRESENTED BEFORE (WHITE) AND AFTER (LIGHT BLUE) THE DISASTROUS OCCURRENCE (BLUE) (ΘΕΟΤΉΣ, 2021)

References

Abramson, L., Lee, T., Sharma, S. & Boyce, G., 2002. *Slope stability and stabilization methods.* 2nd Edition ed.

Abraseys, N. N. & Jackson, J. A., 1989. Seismicity and associated strain of central Greece between 1890 and 1988.

Aleotti, P., 2004. A warning system for rainfall-induced shallow failures. *Engineering geology,* 73(3-4), pp. 247-265.

Andreadakis, E. et al., 2018. *Characteristics and impacts of the November 2017 catastrophic flash flood in Mandra, Greece.* s.l., European Geosciences Union General Assembly 2018.

Bartelt, P. et al., 2013. *Rapid Mass Movements Simulation: User Manual*

Bengtson, H., 2017. *Spreadsheet Use for Partially Full Pipe Flow Calculations*

Berger, C., McArdell, B. & Schlunegger, F., 2011. Sediment transfer patterns at the Illgraben catchment, Switzerland: Implications for the time scales of debris flow activities. *Geomorphology,* 125(3), pp. 421-432.

Bezak, N. et al., 2020. An extreme May 2018 debris flood case study in northern Slovenia: analysis, modelling, and mitigation. *Landslides,* 17(10), pp. 2373-2383.

Bhattaral, B., Kayastha, R., Adhikari, T. & Mool, P., 2015. Estimation of Peak Discharge and Selection of Manning's coefficient for Sangda River and Langtang River of Nepal.

Blijenberg, H., 2007. Application of physical modelling of debris flow triggering to field conditions: Limitations posed by boundary conditions. *Engineering geology,* 91(1), pp. 25-33.

Bollschweiler, M. S., Stoffel, M. & Miklau, F. R., 2012. *Dating Torrential Processes on Fans and Cones.* 1 Online ed.

Brunetti, M. et al., 2010. Rainfall thresholds for the possible occurrence of landslides in Italy. *Natural hazards and earth system sciences,* 10(3), pp. 447-458.

Bühler, Y., Christen, M., Kowalski, J. & Bartelt, P., 2011. Sensitivity of snow avalanche simulations to digital elevation model quality and resolution. *Annals of glaciology,* 52(58), pp. 72-80.

Caine, N., 1980. The rainfall intensity-duration control of shallow landslides and debris flows. *natural resources,* 62(1-2), pp. 23-27.

Calligaris, C. & Zini, L., 2012. Debris Flow Phenomena: A Short Overview?. In: I. A. Dar, ed. *Earth Sciences.* s.l.:s.n., p. 662.

Cannon, S. et al., 2008. Storm rainfall conditions for floods and debris flows from recently burned areas in southwestern Colorado and southern California. *Geomorphology,* 96(3), pp. 250-269.

Casagrande, A., 1936. *Characteristics of cohesionless soils affecting the stability of slopes and earth fills.* Print book : National government publication ed. s.l.:Harvard University, 1936.

Cesca, M. & D'Agostino, V., 2008. Comparison between FLO-2D and RAMMS in debris- flow modelling: A case study in the Dolomites.

Chien-Yuan Chen & Fan-Chieh Yu, 2011. Morphometric analysis of debris flows and their source areas using GIS. *Geomorphology,* 102(102), pp. 1-11.

Chousianitis, K., Ganas, A. & Gianniou, M., 2013. Kinematic interpretation of present-day crustal deformation in central Greece from continuous GPS measurements. *Journal of Geodynamics,* Volume 71, pp. 1-13.

Chow, V., 1955. A note of the Manning Formula. *Transactions American Geophysical Union,* 36(4), p. 688.

Christen, M. et al., 2012. *NUMERICAL SIMULATION TOOL "RAMMS" FOR GRAVITATIONAL NATURAL HAZARDS.*

Christen, M., Kowalski, J. & Bartlet, P., 2010. RAMMS: Numerical simulation of dense snow avalanches in three-dimensional terrain. *Cold regions science and Technology,* 63(1-2), pp. 1-14.

Costa, J. & Fleisher, P., 1984. *Developments and applications of geomorphology || Physical geomorphology of debris flows.* Kindle Edition ed. s.l.:Springer.

Coussot, P. & Piau, J., 1994. On the behavior of fine mud suspensions. *Rheologica Acta,* Volume 33, pp. 175-184.

Cregoretti, C. & Dalla Fontana, G., 2008. The triggering of debris flow due to channel-bed failure insome alpine headwater basins of the Dolomites: analyses ofcritical runoff. *Hyrological Processes,* 22(13), pp. 2248-2263.

Cristen, M., Kowalski, J. & Bartlet, P., 2010. RAMMS: Numerical simulation of dense snow avalanches in three-dimensional terrain.

Cruden, D. M. & Varnes, D. J., 1996. *Landslide Types and Processes,* s.l.: Special Report-National Research Council.

CUI, Y.-F., ZHOU, X.-j. & GUO, C.-x., 2017. Experimental study on the moving characteristics of fine grains in wide grading unconsolidated soil under heavy rainfall. *Journal of Mountain science,* Volume 14, pp. 417-437.

Deligiannakis, G., Papanikolaou, I. D. & Roberts, G., 2018. Fault specific GIS based seismic hazard maps for the Attica region, Greece. *Geomorphology,* Volume 306, pp. 264-282.

Diakakis, M. et al., 2019. An integrated approach of ground and aerial observations in flash flood disaster investigations. The case of the 2017 Mandra flash flood in Greece.

Diakakis, M. et al., 2019. An integrated approach of ground and aerial observations in flash flood disaster investigations. The case of the 2017 Mandra flash flood in Greece. *International Journal of Disaster Risk Reduction,* Volume 33, pp. 290-309.

Earle, S., 2020. *Drainage basins,* s.l.: BCCampus.

El-Hames, A., 2012. An empirical method for peak discharge prediction in ungauged arid and semi-arid region catchments based on morphological parameters and SCS curve number.

Fischenich, C., 2000. Robert Manning (A Historical Perspective). *Technical notes collection.*

FLOODHUB, 2018. *ΑΝΑΛΥΣΗ ΤΗΣ ΠΛΗΜΜΥΡΑΣ ΤΗΣ 15/11/2017 ΣΤΗ ΔΥΤΙΚΗ ΑΤΤΙΚΗ ΜΕ ΑΞΙΟΠΟΙΗΣΗ ΔΟΡΥΦΟΡΙΚΗΣ ΤΗΛΕΠΙΣΚΟΠΗΣΗΣ,* s.l.: Ινστιτούτο Αστρονομίας, Αστροφυσικής, Διαστημικών Εφαρμογών και Τηλεπισκόπησης Εθνικό Αστεροσκοπείο Αθηνών.

Fort, M., Cossart, E. & Arnaud-Fassetta, G., 2010. Catastrophic landslides and sedimentary budgets. In: I. A. a. A. S. Goudie, ed. *Geomorphological Hazards and Disaster prevention.* s.l.:online by Cambridge University Press.

Frank, F., McArdell, B., Huggel, C. & Vieli, A., 2015. The importance of entrainment and bulking on debris flow runout modeling: examples from the Swiss Alps. *Natural Hazards and earth system science,* Volume 15, pp. 2569-2583.

Frank, F. et al., 2017. Debris-flow modeling at Meretschibach and Bondasca catchments, Switzerland: sensitivity testing of field-data-based entrainment model. *Natural hazards and earth system science.*

Gabet, E. & Mudd, S., 2006. The mobilization of debris flows from shallow landslides. *Geomorphology,* 74(1-4), pp. 207-218.

Ganas, A., Pavlides, S. & Karastathis, V., 2005. DEM-based morphometry of range-front escarpments in Attica, central Greece, and its relation to fault slip rates. *Geomorphology,* Volume 65, pp. 301-319.

Gaume, E. & Borga, M., 2008. Post-flood field investigations in upland catchments after major flash floods: proposal of a methodology and illustrations. *Flood risk management,* 1(4), pp. 175-189.

Godt, G. & Coe, J., 2007. Alpine debris flows triggered by a 28 July 1999 thunderstorm in the central Front Range, Colorado. *Geomorphology,* 84(1-2), pp. 80-97.

Graf, C. & McArdell, B., 2011. Debris-flow monitoring and debris-flow runout modelling before and after construction of mitigation measures: an example from an instable zone in the Southern Swiss Alps. *Actes du colloque de la Société Suisse de Géomorphologie,* Issue 3-5, pp. 245-258.

Gregoretti, C. & Dalla Fontana , G., 2007. The triggering of debris flow due to channel-bed failure insome alpine headwater basins of the Dolomites: analyses ofcritical runoff. *Hydrological processes,* 22(13), pp. 2248-2263.

Gregoretti, C. et al., 2019. Relevance of erosion processes when modelling in-channel gravel debris flows for efficient hazard assessment. *Hydrology,* Volume 568, pp. 579-591.

Grimaldi, S., Petroselli, A., Tauro, F. & Porfiri, M., 2012. Time of concentration: a paradox in modern hydrology. *Hydrological sciences.*

Grimaldi, S., Petroselli, A., Tauro, F. & Profiri, M., 2012. Time of concentration: a paradox in modern. *Hydrological Sciences Journal,* 57(2), pp. 217-228.

Guzzetti, F. et al., 2008. Distribution of landslides in the Upper Tiber River basin, central Italy. *Geomorphology,* 96(1-2), pp. 105-122.

Guzzetti, F., Peruccacci, S., Rossi, M. & Stark, C., 2007. The rainfall intensity–duration control of shallow landslides and debris flows: an update. *Landslides,* Volume 5, pp. 3-17.

Haas, T. & Woerkom, T., 2016. Bed scour by debris flows: experimental investigation of effects of debris-flow composition. *Earth surface processes and Landforms,* 41(13), pp. 1951-1966.

Highland, L. & Bobrowsky, P., 2008. The landslide handbook: a guide to understanding landslides. *Geological survey circular ,* p. 129.

Hungr, O., 2000. ANALYSIS OF DEBRIS FLOW SURGES USING THE THEORY OFUNIFORMLY PROGRESSIVE FLOW. *Earth surface processes and Landforms,* 25(5), pp. 483-495.

Hungr, O., Evans, S., Bovis, M. & Hutchinson, J., 2001. A review of the classification of landslides of the flow type. *Environmental and engineering of Geoscience,* 7(3), pp. 221-238.

Hungr, O., Morgan, G. & Kellerhals, R., 1984. Quantitative analysis of debris torrent hazards for design of remedial measures. *Canadian Geotechnical Journal,* pp. 663-677.

Iverson , R., Reid, M. & LaHusen, R., 1997. Debris-Flow mobilization from landslides.

Iverson, R., 1997b. The physics of debris flows. *Reviews of Geophysics ,* 35(3), pp. 245-296.

Iverson, R., 2000. Landslide triggering by rain infiltration. *Water Resources Research,* 36(7), pp. 1897-1910.

Iverson, R., 2005. Regulation of landslide motion by dilatancy and pore pressure feedback. *Journal of Geophysical Research,* 110(F2).

Iverson, R. & Ouyang, C., 2015. Entrainment of bed material by Earth-surface mass flows: Review and reformulation of depth-integrated theory. *Reviews of Geophysics ,* 53(1), pp. 27-58.

Iverson, R. & Vallance, J., 2001. New views of granular mass flows. *Geology,* 29(2), pp. 115-118.

Johnson, B. et al., 2012. In situ observations of volcanic ash clouds from the FAAM aircraft during the eruption of Eyjafjallajökull in 2010. *Journal of Geophysical Research,* 117(D20), p. 26.

Jun-Du, Zhong-jie Fan, Wen-Tao Xu & Lin-yao Dong, 2021. Research Progress of Initial Mechanism on Debris Flow and Related Discrimination Methods: A Review. *frontiers in Earth Science.*

Kaufman de ALMEIDA, I. et al., 2014. Estimation on time of concentration of overland flow in watersheds : A Review. *Geociências,* 33(4), pp. 661-671.

Klubertanz, G., Laloui, L. & Vulliet, L., 2009. Identification of mechanisms for landslide type initiation of debris flows. *Engineering Geology,* 109(1-2), pp. 114-123.

Koukis, G., Sabatakakis, N., Nikolaou, N. & Loupasakis, C., 2005. Landslide Hazard Zonation in Greece. *International Consortium on Landslides,* pp. 291-296.

Koutsoyiannis, D., 2004. Statistics of extremes and estimation of extreme rainfall: I. Theoretical investigation.

Koutsoyiannis, D., 2004. Statistics of extremes and estimation of extreme rainfall: II. Empirical investigation of long rainfall records. *Scientific Journals,* 49(4), pp. 591-610.

Liu, S., Wei, L. & Hu, K., 2020. Topographical and geological variation of effective rainfall for debris-flow occurrence from a large-scale perspective. *Geomorphology,* Volume 358.

Manning, R., 1891. On the flow of water in open channels and pipes. *Hydraulic Engineer ,* pp. 161-207.

Matthias, J., 2005. A size classification for debris flows. *Engineering Geology,* 79(3-4), pp. 151-161.

Matthias, J. & Jordan, P., 2001. Design flood estimates in mountain streams – the need for a geomorphic approach. *Canadian Journal of civil engineering,* 28(3), pp. 425-439.

McGuire, L., Rengers, F., Kean, J. & Staley, D., 2017. Debris flow initiation by runoff in a recently burned basin: Is grain-by-grain sediment bulking or en masse failure to blame?. *Geophysical Research Letters ,* 44(14), pp. 7310-7319.

Miko ˇs, M. & Bezak, N., 2021. Debris Flow Modelling Using RAMMS :Model in the Alpine Environment with focus on the Model Parameters and main Characteristics. *frontiers in Earth Science .*

Montgomery, D. & Dietrich, W., 1994. A psysically based model for the topographic control on shallow landsliding. *Water Resources Research ,* 30(4), pp. 1153-1171.

Nettleton, I., Martin, S., Hencher, S. & Moore, R., 2005. *Debris flow types and mechanisms,* s.l.: s.n.

Nikolopoulos, E. et al., 2014. Impact of uncertainty in rainfall estimation on the identification of rainfall thresholds for debris flow occurrence. *Geomorphology,* Volume 221, pp. 286-297.

O'Brien , J. & Julien, P., 1988. Laboratory Analysis of Mudflow Properties.

O'Brien, J., 2001. FLO 2D user manual.

Plumer, C., Carlson, D. & Hammersley, L., 2016. *Physical Geology.* 15th Edition

Rapp, A., 1960. Recent Development of Mountain Slopes in Kärkevagge and Surroundings, Northern. *Geografiska Annaler ,* 42(2-3), pp. 65-200.

Raymoncd, W. & Angela, J., 1997. *Preliminary maps showing rainfall thresholds for debris-flow activity, San Francisco Bay region, California.* s.l.:BiblioGov.

Rieckenamnn, D. & Zimmermann, M., 1993. The 1987 debris flows in Switzerland: documentation and analysis.

Salm, B., 2017. Flow, flow transition and runout distances of flowing avalanches. *Annals of Glaciology,* Volume 18, pp. 221-226.

Salm, B., Burkard, A. & Gubler, H., 1990. Berechnung von Fliesslawinen : eine Anleitung fuer Praktiker mit Beispielen. *Eidgenössisches Institut für Schnee- und Lawinenforschung*, Volume 47.

Salm, B., Burkard, A. & Gubler, H., 1990. Berechnung von Fliesslawinen: eine Anleitung für Praktiker mit Beispielen.

Sandersen, F., Bakkeoi, S., Hestnes, E. & Lied, K., 1996. The influence of meteorological factors on the initiation of debris flows, rockfalls, rockslides and rockmass stability. *Geology.*

Schimmel, A., Hübl , J., McArdell, B. & Walter, F., 2018. Automatic Identification of Alpine Mass Movements by a Combination of Seismic and Infrasound Sensors. *Physical Sensors ,* 18(5), p. 1658.

Simoni, A. & Graf, C., 2012. Performance of 2D debris flow simulation model RAMMS. Back-Analysis of field events in Italian Alps.

Skilodimou, H. & Bathrellos, G., n.d. *Debris flow: categories,characteristics,hazard assessment,mitigation measures,* s.l.: s.n.

Sosio, R., Crosta, G. & Frattini, P., 2007. Field observations, rheological testing and numerical modelling of a debris-flow event.

Soulios, G., Stournaras, G., Nikas, K. & Mattas, C., 2018. The floods in Greece: the case of Mandra in Attica. *Bulletin of the Geological Society of Greece ,* Volume LII-52, pp. 131-144.

Stancanelli, L., Lanzoni, S. & Foti, E., 2015. Propagation and deposition of stony debris flows at channel confluences. *Water Resources Research ,* 51(7), pp. 5100-5116.

Takahashi, T., 1978. Mechanical characteristics of debris flow. *Journal of the Hydraulics Division,* 104(8).

Takahashi, T., 1981. Debris Flow. Volume 13, pp. 57-77.

Takahashi, T. et al., 1998. Mechanics of the viscous type debris flow (3)–Formation and propagation of the debris flow surge. *Disaster Prevention Research Institute Annuals,* 36(B-2), pp. 433-449.

Tavoularis, N., Papathanassiou, G., Ganas, A. & Argyrakis, P., 2021. Development of the Landslide Susceptibility Map of Attica Region, Greece, Based on the Method of Rock Engineering System. *Land,* 10(2), p. 148.

Terzaghi, K., 1950. Mechanisms of Landslides. *Geotechnical Society of America,* 4(5A), pp. 83-125.

Theule , J. et al., 2015. Channel scour and fill by debris flows and bedload transport. *Geomorphology,* Volume 243, pp. 92-105.

U.S. Army corps of engineers, 1994. Engineering and Design Rock Foundations. *Manual.*

Underwood, S. et al., 2016. Atmospheric circulation patterns, cloud-to-ground lightning, and localy intense convective rainfall associated with debris flow initiation in the Dolomite Alps of northeastern Italy. *Natural hazards and earth system science,* Volume 16, pp. 509-528.

Voellmy, A., 1955. Über die Zerstörungskraft von Lawinen. *E-Periodica,* Volume 73, p. 212.

Washington, S., 1984. Proceedings of a Workshop on Slope Stability : Problems and Solutions in Forest Management. *General Technical Report ,* p. 118.

Wieczorek, G. & Glade, T., 2005. Climatic factors influencing occurence of debris flow. *Debris-flow Hazards and Related Phenomena,* pp. 325-362.

Winter, M. et al., n.d. Landslides Events.

Winter, M., Macgregor, F. & Shackman, L., 2005. *Scottish Road Network Landslides Study,* s.l.: s.n.

WLI, W., 1995. A suggested method for reporting a landslide. *The International Geotechnical Societies' UNESCO Working Party on World Landslide Inventory,* 41(5-12), p. 11.

Zhou, G. et al., 2018. Depositional mechanisms and morphology of debris flow: physical modelling. *Landslides ,* Volume 16, pp. 315-332.

Zhou, S., Gao, L. & Zhang, L., 2019. Predicting debris-flow clusters under extreme rainstorms: a case study on Hong Kong Island. *Bulletin of Engineering Geology and the Environment,* Volume 78, pp. 5775-5794.

Ανδριόπουλος, Π., 2020. *Οπτική κοκκομετρία σε αποθέσεις ξαφνικών πλημμυρών και ροών κορημάτων με χρήση επίγειων μέσων και ΣμηΕΑ.* s.l., Εθνικό Καποδιστριακό Πανεπιστήμιο Αθηνών.

Αντωνιάδη, Σ., 2016. *ΔΙΕΡΕΥΝΗΣΗ ΜΕΤΑΒΛΗΤΟΤΗΤΑΣ ΧΡΟΝΙΚΗΣ ΑΠΟΚΡΙΣΗΣ ΛΕΚΑΝΩΝ ΑΠΟΡΡΟΗΣ,* s.l.: Εθνικό Μετσόβιο Πολυτεχνείο.

Βασιλειάδης, Ε., 2010. *Ζωνοποίηση της επικινδυνότητας των κατολισθητικών φαινομένων στον Ελλαδικό χώρο. Δημιουργία και εφαρμογή μοντέλων με Γεωγραφικό Σύστημα Πληροφοριών,* s.l.: Πανεπιστήμιο Πατρών.

Γραμμένου, Α., 2021. *Ξαφνικές πλημμύρες και ροές κορημάτων. Η περίπτωση της Μάνδρας,* s.l.: Εθνικό Καποδιστριακό Πανεπιστήμιο Αθηνών.

Δουραμάνης, Μ. Ε., 2006. *ΕΦΑΡΜΟΓΗ ΤΟΥ ΣΧΕΔΙΑΣΤΙΚΟΥ ΠΑΚΕΤΟΥ AutoCAD Land Development Desktop R2i ΣΤΗΝ ΜΕΛΕΤΗ ΕΚΜΕΤΑΛΛΕΥΣΗΣ ΤΟΥ ΛΑΤΟΜΕΙΟΥ ΑΣΒΕΣΤΟΛΙΘΟΥ ΚΑΜΑΡΙΟΥ,* s.l.: Πολυτεχνείο Κρήτης.

Εξαδάκτυλος, Γ., 2002. Ανάλυση ευστάθειας υπαίθριων και υπόγειων έργων.

Ερμίδης, Δ., 2018. *Υδρογεωλογικό καθεστώς λεκάνης Θριασίου Πεδίου με έμφαση στα γεωυδραυλικά χαρακτηριστικά των υδροφόρων οριζόντων και στην ποιότητα των υπογείων υδάτων,* s.l.: Γεωπονικό Πανεπιστήμιο Αθηνών.

Θεοδωρίδου, Γ. & Καλούσης, Γ., 2019. *Φαινόμενα Διάβρωσης και Απόθεσης κατά την Ξαφνική Πλημμύρα της Μάνδρας στο ρέμα Κατσιμίδι (Δυτική Αττική, 15 Νοέμβρη 2017). Χαρτογράφηση πεδίου με Υποβοήθηση από ΣΜηΕΑ,* s.l.: Εθνικό Καποδιστριακό Πανεπιστήμιο Αθηνών.

Θεοδωρίδου, Γ. & Καλούσης, Γ., 2019. Φαινόμενα Διάβρωσης και Απόθεσης κατά την Ξαφνική Πλημμύρα της Μάνδρας στο ρέμα Κατσιμίδι (Δυτική Αττική, 15 Νοεμβρίου 2017). Χαρτογράφηση πεδίου με Υποβοήθηση από ΣμηΕΑ.

Θεοτής, Α., 2021. *Δομές ελέγχου για την ανάσχεση ροών κορημάτων και διερεύνηση καινοτόμας διάταξης ανάσχεσης,* s.l.: s.n.

Λέκκας, Ε. et al., 2015. *Σχέδιο Ολοκληρωμένης Διαχείρισης Γεωπεριβαλλοντικών Επιπτώσεων και άμεσων Επεμβάσεων στις Πυρόπληκτες Περοχές του Δήμου Μονεμβασίας-Έρευνα Μείωσης Κατολισθητικού Κινδύνου.* s.l., s.n.

Λουπασάκης, Κ., 2013-2014. *Εδαφομηχανική και Στοιχεία Θεμελιώσεων-Σημειώσεις Διαλέξεων Μαθήματος,* s.l.: Εθνικό Μετσόβιο Πολυτεχνείο-Σημειώσεις μαθήματος.

Μουντράκης, Δ., 2010. *Γεωλογία και Γεωτεκτονική εξέλιξη της Ελλάδας.* s.l.:s.n.

Μπούνου, Α., 2012. *Συγκριτική αξιολόγηση αριθμητικών επιλύσεων του προβλήματος της ευστάθειας πρανών με τις μεθόδους πεπερασμένων στοιχείων, πεπερασμένων διαφορών & οριακής ισορροπίας,* s.l.: Πολυτεχνείο Κρήτης.

Σοφιανός, Α., 2015. *Υποστήριξη Υπογείων Έργων*